



UNIVERSITEIT • STELLENBOSCH • UNIVERSITY
jou kennisvenoot • your knowledge partner

Development of a minimally invasive robotic surgical manipulator

Peter-John Christiane

14030292-2003



In submission for:

Masters of Science in Engineering (MScEng)

December 2008

**Department of Mechanical and Mechatronic Engineering
University of Stellenbosch**

FAKULTEIT INGENIEURSWESE
FACULTY OF ENGINEERING



Development of a minimally invasive robotic surgical manipulator

Peter-John Christiane

14030292-2003

In submission for:

Masters of Science in Engineering (MScEng)

December 2008

Supervisors: Prof C Scheffer & Dr K Schreve

**Department of Mechanical and Mechatronic Engineering
University of Stellenbosch**

Declaration

I, the undersigned, hereby declare that the work contained in this thesis is my own original work and that I have not previously in its entirety or in part submitted it at any university for a degree.

Signature:

Peter-John Christiane

Date:

Copyright © 2008 Stellenbosch University
All Rights Reserved

Abstract

Minimal invasive surgery (MIS) enables surgeons to operate through a few small incisions made in the patient's body. Through these incisions, long rigid instruments are inserted into the body and manipulated to perform the necessary surgical tasks. Conventional instruments, however, are constrained by having only five degrees of freedom (DOF), as well as having scaled and mirrored movements, thereby limiting the surgeon's dexterity. Surgeons are also deprived of depth perception and hand-eye coordination due to only having two-dimensional visual feedback. Surgical robotics attempt to alleviate these drawbacks by increasing dexterity, eliminating the fulcrum effect and providing the surgeon with three-dimensional visualisation. This reduces the risks to the patient as well as to the surgeon. However, existing MIS systems are extremely expensive and bulky in operating rooms, preventing their more widespread adoption. In this thesis, a new, inexpensive seven-DOF primary slave manipulator (PSM) is presented. The four-DOF wrist is actuated through a tendon mechanism driven by five 12 VDC motors. A repeatability study on the wrist's joint position was done and showed a standard deviation of 0.38 degrees. A strength test was also done and demonstrated that the manipulator is able to resist a 10 N opposing tip force and is capable of a theoretical gripping force of 15 N.

Opsomming

Minimale indringende chirurgie (MIC) maak dit vir chirurgie moontlik om operasies uit te voer deur 'n paar klein insnydings wat op die pasiënt se liggaam gemaak word. Deur hierdie insnydings word lang onbuigsame instrumente in die liggaam ingesit en gemanipuleer om die nodige chirurgiese take uit te voer. Konvensionele instrumente is egter beperk vanweë die feit dat hulle net vyf vryheidsgrade het, asook afgeskaalde bewegings en spieëlbewegings, en gevolglik die chirurg se handvaardigheid beperk. Chirurgie word ook onttrek van dieptewaarneming en hand-oog-koördinasie, want hulle is beperk tot tweedimensionele visuele terugvoer. Chirurgiese robotika poog om hierdie nadele aan te spreek deur handvaardigheid te vermeerder, die hefboomeffek uit te skakel en die chirurg driedimensionele visualisering te bied. Dit verminder die risiko's vir die pasiënt én vir die chirurg. Bestaande MIC-stelsels is egter uiters duur en neem baie plek op in teaters, wat verhoed dat hulle op 'n groter skaal gebruik word. In hierdie tesis word 'n nuwe, goedkoop sewevryheidsgrade- primêre slaafmanipuleerder (PSM) voorgelê. Die viervryheidsgrade-pols word beweeg deur 'n tendonmeganisme wat aangedryf word deur vyf 12 VDC-motors. 'n Herhaalbaarheidstudie is op die pols se gewrigsposisie gedoen, wat 'n standaardafwyking van 0.38 grade aangetoon het. 'n Sterktetoets is ook gedoen en het gewys dat die manipuleerder in staat is om 'n 10 N-teenkantelkrag te weerstaan en dat dit oor 'n teoretiese greepsterkte van 15 N beskik.

Acknowledgements

A special thanks to the following people who helped with this thesis and made it all possible through their efforts

- To Prof Cornie Sheffer and Dr Kristiaan Schreve who supervised this thesis and gave their invaluable inputs.
- To Almero Viljoen and Jacob Viljoen who initiated the project. For their contributions and their financial support.
- To the Mechanical Workshop, in particular Ferdie Zietsman and Anton van den Berg, who made the prototypes and were very patient and helpful while doing so.
- To my parents for their continuous support and unfailing love. Without them, everything I have achieved through my life would not have been possible.

Table of Contents

Declaration.....	i
Abstract.....	ii
Opsomming.....	iii
Acknowledgements.....	iv
Table of Contents.....	v
Nomenclature	ix
1. Abbreviations	ix
2. Glossary.....	x
List of Figures	xi
List of Tables.....	xiv
Chapter 1: Introduction.....	1
1. Background	1
2. Minimal Invasive Surgery	1
3. Minimal Invasive Robotic Surgery.....	4
4. Need for an inexpensive MIRS System	5
5. Objectives.....	6
6. Thesis Layout.....	6
Chapter 2: Robotic Systems and Manipulators for Laparoscopy.....	7
1. Minimal Invasive Surgical Systems.....	7
1.1 MIRS Systems at Research Institutes	8
1.1.1 UCB/USCF RTW	8
1.1.2 HISAR.....	8
1.1.3 ARTEMIS.....	9
1.1.4 KaLAR.....	9
1.2 Commercially Developed MIRS Systems.....	10
1.2.1 AESOP.....	10
1.2.2 ZEUS	11
1.2.3 da Vinci.....	12
2. Manipulator Designs for MIRS Systems	13
2.1 EndoWrist.....	13
2.2 Passive mechanical manipulator instrument tip.....	14
2.3 Sensorized and actuated instruments	14
2.4 Multi-Slider Linkage Manipulator	15
2.5 Miniature worm gear manipulator	15
2.6 Miniature hydraulic parallel manipulator	16
2.7 Novel hybrid actuator design.....	16

3. Actuating Technologies	17
Chapter 3: Manipulator Design	19
1. System Analysis	19
1.1 Design Objectives\Considerations	19
1.2 Design Requirements	20
2. Manipulator Concept Design	20
3. Design of the first prototypes	22
4. Design of the final prototype	23
4.1 Working principle of the manipulator.....	24
4.2 Choice of Materials	25
4.3 Design of the Revolute Joint	26
4.4 Design of the Rotation Joint.....	27
4.5 Actuator Drive	28
4.6 Tool Tip.....	29
5. Manipulator Assembly Procedure	29
5.1 Wrist Assembly Procedure	29
5.2 Actuator Drive Assembly Procedure	31
6. Manipulator Sterilization	32
6.1 Sterilization Techniques	32
6.2 Manipulator Modifications for Sterilization.....	33
7. Mechanical Manipulator Costs	33
Chapter 4: Electronics Design	35
1. System Analysis	35
1.1 Design Considerations.....	35
1.2 Functional Requirements.....	36
2. Control Electronics Concept Description	37
3. Design of the control electronics	37
3.1 Working principle of the control electronics	38
3.2 Digital PCB Board.....	38
3.3 Power Drive PCB Board	40
4. Microcontroller Firmware Overview.....	43
4.1 Master Controller Firmware	43
4.2 Slave Controller Firmware.....	44
5. Control Electronics Costs	44
Chapter 5: System Evaluation	46
1. Repeatability Test Experiment	46

1.1	Experimental Setup	46
1.2	Results and Discussion	48
2.	Manipulator Strength Test Experiment	51
2.1	Experimental Setup	51
2.2	Results and Discussion	52
3.	System Evaluation Discussion	54
Chapter 6: Conclusion and Recommendations		56
Ongoing and Future work		58
References.....		59
Appendix A: Cable Tension Test.....		A1
1.	Experimental Setup	A1
2.	Results and Discussion	A2
Appendix B: Basic Manipulator Calculations		B1
1.	Torsional and Bending Analysis of Manipulator	B1
2.	Torsional Spring Calculations	B2
Appendix C: Manipulator Concept Development		C1
1.	Revolute joint	C1
1.1	Cable.....	C1
1.1.1	Pulleys (One turn)	C1
1.1.2	Pulleys (Multiple turns)	C2
1.1.3	Ball-‘n-Chain	C2
1.1.4	Pneumatic piston	C2
1.1.5	Magnets in series	C3
1.1.6	Spur gear runner	C3
1.1.7	Spring joint, cable actuated	C4
1.1.8	Three-link joint	C4
1.2	Gearing.....	C5
1.2.1	Worm gear	C5
1.2.2	Double worm gear.....	C5
1.2.3	Worm gear with big motor	C6
1.2.4	Bevel gear.....	C6
1.3	Other	C7
1.3.1	Pneumatic, three cylinder joint.....	C7
1.3.2	Flexible distal tip	C7
1.3.3	Planetary gear reel for cable actuation.....	C7
1.3.4	Worm gear reel for cable actuation.....	C8
2.	Rotation joint	C8

2.1	Cable.....	C9
2.1.1	Cable rotation mechanism	C9
2.2	Gearing.....	C9
2.2.1	Direct drive actuation.....	C9
2.2.2	Spur/Helical rotational joint.....	C10
2.2.3	Multi-stage planetary gear rotation joint	C10
2.2.4	Harmonic gear joint.....	C11
2.2.5	Harmonic & Planetary joint.....	C11
2.2.6	Helical worm gear mechanism with two motors	C12
2.2.7	Bevel & Spur/Helical gear rotation joint	C12
2.2.8	Angular swivel joint.....	C13
2.3	Other	C14
2.3.1	Drive shaft	C14
2.3.2	Inner tube guided joint	C14
Appendix D: Technical Drawings.....		D1
Appendix E: Electronic Design.....		E1
1.	Noise Reduction Techniques.....	E1
1.1	Board-Level Techniques	E1
1.1.1	Board-structure techniques	E1
1.1.2	Filter techniques.....	E1
1.1.3	Other design techniques	E2
2.	Electronic schematics.....	E3
3.	PCB Layouts.....	E4
4.	PCB Images.....	E6
Appendix F: Experimental Data.....		F1
1.	Repeatability Test.....	F1
2.	Strength Test Data	F2

Nomenclature

1. Abbreviations

2D	two dimensional
3D	three dimensional
ADC	Analog to Digital Converter
AESOP	Automated Endoscopic System for Optimal Positioning
ARTEMIS	Advanced Robot and Telemanipulator Systems for Minimal Invasive Surgery
CAD	Computer Aided Design
CCD	Charge Coupled Device
CMM	Coordinate Measuring Machine
CMOS	Complementary Metal-Oxide Semiconductor
CNC	Computer Numerical Control
CRT	Cathode Ray Tube
CT	Computer Tomography
DC	Direct Current
DMOS	Diffusion Metal Oxide Semiconductor
DOF	Degree(s) of Freedom
EMC	Electromagnetic Compliance
EMI	Electromagnetic Interference
EUSART	Enhanced Universal Serial Asynchronous Receiver Transmitter
FDA	Food and Drug Administration
KAIST	Korea Advanced Institute of Science and Technology
KaLAR	KIAST Laparoscopic Assistant Robot
MCM	Motion Control Module
MIRS	Minimal Invasive Robotic Surgery
MIS	Minimal Invasive Surgery
MSSP	Master Synchronous Serial Port
OCP	Overcurrent Protection
PCB	Printed Circuit Board
PCPWM	Power Control PWM
PSM	Primary Slave Manipulator
PWM	Pulse Width Modulator
RAM	Random Access Memory
RTW	Robotic Telesurgical Workstation
SMA	Smart Memory Alloy
SSM	Secondary Slave Manipulator
SSP	Synchronous Serial Port
TTL	Transistor-Transistor Logic

UCB University of California, Berkley
USCF University of California, San Francisco

2. Glossary

Backlash	The play or loose motion in an instrument due to clearance existing between mechanically contacting parts.
Cholecystectomy	It is the surgical removal of the gallbladder.
Electro Magnetic Compliance	The requirements for both electromagnetic emissions and susceptibility of a piece of equipment to comply with a governing set of standards.
Electro Magnetic Interference	The interference in signal transmissions or receptions caused by the radiation of electrical and magnetic fields.
Endoscope	A thin, fiber optic tube with a light and lens, used to view the internal operating cavity while doing a surgical procedure.
Fulcrum effect	The tool tip moves in the opposite direction to the surgeon's movements due to the pivoting of the tool around the entry point. This is known as the fulcrum effect.
Hysterectomy	The surgical removal of the uterus and, sometimes, the cervix.
Hysteresis	The property that the output depends on the history of the input and current direction of change.
Laparoscopy	The surgical procedure whereby instruments are placed through small incisions made in the patient's skin to view the internal organs and perform the necessary tasks.
Myomectomy	It is the surgical removal of the uterine fibroid tumor
Stewart platform	It is a kind of parallel manipulator using an octahedral assembly of struts.
Tactile feedback	It is the sense of pressure perception by the surgeon based or received from force sensing means to give the surgeon the ability to know how much force is being applied

List of Figures

Figure 1: Illustration of pelvic laparoscopy (NJPCU, 2006)	2
Figure 2: Human anatomy and physiology of the gallbladder (Martini and Bartholomew, 2007)	3
Figure 3: Conventional rigid MIS instrument (Mediflex, 2006)	3
Figure 4: da Vinci from Intuitive Surgical Inc. (Intuitive Surgical Inc., 2007)	5
Figure 5: DOF of laparoscopic instrumentation (Ruurda, 2003)	7
Figure 6: UCB/UCSF robotic telesurgical workstation and milirobotic wrist (Cavusoglu <i>et al.</i> , 2001)	8
Figure 7: ARTEMIS minimal invasive robotic system (Ortmaier, 2003)	9
Figure 8: Schematic of the revised KaLAR system (Sim <i>et al.</i> , 2006)	10
Figure 9: The AESOP endoscopic system (Trueforce, 2004; Sim <i>et al.</i> , 2006)	11
Figure 10: ZEUS Surgical Console (left) and Operating Manipulators (right) (Trueforce, 2004)	11
Figure 11: da Vinci's MIRS system (Intuitive Surgical Inc., 2007)	12
Figure 12: da Vinci's secondary slave manipulator (left) and the EndoWrist instruments (right) (Intuitive Surgical Inc., 2007)	13
Figure 13: da Vinci's EndoWrist (Morley and Wallace, 1994; Intuitive Surgical Inc., 2007)	13
Figure 14: Passive mechanical manipulator instrument tip (Jaspers, 2005; Diks <i>et al.</i> , 2007)	14
Figure 15: Articulate joint (Seibold <i>et al.</i> , 2005)	15
Figure 16: Multi-DOF end-effector (Yamashita <i>et al.</i> , 2003)	15
Figure 17: Miniature worm gear manipulator prototype (Peirs <i>et al.</i> , 2000)	16
Figure 18: Miniature hydraulic parallel manipulator design (Peirs <i>et al.</i> , 1999)	16
Figure 19: Assembly of hybrid actuator needle driver (Kode and Cavusoglu, 2007)	17
Figure 20: Secondary slave manipulator concept	19
Figure 21: Seven DOF Primary slave manipulator showing a multi-DOF wrist	21
Figure 22: First and second iterations of first generation prototypes	22
Figure 23: Third iteration of first generation prototypes	23
Figure 24: Manipulator instrument tip prototype	24
Figure 25: Designed 4 DOF primary slave manipulator	24
Figure 26: Manipulator actuating hub	25
Figure 27: Revolute Joint	26
Figure 28: Sectional views of the Revolute Proximal (left) and Revolute Distal (right)	26
Figure 29: Rotation Joint Rotor Assembly (left) and Cable Guide Assembly (right)	27
Figure 30: Sectional views of Rotor Assembly (left) and Cable Guide Assembly (right) ...	27
Figure 31: Sectional view of Actuator Drive Assembly	28
Figure 32: Tool tip	29

Figure 33: Assembly of Rotor Assembly (left) and Cable Guide Assembly (right)	30
Figure 34: Sectional view of Manipulator Wrist	30
Figure 35: Assembly of Actuator Hub	31
Figure 36: Assembly of Actuator Drive	32
Figure 37: Manipulator Cost Estimation	33
Figure 38: Functional requirements diagram.....	36
Figure 39: Master-slave electronics concept	37
Figure 40: Manipulator's control electronics.....	38
Figure 41: Digital Printed Circuit Board.....	39
Figure 42: Master microcontroller schematic.....	40
Figure 43: Slave microcontroller schematic.....	40
Figure 44: Power Printed Circuit Board	41
Figure 45: L6225 H-Bridge Parallel Configuration Schematic	41
Figure 46: 5 V Regulator Circuit	42
Figure 47: Master Controller Firmware Flowchart	43
Figure 48: Slave Controller Firmware Flowchart	44
Figure 49: Control Electronics Cost Estimate	45
Figure 50: Repeatability test setup	46
Figure 51: Repeatability test procedure	47
Figure 52: Sample 1 repeatability graph	48
Figure 53: Short arm hysteresis error	50
Figure 54: Manipulator Strength Test Experimental Setup	51
Figure 55: Strength test weights	52
Figure 56: Strength test deflection moving from extension to flexion.....	52
Figure 57: Strength test deflection moving from flexion to extension.....	53
Figure 58: Drawing of the Gripper jaws and the drive rod (Peeters, 2002).....	53
Figure 59: Force factorisation for the torque balance.....	54
Figure 60: Cable Tension Test Apparatus.....	A1
Figure 61: Cable Tension Test Setup	A2
Figure 62: Force vs. Time plot for first trail.....	A2
Figure 63: Displacement vs. Time plot for first trail.....	A2
Figure 64: Force vs. Time plot for Second Trail.....	A3
Figure 65: Displacement vs. Time for Second Trail	A3
Figure 66: Force vs. Time plot for Third Trail	A4
Figure 67: Displacement vs. Time for Third Trail	A4
Figure 68: Pulley concept.....	C1
Figure 69: Ball-'n-Chain concept	C2
Figure 70: Pneumatic piston concept	C2
Figure 71: Magnets in series concept	C3
Figure 72: Spur gear runner concept	C3
Figure 73: Spring joint, cable actuated concept	C4

Figure 74: Three-link concept	C4
Figure 75: Worm gear concept	C5
Figure 76: Double worm gear concept.....	C5
Figure 77: Big motor worm gear concept	C6
Figure 78: Bevel gear concept.....	C6
Figure 79: 3 Cylinder pneumatic joint concept.....	C7
Figure 80: Flexible distal tip concept	C7
Figure 81: Planetary gear reel concept	C7
Figure 82: Worm gear reel concept	C8
Figure 83: Cable rotation joint concept	C9
Figure 84: Direct drive rotational joint concept.....	C9
Figure 85: Spur/Helical rotational joint concept.....	C10
Figure 86: Multi-stage planetary gear rotational joint concept.....	C10
Figure 87: Harmonic gear rotational joint concept.....	C11
Figure 88: Harmonic & Planetary gear rotational joint concept.....	C11
Figure 89: Helical worm gear rotational joint concept	C12
Figure 90: Bevel & Spur/Helical gear rotational joint concept	C12
Figure 91: Angular swivel joint concept.....	C13
Figure 92: Drive shaft concept	C14
Figure 93: Inner tube guided rotational joint concept.....	C14
Figure 94: PIC18F2550 (Master) Schematic	E3
Figure 95: PIC18F2431 (Slave) Schematic	E3
Figure 96: L6225 H-Bridge Schematic	E3
Figure 97: Digital PCB Top Layout (Not to scale).....	E4
Figure 98: Digital PCB Bottom Layout (Not to scale)	E4
Figure 99: Power PCB Top Layout (Not to scale)	E5
Figure 100: Power PCB Bottom Layout (Not to scale)	E5
Figure 101: Close ups of Digital PCB (left) and Power PCB (right)	E6

List of Tables

Table 1: MIRS vs. Conventional MIS in laparoscopy (adapted from Lanfranco <i>et al.</i> , 2004)	4
Table 2: Comparison of different actuating technologies (Kode and Cavusoglu, 2007) ..	18
Table 3: Design requirements for the manipulator	20
Table 4: Manipulator's major dimensions	25
Table 5: Recommended Values for the Components in Figure 45	42
Table 6: Mean and standard deviation for short arm.....	49
Table 7: Mean and standard deviation for long arm	50
Table 8: Variables of gripper motion mechanism	54
Table 9: Repeatability Test Experimental Data	F1
Table 10: Strength Test Experimental Data	F2

Chapter 1: Introduction

Recent developments in the field of materials, actuation and mechatronics have opened a new and promising frontier in the development of minimal invasive surgery (MIS) instrumentation. Existing conventional instrumentation limits MIS to less complicated procedures due to their imposed visual and dextrous constraints. Robotics therefore attempt to eliminate these constraints and advance MIS even further.

In this thesis, a new seven degree of freedom (DOF) manipulator is designed for minimal invasive surgery. The manipulator is aimed to form part of a new inexpensive robotic surgical system to focus on simple procedures done frequently at all medical centres.

1. Background

In 1921, when the Czech playwright Karel Capek coined the term “robot” in his play *Rossum’s Universal Robots*, robots became more popular in imagination and in reality. The word robot is derived from the Czech word *robot*, meaning forced labour, and has evolved in meaning “dumb” machines performing repetitive tasks, to highly intelligent anthropomorphic robots of popular culture (Lanfranco *et al.*, 2004). Today robots are still relatively dumb but are useful for performing highly specific, highly precise and possibly even dangerous tasks repetitively. However, robots have been slow to enter the field of medicine.

Only in 1985 did the first robot, the Puma 560, help to perform a CT-guided stereotactic brain surgery, which led to the development of the PROBOT and ROBODOC (Lanfranco *et al.*, 2004). ROBODOC received FDA (Food and Drug Administration) approval in the late 1980s for machining the femur with greater precision during hip replacements. Further advancements in surgical robotics led to the FDA approving the AESOP endoscopic system, the ZEUS surgical system for minimal invasive surgical procedures and also the technologically advanced da Vinci surgical system from Intuitive Surgical Inc. In 2003 Intuitive Surgical Inc. merged with Computer Motion Inc. after which the ZEUS system was discontinued. Today, the da Vinci is the only complete minimal invasive robotic surgical (MIRS) system commercially available and has sold over 500 systems (Hockstein *et al.*, 2007), mostly to academic institutes across the world.

2. Minimal Invasive Surgery

In the late 1980s and early 1990s surgical procedures were revolutionized through the introduction of minimally invasive techniques (see Figure 1). MIS is a technique whereby surgeons use specially designed instruments to operate through small incisions made through the patient’s skin. The surgical site is usually viewed by means of a miniature CCD video camera or endoscope placed in one of the incisions and displayed on a CRT monitor. Benefits in using MIS techniques rather than open surgery methods include a quicker recovery time, reduced discomfort to the patient and reduced incidence of post-

surgical complications, such as adhesions. Reduced hospitalization time and therefore procedural costs are also major benefits, as well as less time away from productive work for the patient.

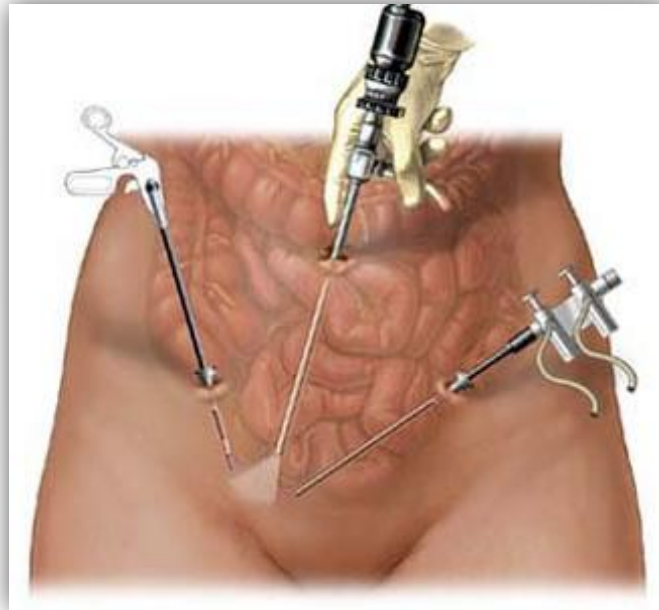


Figure 1: Illustration of pelvic laparoscopy (NJPCPU, 2006)

Several surgical specialties have benefited greatly from the development of techniques in minimal invasive surgery over the past decade. One such example is laparoscopic cholecystectomy, which was first performed by Prof. Erich Mühe on September 12, 1985 (Reynolds, 2001). A cholecystectomy is the surgical removal of the gallbladder. The gallbladder is a hollow, muscular pear-shaped organ situated as shown in Figure 2. The function of the gallbladder includes the storage of bile before being released into the duodenum, as well as bile modification. When the bile salts become too concentrated, gallstones may form which can cause a variety of clinical problems. Gallstones can sometimes be dissolved using oral ursodeoxycholic acid, but may recur once treatment is stopped. A cholecystectomy has a higher chance of eliminating the recurrence of gallstones.

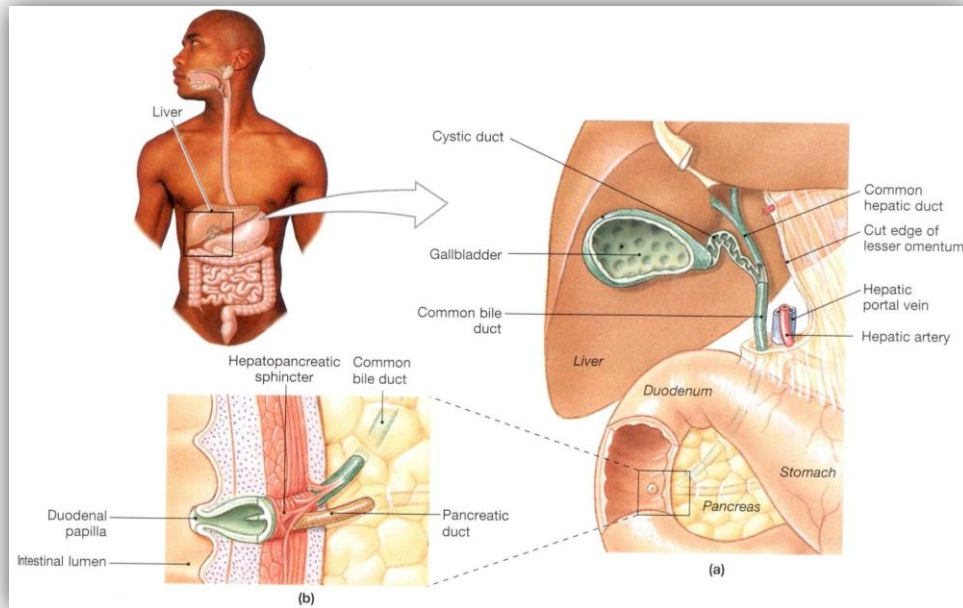


Figure 2: Human anatomy and physiology of the gallbladder (Martini and Bartholomew, 2007)

In laparoscopic cholecystectomy the surgeon operates through three to five small incisions (Howe and Matsuoka, 1999). Long rigid instruments, such as the one shown in Figure 3, are passed through trocars and manipulated by sliding them in and out, rotating them about their long axis and pivoted about their centres of rotation, defined roughly by the incision site in the abdomen wall to grip and cut tissue inside the patient. A video endoscope manipulated by an assistant provides a view of the internal operating space. During the procedure, the patient's abdomen is insufflated with CO₂ to increase the operating cavity and allow the surgeon to operate more easily.



Figure 3: Conventional rigid MIS instrument (Mediflex, 2006)

Minimal invasive surgery, however, has its drawbacks in that the conventional instruments have only five DOF through their entry port, preventing arbitrary orientation of the instrument tip. MIS is also technically more difficult, because the tool tip moves in the opposite direction to the surgeons' movements due to the pivoting of the tool around the entry point. This phenomenon is known as the fulcrum effect. In addition, the image displayed on the CRT monitor is a 2-dimensional image and therefore deprives the surgeon from depth perception and hand-eye coordination, making the procedure more difficult to perform due to the surgeon having to

continuously correlate hand motions to the end effectors' motions. Despite these dextrous and visual constraints related to conventional MIS equipment, robotics in surgery attempt to alleviate these constraints and further advance MIS, making robotics a promising field for innovation to improve the capabilities of surgeons in minimal invasive surgery.

3. Minimal Invasive Robotic Surgery

Minimal invasive robotic surgery (MIRS) systems use state of the art technologies to directly address the drawbacks of conventional MIS instrumentation. Improvements in MIS due to MIRS developments include 3-dimensional visualization, increased manoeuvrability, precision and in some cases smaller incisions. A complete list which compares conventional MIS instrumentation to robotic instrumentation in laparoscopy is given in Table 1.

Table 1: MIRS vs. Conventional MIS in laparoscopy (adapted from Lanfranco *et al.*, 2004)

	Conventional Laparoscopic Surgery	Robot-Assisted Surgery
Advantages	Well-developed technology Affordable and ubiquitous Proven efficacy	3D Visualization Improved dexterity Seven degrees of freedom Elimination of the fulcrum effect Elimination of physiological tremors Ability to scale motions Tele-surgery Ergonomic position
Disadvantages	Loss of touch sensation Loss of 3D visualization Comprised dexterity Limited degrees of freedom The fulcrum effect Amplification of physiological tremors	Absence of touch sensation High start-up costs High maintenance costs May require additional staff Unproven benefit

One advantage listed in Table 1 under Robot-assisted surgery is tele-surgery. This implies that procedures can be performed over a distance, and was proved in 2001 when the first demonstration of a trans-Atlantic tele-surgery was reported when surgeons in New York operated on a 68 year old woman in Strasbourg, France, and remote controlled robots were used to perform a laparoscopic cholecystectomy (Satava, 2006). Also, the first unmanned robotic surgery took place in May 2006 in Italy (Intuitive Surgical Inc., 2007).

Commercially available MIRS systems, such as the advanced da Vinci surgical system (from Intuitive Surgical Inc.) shown in Figure 4, generally have a surgeon's console and a patient-side cart with interactive robotic arms (also known as a master-slave system). These systems attempt to improve surgical dexterity and visual feedback through features including articulating end effectors, tremor filtering, motion reversal correction, stereoscopic vision and motion scaling (Lehman *et al.*, 2007). However, existing robotic

master-slave systems are not without shortcomings. The main factor preventing more widespread adoption of such systems is their prohibitive cost (Sim *et al.*, 2006).



Figure 4: da Vinci from Intuitive Surgical Inc. (Intuitive Surgicals Inc., 2007)

4. Need for an inexpensive MIRS System

Currently available MIRS systems, such as the da Vinci (costing an estimated USD\$1 million), are hugely expensive and have high maintenance costs to keep the system in a continuous working condition. Furthermore, employment of additional staff to maintain the system and possibly even the development of a new and bigger operating room to accommodate the sizable system is required in some instances (Sim *et al.*, 2006). For this reason alone, most medical centres discard the consideration of such a system and continue using conventional instrumentation, accepting their related drawbacks.

To address this shortcoming, an inexpensive MIRS system should be designed and developed to cater for those simple procedures done more frequently, leaving the complex and precise procedures to the more sophisticated MIRS systems. This would allow most medical centres to offer a MIS facility in which there are reduced risks to the patient and the surgeon at a lower cost.

From a business venture point of view; there are approximately 143 private hospitals performing laparoscopic operations in South Africa alone. If each one of these were to purchase an MIRS system for a more conservative price of R1 million each, the total would amount to R143 million. Eventually, if the system enters the international market the profits would increase tenfold, making the development of such a system an extremely attractive business endeavour.

5. Objectives

The objective of this thesis is to develop an inexpensive primary slave manipulator for a MIRS system. The manipulator should have seven DOF to increase the surgeon's manoeuvrability as well as to reduce the manipulator's diameter to benefit from the minimal invasive surgery technique's advantages. Control electronics for the manipulator should also be developed to control the manipulator. It must be noted, however, that the design of the manipulator is mainly focused on the multi-DOF wrist of the manipulator. The implementation of the control electronics is only to prove the manipulator's functionality and to perform the required experiments. Sterilizability is also not considered at this stage in the design.

To determine the manipulator's feasibility, a repeatability test and a strength test must be done. These should show the functional capability of the manipulator, based on the literature found and the design requirements generated.

Although the relevant standards were perused and taken into account to some extent during the development of the manipulator, the complete certification of the system to the relevant medical standards were also beyond the scope of this work.

6. Thesis Layout

Chapter 2 presents a number of surgical robotic systems at various research institutes as well as miniature manipulator designs for minimal invasive surgery. Chapter 3 then discusses the design of a new manipulator for minimal invasive surgery adopting a tendon mechanism actuation method using DC motors. Chapter 4 goes on to discuss the electronics to drive and control the motors, and Chapter 5 explains the repeatability and strength of the manipulator. Finally, in Chapter 6, a summary of the work is given with a few recommendations for future work.

Chapter 2: Robotic Systems and Manipulators for Laparoscopy

The ability of surgeons to work through a few small incisions presents a number of benefits to the patient as well as the surgeon. However, the surgeon's limiting five DOF (see Figure 5) of conventional MIS instrumentation is the principal disadvantage in laparoscopic procedures (Ruurda, 2003). Moreover, the fulcrum effect requires the surgeons to perform difficult mental transformations between visual and motor coordinate frames (Howe and Matsuoka, 1999).

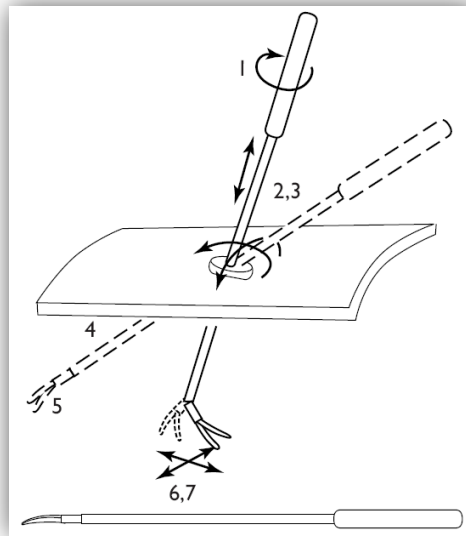


Figure 5: DOF of laparoscopic instrumentation (Ruurda, 2003)

Robotics in surgery therefore attempts to alleviate these drawbacks and further advance MIS by giving the surgeon more manoeuvrability within the operating cavity as well as eliminating the fulcrum effect. Hence, this chapter presents robotic surgical systems at research institutes and those which are commercially available. Robotic manipulator designs and different actuating technologies are also discussed.

1. Minimal Invasive Surgical Systems

Robotics in surgery began with the Puma 560, a robot used in 1985 by Kwoh *et al.* (1988) to perform CT-guided stereotactic brain surgeries with improved absolute positioning accuracy. Three years later, Davies *et al.* (2000) used the Puma 560 for a transurethral resection of the prostate. This eventually led to the development of PROBOT, a robot specifically intended for transurethral resection procedures. While PROBOT was still being developed, ROBODOC was being developed by Integrated Surgical Supplies Ltd., of Sacramento, California. The ROBODOC robotic system was designed to machine the

femur with greater precision in hip replacement surgeries and became the first surgical robot to receive FDA approval in the late 1980's.

1.1 MIRS Systems at Research Institutes

Over the last two decades, many minimal invasive surgical robots and robot enhancements were researched and developed, among these were the UCB/USCF RTW, HISAR, ARTEMIS, and the KaLAR. These will be briefly discussed in this section.

1.1.1 UCB/USCF RTW

In a joint venture between the University of California, Berkley (UCB) and the University of California, San Francisco (UCSF), a robotic telesurgical workstation (RTW) was developed (Cavusoglu *et al.*, 2001). The second generation RTW is shown in Figure 6 on the left with its milirobotic wrist on the right.

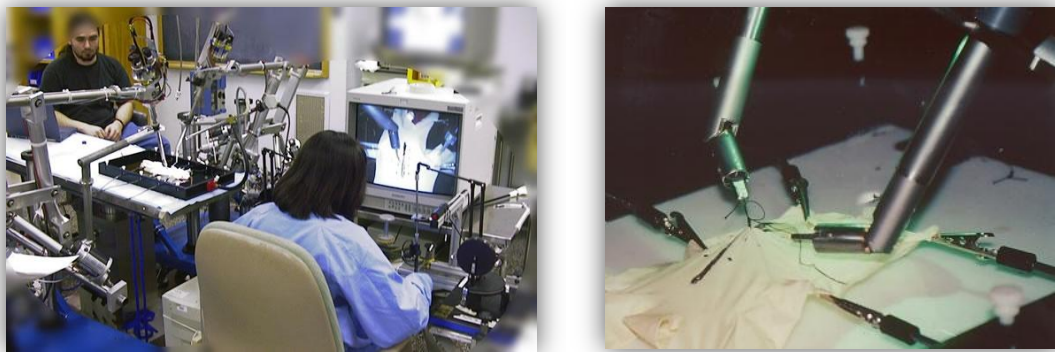


Figure 6: UCB/USCF robotic telesurgical workstation and milirobotic wrist (Cavusoglu *et al.*, 2001)

The slave manipulator consists of the primary slave manipulator or gross positioning stage (responsible for the positioning of the milirobot) and the milirobot itself (primary slave manipulator) which performs the operation inside the patient. Figure 6 (left) also shows the master manipulator used to control the slave manipulators.

The milirobot has a two DOF wrist, with yaw and roll axis rotations, and a gripper. The tendon actuated wrist is 15 mm in diameter and has a wrist-to-gripper length of 50 mm. The tendons are jointly actuated by three DC servo motors located on the four-bar linkage primary slave manipulator. This gross stage is responsible for actuating the primary slave manipulator through the same four DOF as that of a conventional laparoscopic instrument.

1.1.2 HISAR

In 1995 researchers at IBM Research and Johns Hopkins Medical Center developed a seven DOF ceiling-mounted surgical robot for laparoscopic camera navigation called HISAR (Funda *et al.*, 1995). The HISAR's first three DOF was actuated, the next two were passive, and the last two rolled and zoomed the camera. The ceiling-mounted concept

also helped to keep the accessory rails off the surgical table as well as the floor space around the table clear. The HISAR was, however, never commercialized.

1.1.3 ARTEMIS

The Advanced Robot and Telem manipulator Systems for Minimal Invasive Surgery (ARTEMIS) was one of the first and most advanced MIRS systems in the early 1990's. It was developed in Germany at the "Forschungszentrum Karlsruhe". A prototype was built, shown in Figures 6 and 7, and proved to be very effective. However, funding for the project was not renewed which discontinued the research.



Figure 7: ARTEMIS minimal invasive robotic system (Ortmaier, 2003)

The controls for the ARTEMIS (shown in Figure 7 on the right) system's manipulators consisted of various input devices: two haptic manipulators for controlling the robot manipulators, voice recognition for the endoscope, and foot pedals. The slave manipulators (on the left in Figure 7) consisted of three manipulators: two manipulators for holding and manipulating surgical instruments, while the other holds the endoscope. The major drawback of the ARTEMIS system was that it did not have force feedback at the controller side and there were not any instruments with additional degrees of freedom at the robot manipulator side (Schur *et al.*, 2000).

1.1.4 KaLAR

Lee *et al.* (2003) developed a laparoscopic assistant robot termed the KIAS T Laparoscopic Assistant Robot (KaLAR) at Korea Advanced Institute of Science and Technology (KAIST). However, as it is mainly designed for cholecystectomy, Shin *et al.* (2006) presented a modified version of the KaLAR for application to general surgery. The system shown in Figure 8 consists of a passive base to hold the robotic system, a two DOF external manipulator and a bending laparoscope. The bending laparoscope provides one DOF linear motion and two DOF bending motion. The external manipulator provides external motion about the trocars insertion by means of the robotic system.

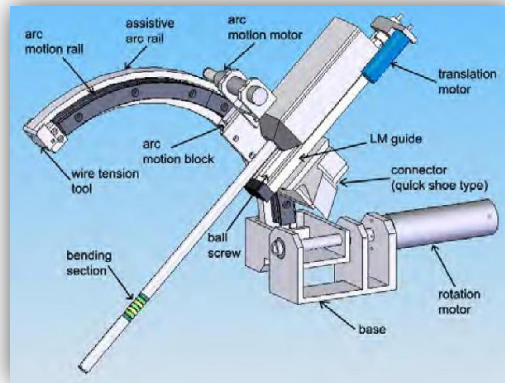


Figure 8: Schematic of the revised KaLAR system (Sim *et al.*, 2006)

1.2 Commercially Developed MIRS Systems

In addition to the robotic systems discussed above, several other systems have been commercially developed and approved by the FDA. These include the AESOP system (from Computer Motion Inc.), a voice-activated robotic controlled laparoscope, and the comprehensive MIRS systems, the da Vinci (from Intuitive Surgical Inc.) and Zeus (from Computer Motion Inc.). In June 2003, Computer Motion was merged with Intuitive Surgical, discontinuing the ZEUS robotic system and making AESOP a part of Intuitive Surgical Inc.'s product line.

1.2.1 AESOP

In Figure 9 the Automated Endoscopic System for Optimal Positioning (AESOP), a robotic manipulator for endoscope control, received FDA approval in 1994 and was the first actively marketed tele-robotic manipulator system (Hockstein *et al.*, 2007). The manipulator holds the endoscopic camera and is manipulated through commands given by the surgeon. The first system, the AESOP 1000, was controlled by the surgeon using foot pedals but was changed to voice control in the AESOP 2000 to make the system more user-friendly, especially to new users. The third revision followed, the AESOP 3000, which allowed seven DOF through four motorized joints, two passive joints and one manual DOF. The latest revision is the AESOP HR from Intuitive Surgical Inc. after its merger with Computer Motion Inc. in 2003. The AESOP HR's advancements are directed towards site movement, position memory, picture stability while allowing minor adjustments, and the presence of slip clutches to limit the amount of force used (Sim *et al.*, 2006).



Figure 9: The AESOP endoscopic system (Trueforce, 2004; Sim *et al.*, 2006)

1.2.2 ZEUS

The Zeus MIRS system from Computer Motion Inc. was based on the AESOP platform to provide a complete MIRS system. The system shown in Figure 10 consisted of a surgeon's console, two robotic manipulators fixed to the operating table and an AESOP endoscopic manipulator. The surgeon could view a 3D image of the surgical site on the monitor in the surgeon's console through polarized glasses while manipulating the integrated arms as needed. The robotic manipulators that are fixed to the operating table had reusable 3.5 to 5 mm instruments, having the six DOF MicroWrist articulating tip. The robotic manipulators were controlled through the manipulation of the integrated arms in the surgeon's console while the endoscope was controlled through voice commands. The Zeus MIRS system received FDA approval in September 2002. In 2003 Computer Motion Inc. merged with Intuitive Surgical Inc. after which the Zeus was discontinued.

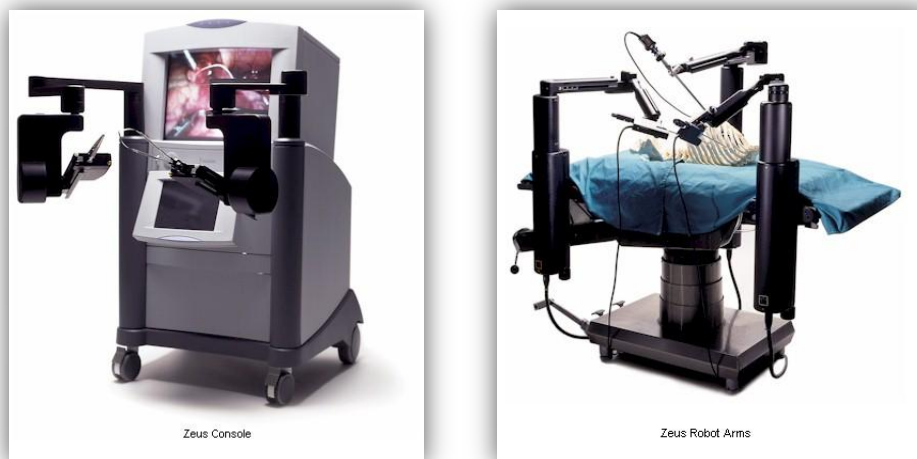


Figure 10: ZEUS Surgical Console (left) and Operating Manipulators (right) (Trueforce, 2004)

1.2.3 da Vinci

The da Vinci MIRS system from Intuitive Surgical Inc. was commercially recognised in 1997 when it performed a laparoscopic cholecystectomy in Belgium (Ballantyne, 2002). The surgical system, shown in Figure 11, consists of a surgeon's console and a patient side cart. The surgeon's console allows the surgeon a three dimensional 0° or 30° view of the surgical site with a high resolution 10 mm endoscope (with two three-chip charge coupled device - CCD cameras) capable of 10x to 15x magnification, giving the surgeon better depth perception (Lobontiu and Loisanca, 2007). The ergonomic console design also integrates control grips which allow for comfortable arm, wrist and pincer movements (Hockstein *et al.*, 2007) to control the motor controlled robotic manipulators on the patient side cart. The surgeon's movements are tracked at a rate of 1300 Hz to seamlessly manipulate the EndoWrist with scaled motion and tremor filtering – translating the surgeon's large movements into fine and steady movements (Hockstein *et al.*, 2007).

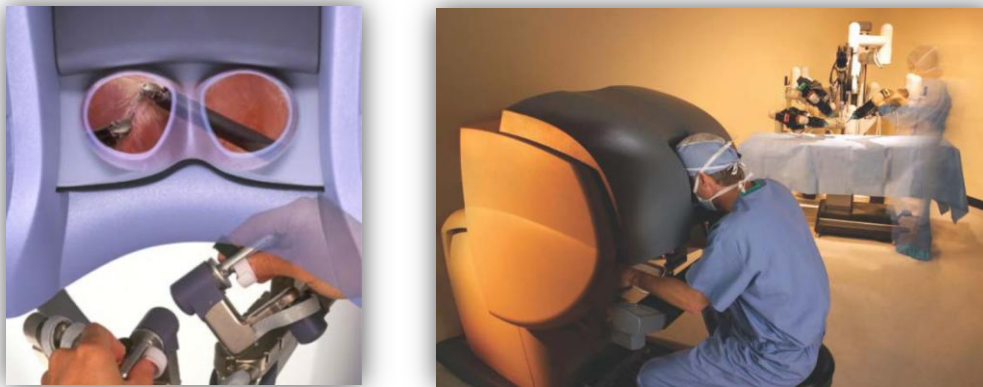


Figure 11: da Vinci's MIRS system (Intuitive Surgical Inc., 2007)

The interchangeable instruments attached to the patient side cart have additional cable-driven articulating joints near the tip (EndoWrist), enabling four more degrees of freedom (internal pitch, internal yaw, rotation and grip) for easier suturing and dissection during surgery (Sim *et al.*, 2006). The instruments, shown in Figure 12, are available in 5 to 8 mm diameters and are under direct control of the surgeon through the surgeon's console. The motion scaling is set to 3:1 (allowing instrument to move 1 mm to every 3 mm the surgeon moves) and the tremor filtering is activated at 6 Hz. A grip force of 1.0 Newton is also programmed into the system (Lobontiu and Loisanca, 2007).



Figure 12: da Vinci's secondary slave manipulator (left) and the EndoWrist instruments (right) (Intuitive Surgical Inc., 2007)

2. Manipulator Designs for MIRS Systems

The challenge in designing a robotic manipulator is to design a manipulator with increased dexterity (e.g. six and seven DOF shown in Figure 5) with intuitive control, while still able to be inserted through small incisions (Howe and Matsuoka, 1999). A number of these robotic manipulators have been developed in research centres across the world and are discussed in the subsequent sections.

2.1 EndoWrist

The da Vinci's advanced EndoWrist, designed by Morley and Wallace, and patented in 1994, is shown in Figure 13. The manipulator is mostly driven by a pulley and cable mechanism to rotate and actuate the wrist. The wrist has three DOF, employing a roll-pitch-roll configuration. The elongated shaft can rotate to roll around its centre axis and the distal part of the wrist, of which the centre of rotation axis is perpendicular to the elongated shaft, has a maximum pitch of approximately 135°.

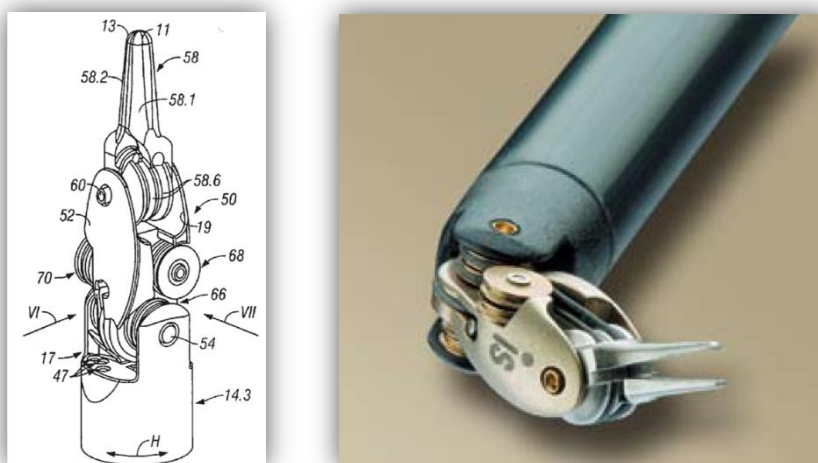


Figure 13: da Vinci's EndoWrist (Morley and Wallace, 1994; Intuitive Surgical Inc., 2007)

The gripper or end effector is pivotally mounted onto the distal wrist member to roll around the wrist axis of the wrist member. The ability to operate the end effector at about 90° pitch and to bend back the end effector gives the wrist mechanism more manoeuvrability and is therefore more adaptable to accessing hard to reach locations, particularly with small entry points (Morley and Wallace, 1994).

2.2 Passive mechanical manipulator instrument tip

Jaspers *et al.* (2004) designed a mechanical manipulator for minimal invasive surgery. A detailed view of the 8 mm instrument tip or end effector is shown in Figure 14 (left) with the prototype also shown on the right. The end effector actuator design is based on a tendon mechanism in which the two gripper jaws are pushed open (approximately 60°) by means of a torsion spring (S) shown in the detailed view in Figure 14. The two gripper jaws are actuated separately using cables (one per jaw) to close the jaws (sixth DOF) or simultaneously deflect them (seventh DOF) about their axis of rotation (ag6, 7) to a maximum of 90° in both directions. The fifth DOF, shown also in the detailed view, is activated through a steel rod (5r) together with a linkage or lever (l), which deflects the tip by pushing the rod up or down. DOF five can be actuated around ag5 to an estimated maximum of 90° in both directions (Jaspers, 2005).

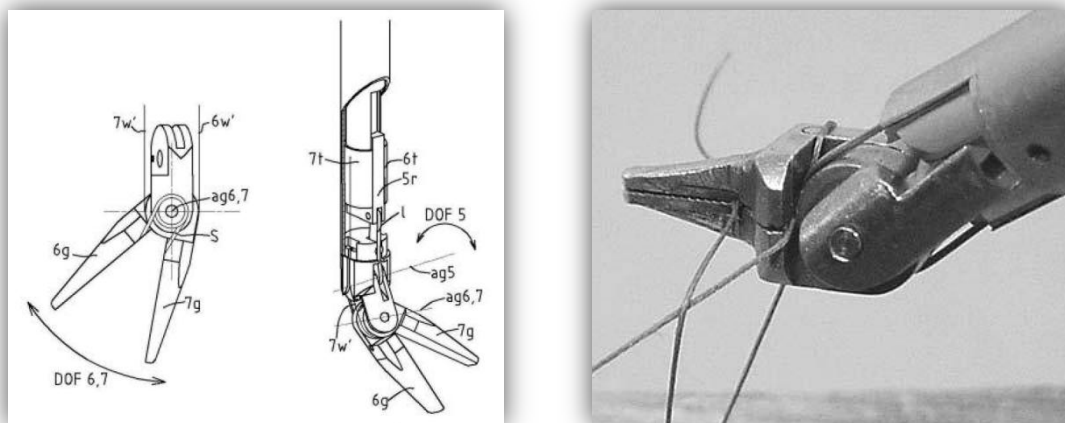


Figure 14: Passive mechanical manipulator instrument tip (Jaspers, 2005; Diks *et al.*, 2007)

2.3 Sensorized and actuated instruments

The four DOF articulate joint developed by Seinbold *et al.* (2005) shown in Figure 15, allowed the gripper to twist about its longitudinal axis (due to its intersecting axes) without pivoting the instrument shaft about the point of intersection. The joint has a restricted movement of about 40° in both directions. The pre-tensioned VectranTM cables are such that they are always tangent to the driving pulley and were configured in such a manner that the two loops were always the same length. This allowed for only two motors to fully actuate the joint. The design parameters were 20 N on the tool tip and a gripping force of 20 N. The gripper was manipulated by means of a cable and

opposing spring. A 70 N needle-holding force was calculated with a maximum actuation driving force of 100 N. The cables were pre-tensioned at 200 N (Seibold *et al.*, 2005).

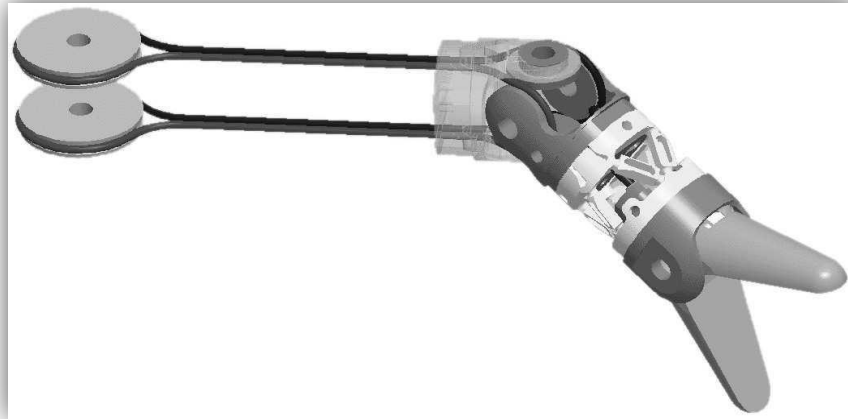


Figure 15: Articulate joint (Seibold *et al.*, 2005)

2.4 Multi-Slider Linkage Manipulator

A handheld forceps manipulator, shown in Figure 16, for endoscopic surgery was proposed using the basic concept of two bending joints joined by a short frame and pin joints which can be manipulated by a multi-slider linkage mechanism. This mechanism serves as a drive and restraint by pulling and pushing the linkages respectively, resulting in a movement restriction of roughly 90° in both directions, 45° for each pin joint. This mechanism allowed for one DOF, and therefore a second mechanism was added to yield a two DOF manipulator. The forceps were used in an in-vivo experiment and was found to have a holding power of 0.55 kg force, showing high repeatability (Yamashita *et al.*, 2003). This manipulator was improved by reducing the number of components and miniaturizing the manipulator even further to 3.5 mm (Yamashita *et al.*, 2006).



Figure 16: Multi-DOF end-effector (Yamashita *et al.*, 2003)

2.5 Miniature worm gear manipulator

Figure 17 shows a single DOF manipulator design by Peirs *et al.* (2000). The manipulator is 8.5 mm in diameter and approximately 20 mm long. It can pivot a maximum of 40° in both directions of rotation. The joint is driven by a locally situated miniature gearmotor

through a worm gear reduction. The gearmotor's measured output torque is estimated at 0.02 mN.m while the worm gear's reduction gear ratio of 1:28 which further increases the torque of the joint. The maximal rotational speed of the joint is therefore estimated to be 260°/s.

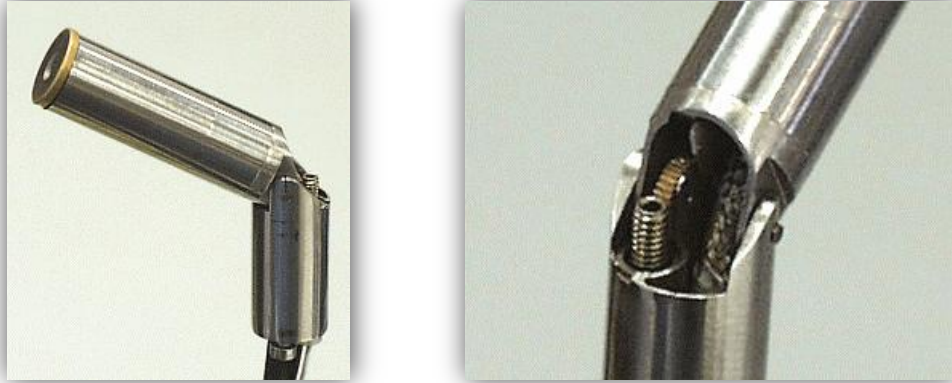


Figure 17: Miniature worm gear manipulator prototype (Peirs *et al.*, 2000)

2.6 Miniature hydraulic parallel manipulator

Peirs *et al.* (1999) presented the design of a miniature hydraulic manipulator shown in Figure 18. The design of the manipulator is based on a three DOF Stewart platform. It has a 12 mm outer diameter and a 30 mm length. The platform is manipulated by three hydraulic pistons, each placed inside a 3 mm inner diameter cylinder and connected to the upper platform through ball joints. The pistons are extended outwards with a 10 bar pressure to generate a 7 N force on each piston. The return force is generated using springs and an elastic membrane covering the whole system. A six DOF manipulator system can be created by placing two of these Stewart platforms in series.

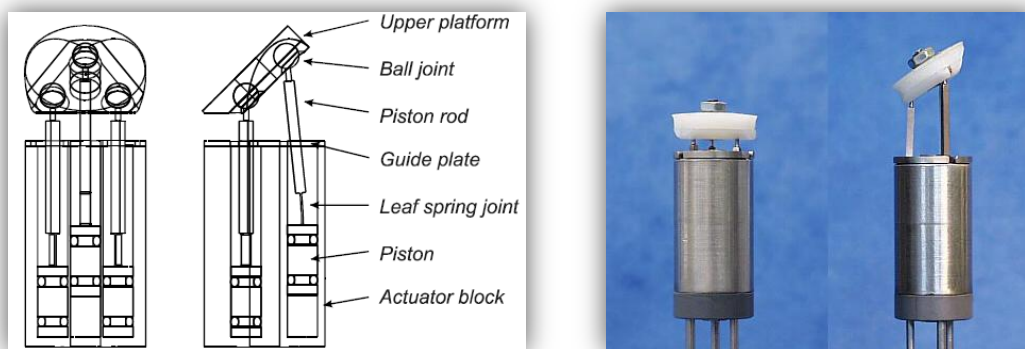


Figure 18: Miniature hydraulic parallel manipulator design (Peirs *et al.*, 1999)

2.7 Novel hybrid actuator design

Kode *et al.* (2007) proposed a local actuator system with a novel hybrid actuation design. The goal was to design a millimeter scale (5.14 mm in diameter and approximately 60 mm in length) local actuator for laparoscopic needle driver jaws and

thereby enabling the design of a manipulator with increased DOF. The local actuator system consists of two stages, namely a DC micromotor stage and an SMA microwire stage. The two stages are connected in series to enable long strokes with smaller forces (in the order of 1 N) and shorter strokes with substantially larger forces (about 15 N for gripping force of 5.5 N) (Kode and Cavusoglu, 2007). The DC micromotor stage is used for the long strokes to open and close the gripper jaws while the SMA microwire stage allows for larger forces for gripping and holding the needle. Both the DC micromotor stage and SMA microwire stage is used for closing the gripper jaws and hold the suture needle while only the DC micromotor was used to open the gripper jaws together with a compression spring. Figure 19 shows the prototype actuator design as well as a transparent CAD model clearly showing the SMA microwires and embedded compression spring.

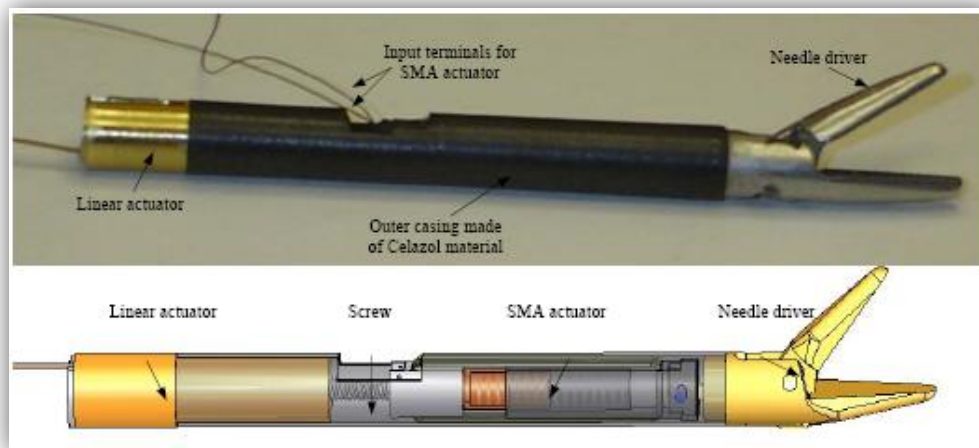


Figure 19: Assembly of hybrid actuator needle driver (Kode and Cavusoglu, 2007)

3. Actuating Technologies

Table 2 shows a number of different actuator technologies which were considered to actuate the manipulator. From this table it can be seen that the amount of work per unit volume, or work density, is high for SMA and Piezoelectric actuators. However, the actuator efficiency for SMA actuators is very low and large power is required. SMA actuators also have low speeds and small stroke lengths, whereas piezoelectric actuators have higher speeds but also short stroke lengths. A hybrid actuator using SMA wires and DC motors were used by Kode and Cavusoglu (2007).

Table 2: Comparison of different actuating technologies (Kode and Cavusoglu, 2007)

Actuator type	Strain (Max, %)	Pressure (Max, MPa)	Efficiency (Max, %)	Relative Speed (Full Cycle)	Power Density
Electromagnetic (Voice Coil)	50	0.10	>90	Fast	High
Piezoelectric					
Ceramic (PZT)	0.2	110	>90	Fast	High
Single Crystal (PZN-PT)	1.7	131	>90	Fast	
Polymer (PVDF)	0.1	4.8	n/a	Fast	
Electrostatic Devices (Integrated force array)	50	0.03	>90	Fast	Low
Shape Memory Polymer	100	4	<10	Slow	Medium
Thermal (expansion)	1	78	<10	Slow	Medium
Magnetostrictive (Terfenol- D. Etrema Products)	0.2	70	60	Fast	Very High

Although electromagnetic actuators are shown in Table 2 to have low work density, or low output torques, advances in miniaturization and the production of miniature DC motors with small gearheads makes the actuating technology feasible for the use in miniature manipulators. These actuators work with high efficiency giving large stroke lengths at high speeds (Gilbertson and Busch, 1996; Smith and Seugling, 2006). Also, by placing the motors outside the manipulator (or human body) and driving the manipulator wrist using cables, allows for high gripping forces while still keeping the manipulator's diameter small. This was the case for da Vinci's EndoWrist and Zeus' MicroWrist.

Chapter 3: Manipulator Design

This thesis' main objective is to design and develop an inexpensive robotic manipulator, or otherwise known as a primary slave manipulator (PSM), for laparoscopic procedures. In this chapter the design of a new seven DOF PSM is presented. The revolute joint and rotational joint as well as the gripper joint allow for a three DOF wrist while the manipulator is also able to rotate about its elongated axis, making a fourth DOF possible. The additional three DOF are made possible by sliding the instrument in and out, and pivoting it about its centre of rotation defined roughly by the point of insertion into the abdomen. This is accomplished through the use of an additional robotic manipulator, or secondary slave manipulator (SSM). Figure 20 shows a SSM holding the PSM.

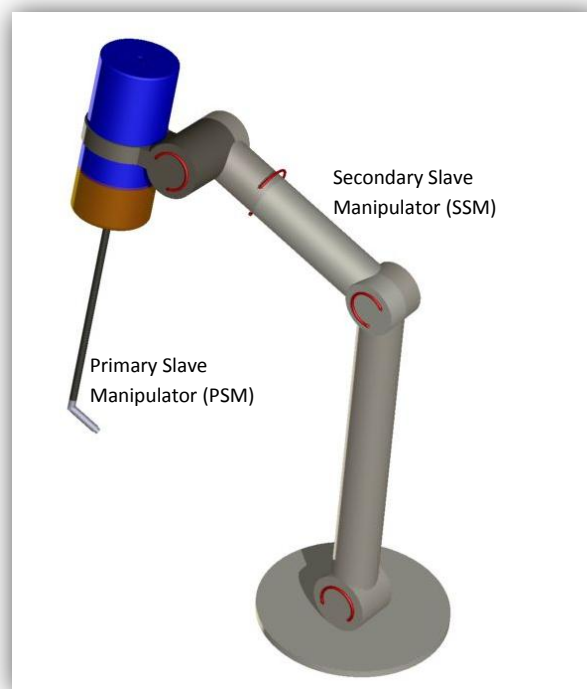


Figure 20: Secondary slave manipulator concept

1. System Analysis

Conventional MIS instrumentation has only five DOF, therefore if a seven DOF manipulator were designed, essentially increasing the instrument's manoeuvrability, it would allow the surgeon to operate with more dexterity. However, a more challenging objective is to design such a manipulator while keeping or reducing the instrument's diameter to still benefit from minimal invasive surgery's advantages (Kode *et al.*, 2005). To reach this goal, a number of design objectives, considerations and requirements were generated.

1.1 Design Objectives\Considerations

The design objective and/or considerations for the primary slave manipulator are:

- To design and develop a seven DOF manipulator, essentially increasing the instrument's manoeuvrability and as a result allow the surgeon to operate with more dexterity. It must be made clear, however, that the PSM itself is capable of only four DOF. The other three DOF are made possible by attaching the PSM to a SSM, which allows the PSM to slide in and out and pivot about the incision point. The design and development of the SSM was not part of this project.
- To reduce the diameter of the instrument to benefit from the minimal invasive surgery technique's advantages.
- Design a manipulator for a system which allows the surgeon to take up a more ergonomic position over the duration of the procedure. The manipulator should be designed such that it is easy to learn how to manoeuvre it, avoiding the surgeon having to make technically difficult translations while operating.
- Design a manipulator which is inexpensive compared to other MIRS systems and is within budget of regular public or private hospitals.

1.2 Design Requirements

The goal is to design a seven DOF manipulator (of which three are made possible by another manipulator) which can be used for minimal invasive surgery procedures. The manipulator should be 10 mm in diameter so that it can fit through a standard 11 mm trocar. The manipulator should be able to rotate 360° about its elongated axis and the wrist able to deflect 55° to allow for maximum accessibility inside the operating cavity. The tool tip should also rotate a minimum of 90° about the wrist axis to allow for gripping at different orientations.

In addition, from the literature (Jaspers *et al.*, 2004; de Visser *et al.*, 2002), a gripping force of at least 5 N is needed for grasping the needle during suturing or pulling and stretching tissue during an MIS procedure. From Greeff (2007) it was decided that a 10 N opposing tip force is also needed to perform most of the necessary tasks in a typical MIS procedure. The design requirements for the manipulator are summarized in Table 3.

Table 3: Design requirements for the manipulator

Parameter	Value
Overall instrument diameter	< 10mm
Rotation about instrument axis	360°
Wrist deflection	> 55°
Tip Rotation about wrist axis	> 90°
Gripper opening angle	> 60°
Gripping Force	> 5N
Opposing tip Force	> 10N

2. Manipulator Concept Design

The primary slave manipulator's wrist was subcategorized into a revolute joint, a rotation joint and a gripper joint. A number of actuation concepts were generated for these joints and are given in Appendix C. From these, a tendon or cable actuating

mechanism was thought best to allow for high gripping forces while still maintaining a small tool size. This is thought to be mainly due to the power transmission mechanisms being placed outside the human body, which was the case for da Vinci's EndoWrist and Zeus's MicroWrist (Kode and Cavusoglu, 2007). Therefore it was thought that if using the "Pulley (One turn)" revolute joint configuration and the "Three-link joint" cable attachment method, a simple and small revolute joint can be developed. For the rotation joint, a modified version of the "Cable rotation mechanism" can be implemented.

The proposed concept therefore consists of cables attached to the different joints and when pulled, will actuate the joint as required. The cables are actuated using reels. These reels will be turned by motors to wind up the cable onto them, therefore pulling the cable and ultimately actuating the joint. Each joint will be actuated in one direction using a cable and then opposed by another cable or a passive component, such as a spring, actuating the joint in the opposite direction.

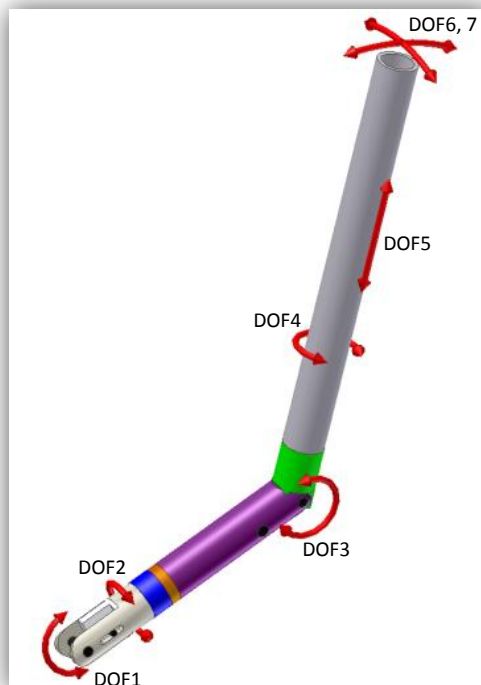


Figure 21: Seven DOF Primary slave manipulator showing a multi-DOF wrist

The tendon mechanism would essentially actuate the three DOF wrist. The fourth DOF of the PSM will be made possible through the use of a spur gear and internal spur gear. These gears would therefore roll the long arm about its own axis, also rotating the actuating mechanism for the wrist along with the long arm to prevent the wrist's cables from intertwining. Figure 21 shows the degrees of freedom associated with the PSM (DOF 1, 2, 3, and 4) as well as those enabled by the SSM (DOF 5, 6 and 7).

3. Design of the first prototypes

The above-mentioned concept was realized in the prototypes manufactured in the Mechanical Workshop at the Faculty of Engineering, University of Stellenbosch. During the development of the first PSM prototypes, the main objective was to verify the functionality of both the revolute and rotation joints of the wrist. The revolute joint worked suitably in the first prototype whereas the rotation joint proved to be a problem. Consequently two more iterations were done before the fourth and successful prototype was developed. The first two iterations' CAD models are shown in Figure 22.

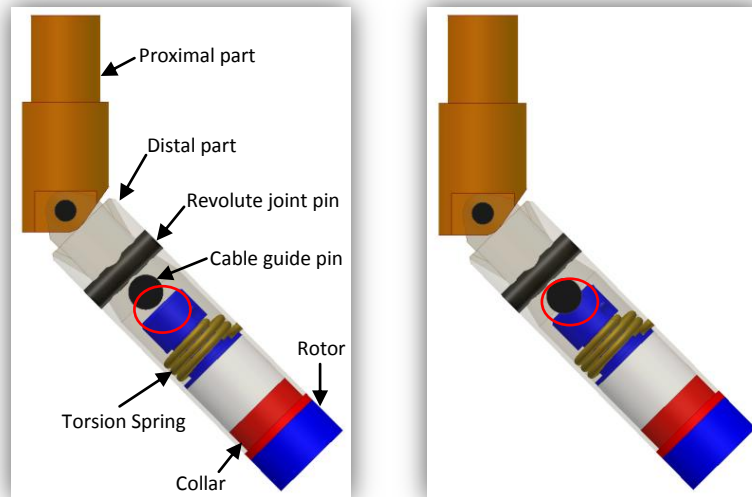


Figure 22: First and second iterations of first generation prototypes

In the first and second iterations, the wrist prototypes were designed as shown in Figure 22 left and right, respectively. Note the difference between iterations one and two as indicated by the red circles. The rotation joint's main components were the wrist's distal part, the cable guide pin, the rotor, the collar and the torsion spring. The main function of the cable guide pin was to alter the direction of the rotation cable from along the distal part's centre axis to around it. This allowed the cable to wound up around the rear end of the rotor and when pulled it would've turned the rotor. The torsion spring was supported by the distal part as well as by the rotor on its radial external and radial internal arms respectively, allowing the spring to counter the rotor's rotation caused when pulling the rotation cable. During assembly, the cable was wound up onto the rear end of the rotor by first pressing the torsion spring's radial external arm towards the distal part's centre (out of the supporting hole) and then turning the rotor to wind up the cable until the spring's arm jumped back into the supporting hole in the distal part. The first iteration prototype's rotation joint proved unsuccessful due to the cable (when being wound up onto the rear end of the rotor or when pulled on to rotate the rotor) slipping into the space between the cable guide pin and the rear end of the rotor. As a result, the space was eliminated in the second iteration prototype. The second iteration prototype worked in principle, however, the manner in which the wrist was assembled proved to be very difficult and time-consuming. Also, the torsion spring had to be bent to place it over the rear end of the rotor as well as in the attempt to wind up the

rotation cable, causing the spring to deform and therefore slip out of its supporting holes at times.

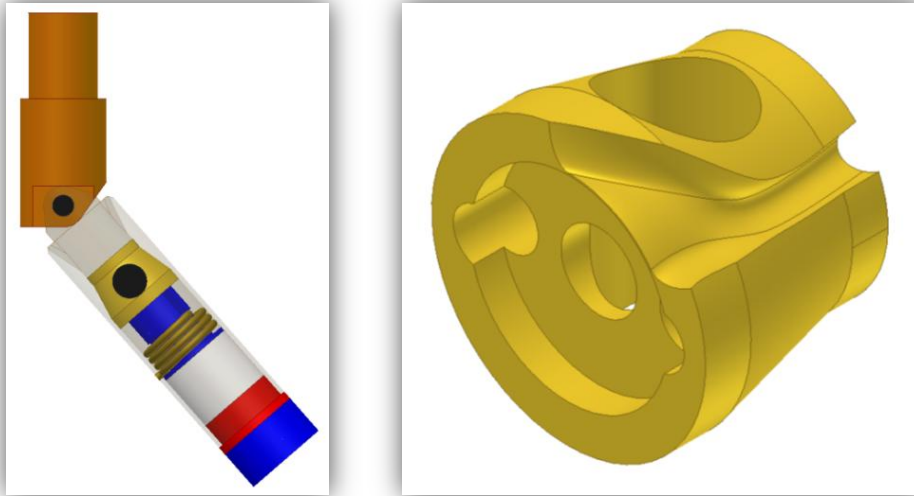


Figure 23: Third iteration of first generation prototypes

The third iteration prototype was designed as shown in Figure 23 (left). To overcome the assembly problem, a modified cable guide component was developed with a curved slot, shown in Figure 23 (right). The curved slot was milled by a CNC machine using a 1.5 mm ball nose cutter, whereas the rest of this part was done using a conventional lathe. The modified cable guide also served as a fixture for the revolute joint cables, replacing the revolute joint pin in the previous iterations. However, the main advantage of the new cable guide was that during assembling a flat screw driver could be used from the rear end of the distal part to turn the cable guide, subsequently winding up the cable onto the rotor. A slot was also machined into the rear end of the rotor, along its axis, allowing for easier assembly of the torsion spring.

Even though these changes solved some of the problems mentioned in the previous iterations, other problems arose. The main problems which eventually caused this iteration to fail included the friction on the cable, mainly in the slot, which caused the rotor not to return to its original position as well as the manner in which the rotation cable was fixed to the rotor. The torsion spring's assembly method and the way in which it was being supported also proved to be a problem. Furthermore, the number of coils of the torsion spring as well as there being no spaces between the coils proved to be a major problem and therefore also contributed to the failure of this third iteration.

4. Design of the final prototype

The preceding prototypes helped identify all the major issues related to the concept which led to the design and development of a successful wrist prototype shown in Figure 24. The subsequent sections discuss the final prototype in more detail.



Figure 24: Manipulator instrument tip prototype

4.1 Working principle of the manipulator

The designed manipulator's wrist consists of a revolute joint, a rotational joint as well as a detachable tool tip (shown in Figure 25 (right)) which commutatively allows for three DOF. The wrist is attached to an elongated shaft which can rotate or roll around its own axis, giving the manipulator a fourth DOF.



Figure 25: Designed 4 DOF primary slave manipulator

The PSM's wrist joints are actuated by means of a tendon mechanism using five DC micromotors to wind up the cables. In Appendix A it was determined that a minimum tensile force of 263 N was needed to produce a 1 N.m torque in the revolute joint, and should therefore be able to resist a 10 N opposing tip force. The cables used were 0.1 mm stainless steel fibres woven into 1.1 mm cables, giving it a tensile strength of close to 100 kg and an approximated bending radius of 2 mm (see Appendix A for "Cable Strength Test"). The five motors and their control electronics are all fixed to an actuator hub situated inside the actuator drive housing, shown in Figure 26. 12 VDC Faulhaber DC brushed motors were chosen due to their small size, their high start-up torque and their ease to be controlled. A 1:1512 gearhead is attached to each motor to allow the reel to

rotate about 60° in three seconds, which for this prototype was thought to be an adequate speed to fully manipulate the revolute joint.



Figure 26: Manipulator actuating hub

Four of the motors' gearhead output shafts are coupled to reels around which the cables are wound up on. The fifth motor's gearhead output shaft is coupled to a spur gear to rotate the manipulator around its elongated axis. The four cables wound around the reels pass over a bronze cable guide and extend down the elongated shaft to the manipulator's wrist joints. Two of these cables are fixed to the revolute joint to allow for flexion and extension of the distal part of the wrist. A third cable, passing through the revolute joint, is fixed to the rotation joint to allow the tool tip to rotate around the wrist's distal part's centre axis and is countered by a torsion spring. The last cable passes through both the revolute and rotation joints and is used to close the gripper jaws while a compression spring opposes the cable to open the gripper jaws again. Figure 25 (right) shows the deflected prototype. Major dimensions of the manipulator are given in Table 4.

Table 4: Manipulator's major dimensions

Dimension	Value
Instrument diameter	10 mm
Wrist length	80 mm
Elongated shaft length	270 mm
Actuator drive diameter	104 mm
Actuator drive length	280 mm

4.2 Choice of Materials

Stainless steel 316 (SS316), medical grade, is often used in medicine due to it being strong, tough and ductile (Enderle *et al.*, 2005). SS316 is also less expensive compared to other bio-metals, making it the choice for many medical instruments. Therefore, mainly for this reason, SS316 is the choice of material for this manipulator. However, SS304 was used for the prototype due to it being more readily available (therefore slightly

cheaper), it having similar mechanical properties as that of SS316, with similar machineability.

4.3 Design of the Revolute Joint

The revolute joint, as shown in Figure 27, consists of the proximal part, the distal part and a revolute pin. The outer diameters for the proximal and distal parts are 10 mm. Both parts were manufactured, using SS304.



Figure 27: Revolute Joint

The proximal part in Figure 28 (left) is 25 mm long with a 5.5 mm through hole. The part also has two 1.2 mm oblique holes (perpendicular to the revolute joint rotation pin or axis) to accommodate the revolute joint's manipulation cables. The primary function of this part is to act as a fixture for the distal part and guides the cables used to deflect the distal part to a maximum of 55° from the elongated axis of the proximal part.

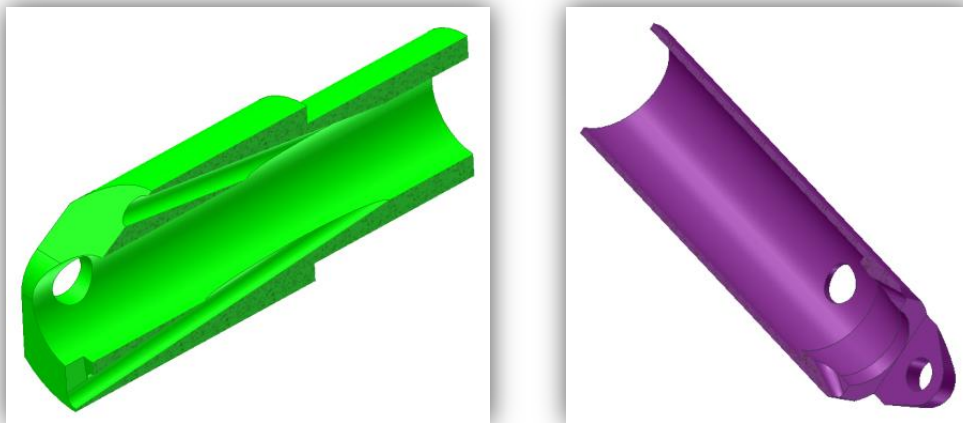


Figure 28: Sectional views of the Revolute Proximal (left) and Revolute Distal (right)

The distal part, shown in Figure 28 (right) is approximately 40 mm long and has a counterbore with a major diameter of 9 mm to house the cable guide and rotation cable assembly. The manipulation cables used for the revolute joint are fixed to the cable guide which in turn pushes against the counterbored shoulder in the distal part to cause the deflection of the distal part.

4.4 Design of the Rotation Joint

The rotation joint consists of the rotor assembly shown in Figure 29 (left) and the cable guide in Figure 29 (right). The rotor assembly slides into the revolute distal part, after the cable guide, and rotates about its longitudinal axis while the cable guide serves as a fixture point for the revolute joint's manipulation cables and also a means to change the direction of the rotation joint's manipulation cable to around the longitudinal axis. All parts (except for the SS302 torsion spring and the Delrin bushes) were manufactured using SS304.

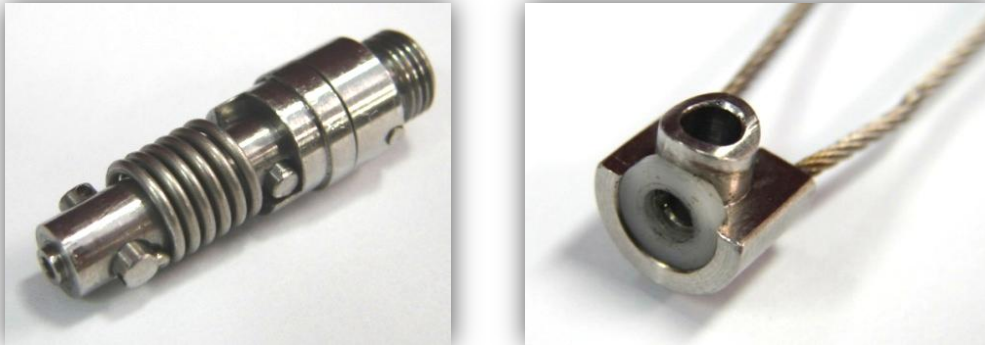


Figure 29: Rotation Joint Rotor Assembly (left) and Cable Guide Assembly (right)

The rotor assembly (see Figure 30 (left)) includes the rotor, collar, collar bush, sweep pin, torsion spring and the support pin. The rotor serves as the base for the assembly and is approximately 35 mm in length. The collar is press-fitted into the distal part's 9 mm end hole and supports the rotor while it rotates in the collar bush. Also, the collar together with the sweep pin allows a maximum of a 100° sweep or rotation. The torsion spring's axial arms are supported by the collar and the support pin; it is pre-tensioned and serves to counter the rotation cable action. The support pin not only supports the torsion spring but also serves as a fixture point for the rotation manipulation cable.

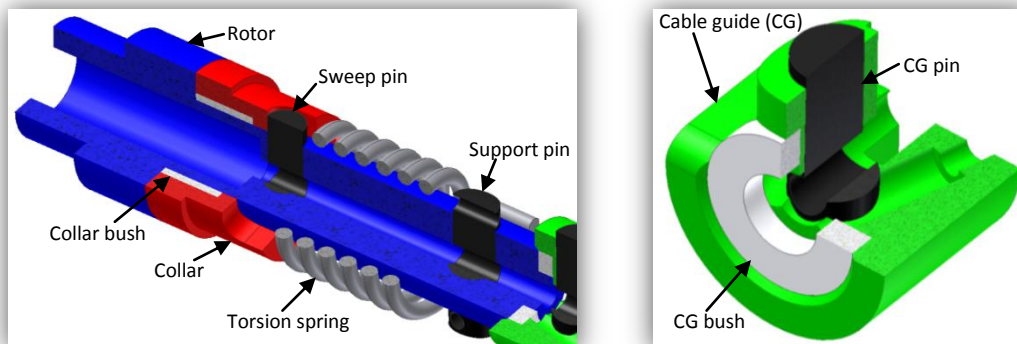


Figure 30: Sectional views of Rotor Assembly (left) and Cable Guide Assembly (right)

The cable guide in Figure 30 (right), as previously mentioned, serves as fixture points for both the revolute joint's flexion and extension manipulation cables. Also, the protruding 5 mm feature serves a means to alter the direction of the rotation joint's manipulation cable from along the distal part's centre axis to around it. This essentially allows the cable (when fixed to the support pin and wound up around the rotor assembly's end),

when pulled, to rotate the rotor and therefore the tool tip which will be screwed onto the tip of the rotor. The cable guide bush supports the end of the rotor while the rotating transverse force is applied.

4.5 Actuator Drive

The actuator drive, shown in Figure 31, consists primarily of five motors with cable reels attached to four of them, the top and bottom actuator hubs, a cable guide, a 28 tooth spur gear, an 84 tooth internal spur gear, and lastly the actuator drive enclosure. The drive essentially works as a tendon mechanism in which one motor reels up a cable while another cable or spring would oppose the motion, while still allowing the joint to move to the desired position. The actuator drive hubs and the drive enclosure were made of aluminium 6 series to reduce the weight and the costs involved, whereas the reels and the 28 tooth spur gear were made of SS304. The internal spur gear and the drive cable guide were made of bronze to prevent damage to the mating spur gear and the sliding cables respectively due to bronzes' ideal material contact properties with stainless steel.

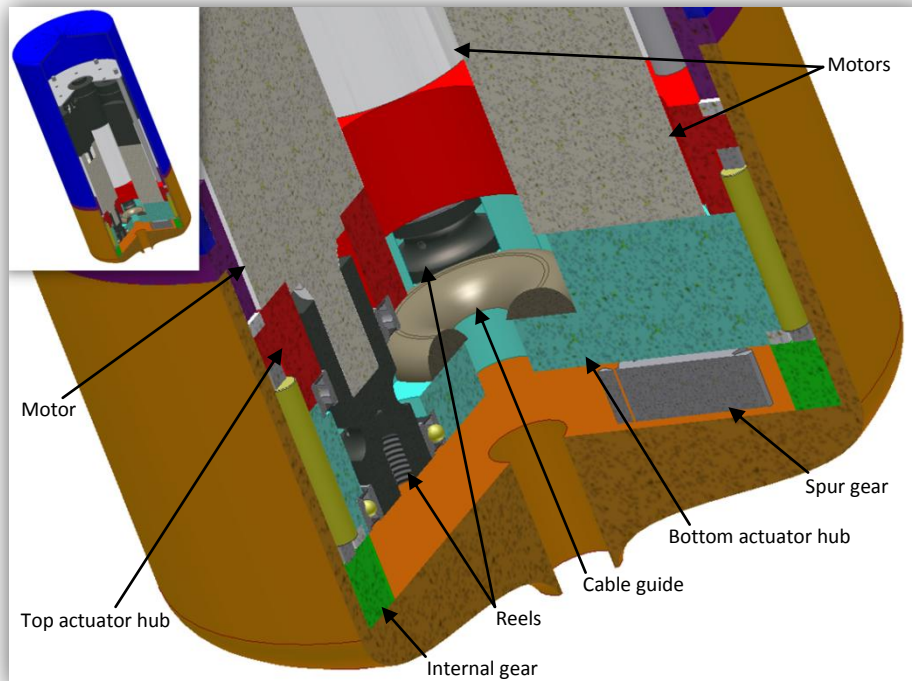


Figure 31: Sectional view of Actuator Drive Assembly

The drive hubs serve as a base on which all the motors are screwed on to as well as a housing in which the bearings can be secured to support the reels while forces are being applied by the wound-up cables. The four cables from the wrist run through the extension arm, over the bronze cable guide and are then attached to the reels. The two cables from the revolute joint would oppose each other to accomplish the extension and flexion movements of the joint while the rotation joint's cable is opposed by the torsion spring and the tool tips' opposed by the compression spring. These four cables and their opposing springs provide only three DOF while the fourth lies in the rotation of the

extension arm by means of the spur gear mating with the internal spur gear. This therefore causes the hubs with their attached components to rotate within the actuator drive enclosure.

4.6 Tool Tip

The tool tip, illustrated in Figure 32, consists of the tool tip base, pivot pin, tool tip bush, slide pin and pull pin. The gripper jaws used in Figure 32 (left) were taken from another laparoscopic instrument to prove the tool tip's working principle, however the jaws could be anything from grippers, claspers, scissors, etc, for the use in laparoscopic MIS procedures. The parts were manufactured in-house and were made of SS304.

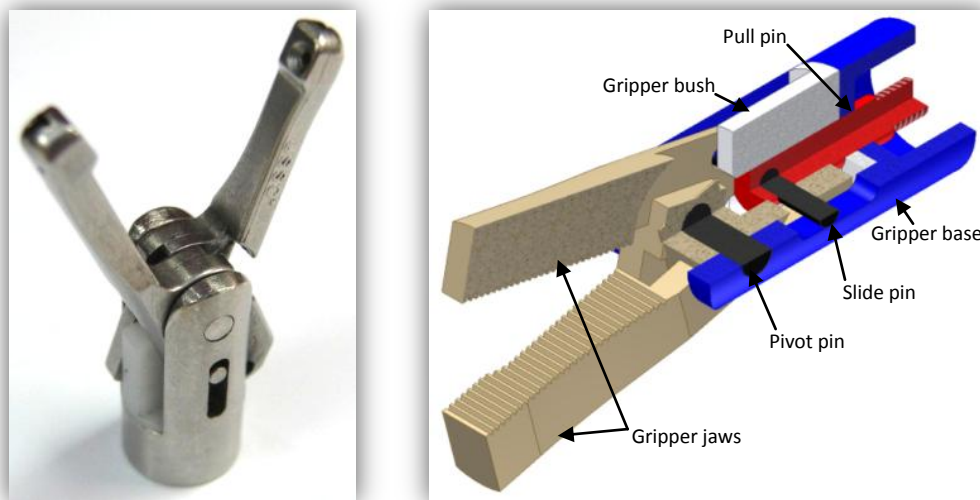


Figure 32: Tool tip

The base of the tool tip shown in Figure 32 (right) holds all the parts to allow the jaws to rotate around the pivot pin. In each finger there is a machined slot angled at about 30° to its longitudinal axis. Therefore, when the slide pin moves up or down the slot in the base the fingers open or close, respectively. The pull pin is fixed to the slide pin and when the base is screwed onto the rotor of the rotation joint, the pull pin is screwed into another sliding part inside the rotor. This part, called the rotation joint pull pin, has a cable attached to it and when pulled it compresses the opposing compression spring behind it. This mechanism then serves as the means to open and close the tool tip jaws.

5. Manipulator Assembly Procedure

5.1 Wrist Assembly Procedure

During the assembly of the wrist, the collar bush is first fitted into the collar and then slid over the rotation joint rotor followed by the torsion spring, as shown in Figure 33 (left). The rotation joint support pin is then pressed into its hole while keeping in mind which side is to support the torsion spring. The torsion spring's axial arms must then be secured into their respective supporting holes before the collar can be rotated (pre-

tensioning the torsion spring) to press the sweep pin into place. Finally, the rotation joint manipulation cable is threaded through the hole in the support pin.

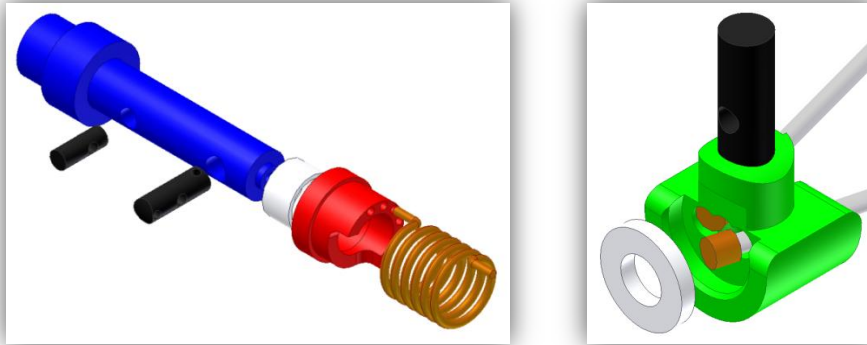


Figure 33: Assembly of Rotor Assembly (left) and Cable Guide Assembly (right)

The rotation joint cable guide (see Figure 33 (right)) is assembled by inserting the manipulation cables for the revolute joint and then pressing the cable guide bush into place. Next, the cable guide assembly is placed into (cables first) the 9 mm end hole of the revolute distal part up against the counterbored shoulder, as shown in Figure 34. The rotor assembly then follows by placing the cable through the left side opening formed by the cable guide and distal part, and pulled through until the collar is against the distal part's front end and can be pushed tightly into the front end of the distal part. After that, the cable guide is rotated anti-clockwise from the back opening of the distal and to wind up the cable onto the rotor assembly's end section. The person assembling should turn the cable guide a full 360° to wind the rotation joint's manipulation cable once around and in so doing, and must take care not to damage any of the cables protruding from the back. Once completed, the cable guide support pin should be placed through its intended hole to prevent the cable guide from rotating with respect to the distal part, after which the rotation joint should work. The tool tip cable with its pull pin and compression spring can then be threaded through the rotation joint assembly.

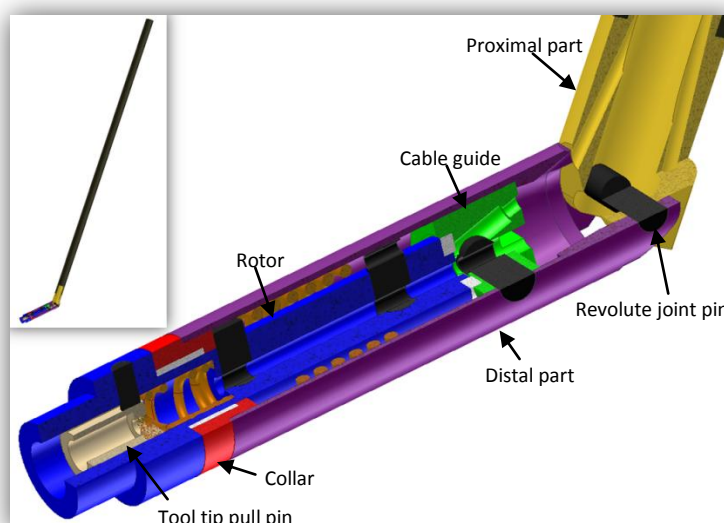


Figure 34: Sectional view of Manipulator Wrist

In assembling the distal assembly of the wrist to the revolute proximal part, the revolute joint cables are threaded through the oblique holes. The rotation joint's cables, as well as the tool tip cables, are placed through the proximal part and down into the manipulator arm. Then the revolute joint pivoting holes of the distal and proximal parts are lined up and the revolute joint pin is pressed in. It should be noted, however, that the two cables from the rotation joint and tool tip must be below the pin if the chamfer of the proximal were facing upwards to allow for a more direct pathway for the cables while being manipulated, and to reduce any influence they may have on the revolute joint.

5.2 Actuator Drive Assembly Procedure

The actuator drive is assembled by first placing the four reels onto the output shafts of their motors and secured using two M3 grub screws per reel (see Figure 35). The four motors are then screwed onto the top actuator drive hub after which sealed ball bearings are slid over the reels and into the 2.5 mm counterbores in the top drive hub. After that, the bronze cable guide is pressed into the $\varnothing 30$ mm hole of the bottom drive hub (with the rounded side facing upwards) before sandwiching and screwing the two drive hubs together. Next, the other ball bearings are pressed over the bottom part of the reels and the fifth motor is screwed onto the bottom actuator drive hub, through the top hub, after which the spur gear is mounted onto its output shaft using M3 grub screws.

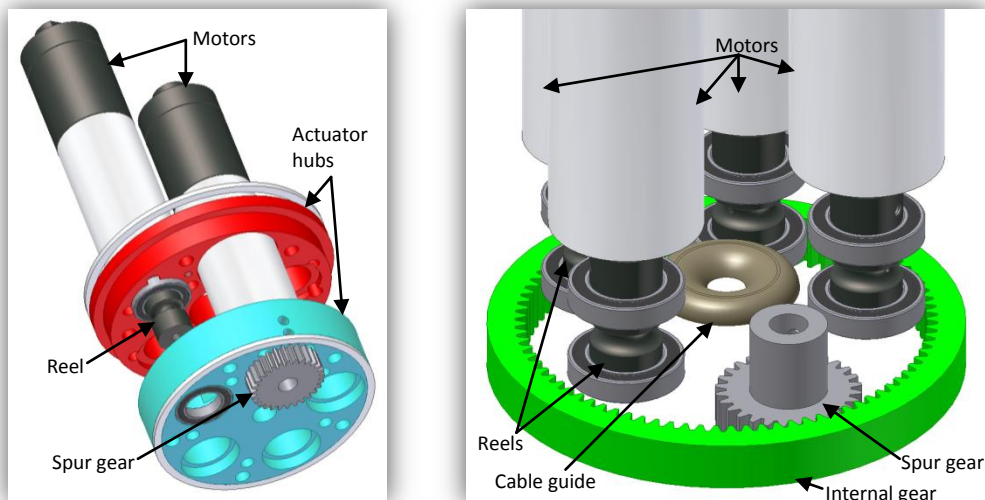


Figure 35: Assembly of Actuator Hub

The internal gear is slid into the bottom actuator drive enclosure with the $\varnothing 90$ mm thrust ring and the needle bearing placed on top of it. Only then is the actuator drive hub assembly placed carefully into the needle bearing and carefully wiggled until the gear teeth slide between each other, as shown in Figure 35 and Figure 36. The other $\varnothing 98$ mm thrust ring is then placed over the motors onto the top drivehub followed by the enclosure lock ring. Finally, the electronic stand's legs and plate are screwed onto the top hub before connecting and mounting the control electronic boards. The top actuator enclosure is then placed over the actuator drive assembly.

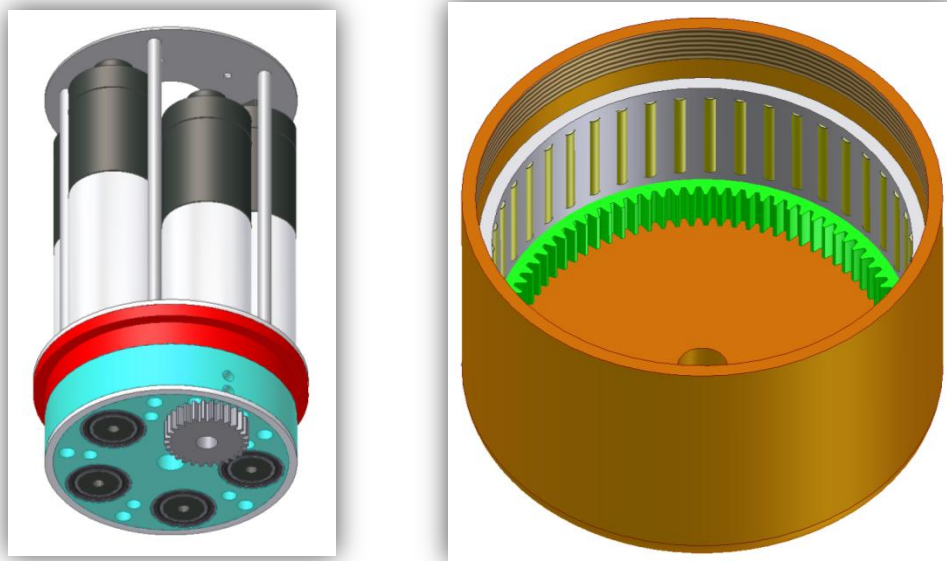


Figure 36: Assembly of Actuator Drive

6. Manipulator Sterilization

The sterilization of the manipulator was not the primary focus of this thesis, but instead to design and test the functionality of a new multi-DOF wrist for minimal invasive surgery. The author, however, thought it important to explain what sterilization techniques are available and elaborate on those which are suited for the manipulator. Also, the required modifications to the manipulator in order for it to be sterilized are discussed. Through this the author hopes to convince the reader that no fundamental changes are necessary in order for the manipulator to be sterilizable.

6.1 Sterilization Techniques

Sterilization is the destruction of all micro-organisms, including spores (Kingsnorth and Majid, 2006). There are various sterilization techniques available for surgical equipment (Lawrence et al., 2002; Pattenale, 2004; Kingsnorth and Majid, 2006):

- Heat sterilization
 - autoclaving (steam under pressure)
 - dry heat
 - low temperature steam
- Cold sterilization
 - g-irradiation
 - ethylene oxide
 - glutaraldehyde

The technique used depends on the equipment's material heat sensitivity and the risk of infection to the patient. The most effective method of sterilization is moist heat (or autoclave) which destroys organisms by coagulation of the protoplasm (Kingsnorth and Majid, 2006). However, only heat-tolerant items such as stainless steel surgical equipment may be autoclaved (sharp surfaces, such as scalpels may, however, be dulled

when autoclaved). The principle; Distilled water is heated in a chamber to above boiling point. The increased temperature causes an increase in pressure in the chamber. The higher the temperature, the higher the pressure and therefore the faster the micro-organisms are killed. Pressure also forces the steam into the micro-cavities of the equipment (Pattenale, 2004).

The exposure time to adequately sterilize an instrument depends on the temperature reached and held as well as the instrument's geometric properties. Most steam autoclaves operate at 121°C (pressure 100kPa) with a holding time of 15 minutes. Raising the temperature to between 126° and 129°C reduces the time to 10 minutes, and temperatures of 134° - 138°C requires a holding time of only three minutes (cycle time 15- 20 minutes) (Lawrence *et al.*, 2002).

6.2 Manipulator Modifications for Sterilization

In order to make the manipulator sterilizable, the primary modifications to the manipulator would be to separate the actuator drive from the extension arm. The incentive for this is due to the fact that the extension arm, with its multi-DOF wrist, is the only part of the manipulator making contact with the patient during surgery and therefore the only part that should be sterilized after each procedure. Also, the actuator drive consists of the DC motors and their control electronics which can not be wetted or heated excessively and should preferably not be sterilized. Placing a sterilized plastic cover over the actuator drive (as in the case of the da Vinci system) should be adequate and therefore sterilization of the actuator drive would probably not be necessary. Therefore, by designing a linking mechanism between the actuator drive and the extension arm, the manipulator, or at least those parts making contact with the patient, can be sterilized without making fundamental changes to the manipulator.

7. Mechanical Manipulator Costs

One of the main objectives for designing a primary slave manipulator was for it to be inexpensive. Figure 37 shows the cost breakdown for the manipulator.

Mechanical Cost Estimation				
No.	Description	Qty	Unit Price	Price
1	Manipulator Wrist: Material (SS304)	NA	R 300.00	R 300.00
2	Manipulator Wrist: Labour	80	R 250.00	R 20 000.00
3	Wrist's Passive Components (Springs, etc)	NA	R 150.00	R 150.00
4	Manipulator Actuator Drive: Material	NA	R 1 350.00	R 1 350.00
5	Manipulator Actuator Drive: Labour Costs	60	R 250.00	R 15 000.00
6	Drive's Passive Components (Bearings, etc)	NA	R 290.00	R 290.00
7	DC motor assembly	5	R 5 313.64	R 26 568.20
			Total:	R 63 658.20

Figure 37: Manipulator Cost Estimation

The material needed to make the manipulator amounted to approximately R1650, whereas the labour costs were estimated by the Mechanical Workshop to be R35000 for

140 hours of labour. The motors used for the prototypes were R26570, therefore making up a total manipulator cost of R63658.20. This does not include the control electronics for the manipulator, which is described in the next chapter.

Chapter 4: Electronics Design

Part of this thesis was to also design the electronics to drive the motors and in so doing control the manipulator's movements. However, only basic control was to be implemented to prove the manipulator's functionality and to perform the repeatability and strength test experiments. This chapter discusses the requirements for such a manipulator and describes the control electronics. The detail design of two printed circuit boards (PCBs), the digital board and the power drive board, are then discussed. A general overview of the microcontroller firmware is also given.

1. System Analysis

The electronics' primary function is to drive the motors to ultimately move the manipulator's wrist to any given position. In order to accomplish this goal, a number of design considerations were looked at and some functional requirements for the control electronics were generated.

1.1 Design Considerations

The design considerations for the control electronics are as follows:

- Five 12 VDC minimotors (from Faulhaber) with graphite commutation are used due to their small size, their high start-up torque and their ease of control. Each motor is attached to a five stage planetary gearhead with a 1:1512 reduction gear ratio to increase the output torque and reduce the output shaft's rotation speed. On the back of each motor a 16 lines per revolution quadrature encoder with Hall effect sensors is also attached.
- Four of the motor assemblies are coupled to the reels which wind up the cables to manipulate the wrist. Two of these four motors oppose each other, while the other two are opposed by a torsion spring and a compression spring. The fifth motor is coupled to the 28 tooth spur gear which meshes with the internal spur gear, making the fourth DOF of the manipulator possible.
- The positional feedback received is that from the motor, allowing closed loop control of the gearhead output shaft. The positions of the wrist joint, however, are unknown; this therefore making it an open loop system. As a result, the mechanical calibrations may have to be done manually each time the manipulator's electronics are switched on. (Note that if moving the manipulator back to its default or zero position before switching the electronics off, the electronics can then assume this position as its zero position upon startup.)
- The intention was to place the electronics in the actuator console, giving a dimensional limitation of approximately $\varnothing 95$ mm. A maximum height of only 30 mm for the electronics board(s) was also allowed.

1.2 Functional Requirements

The functional requirements for the control electronics include that the electronics should make provision to drive the five motors while continuously receiving positional feedback. While doing so, the controller should also communicate with a host to allow user interaction with the embedded firmware, and through this with the manipulator.

The functional requirements for the control electronics are as follows:

- The electronics should drive five motors bi-directionally and simultaneously receive positional feedback. Current feedback of the motors should also be made provision for, for the possible future implementation of auto-calibration and even tactile feedback.
- The control board should be capable of connecting to a PC-based host using HyperTerminal to allow the user to interact with electronics by checking various parameters as well as setting parameters such as the reference position or the upper and lower positional limits. On-board communication links between various hardware components should also be considered.
- The controller should also do 'on-board' diagnostic checks on start up as well as failsafe checks periodically to ensure all hardware is functioning properly and all communication links are up and running.

Figure 38 shows the functional requirements diagrammatically.

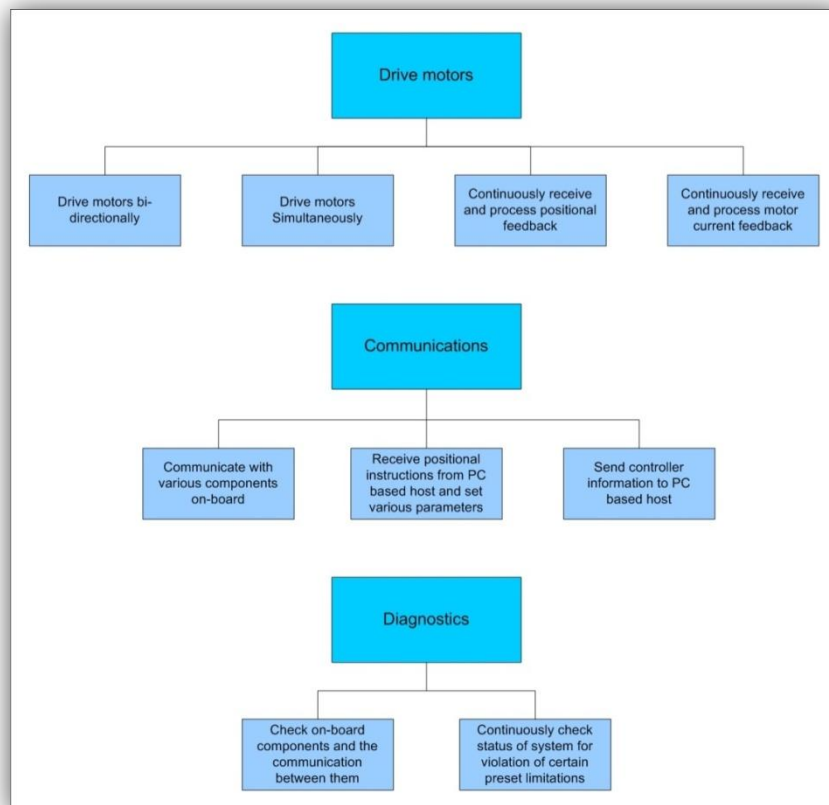


Figure 38: Functional requirements diagram

2. Control Electronics Concept Description

In light of the above-mentioned design considerations and to meet the functional requirements, a master-slave type system concept was thought best to achieve the electronics' primary goal, which is to drive the motors to ultimately manipulate the wrist. The theoretical master-slave type concept is shown diagrammatically in Figure 39.

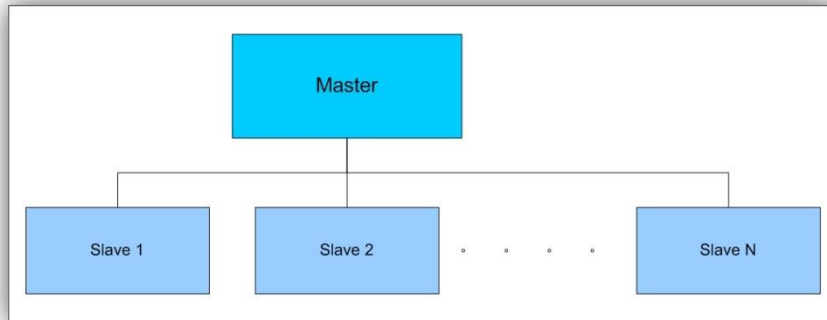


Figure 39: Master-slave electronics concept

The main advantage of such a master-slave type system is that if one slave malfunctions, it should not influence any of the other slaves directly. Also, the master-slave system, compared to a 'single unit' system, is that each slave would only perform those few important tasks directly related to its own activities. This would allow all the tasks to be performed quickly and seamlessly while those unrelated and time-consuming tasks are performed by the master. Furthermore, the master is in control of all the slaves, keeping backup copies of all their parameters. Therefore, in the case that one of the slaves malfunction, the master could attempt to reset the slave and reload its parameters. Finally, the master also acts as a shield to the very important slaves in the case that the host could possibly malfunction and as a result send invalid instructions or data.

3. Design of the control electronics

This master-slave concept was realized in the manipulator's control electronics shown in Figure 40. The control electronics were separated into two PCBs: the digital board and the power drive board. The main reason for this separation was due to the EMC design guidelines given in Appendix E. From these guidelines the circuit was separated according to frequency and type. This made it difficult to fit all the components in on one double-sided PCB due to dimensional limitations. Hence, two round double-sided PCBs were manufactured by TraX Interconnect in Cape Town, South Africa. The board schematics and the PCB layout drawings are given in Appendix F.

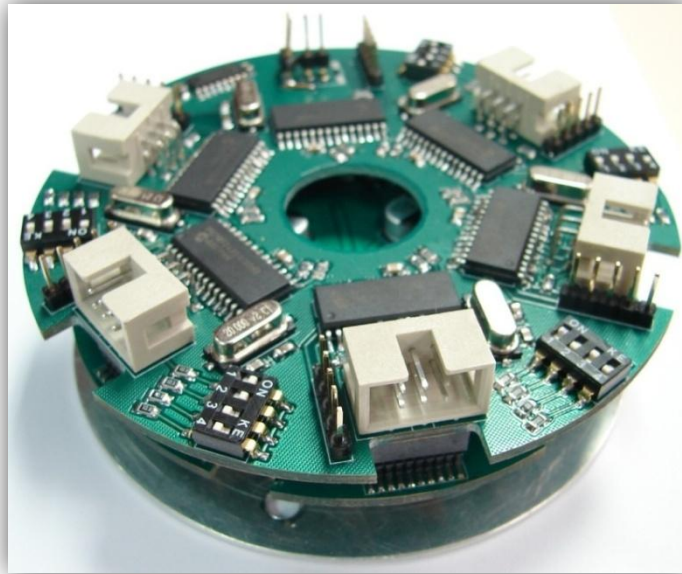


Figure 40: Manipulator's control electronics

In the sections that follow the working principle of the control electronics will be explained and then the PCBs will be discussed in more detail. The master and slave microcontrollers' firmware will also be discussed to show how each slave controls its own hardware and deals with its own tasks while the master interacts with a PC-based host to then send relevant instructions to the different slaves.

3.1 Working principle of the control electronics

While in operation, each slave microcontroller on the digital board controls an H-Bridge which in turn drives a motor. The motor's encoder is connected to the digital board to allow the slave microcontroller to monitor the motor's 'current' position. Using this 'current' position and subtracting it from a reference position (typically received from the master) the microcontroller can then drive the motor to any desired position, therefore forming a proportional closed loop system controller. Also, current feedback from the motor is sampled using the slave's ADC module. Furthermore, each slave is responsible to diagnose its own hardware, e.g. motor position, motor current, etc., and the results are then sent to the master microcontroller using a 2-wire I2C bus.

The master, on the other hand, receives instructions from the PC-based host through an RS-232 communication protocol. These instructions are processed and if, for instance, a new reference position was received, the master would then send this new reference position using the I2C bus to the related slave(s) to then drive the motor(s) to a new position.

3.2 Digital PCB Board

The digital board, shown in Figure 41, mainly consists of one master microcontroller and five slave microcontrollers with their associated components.

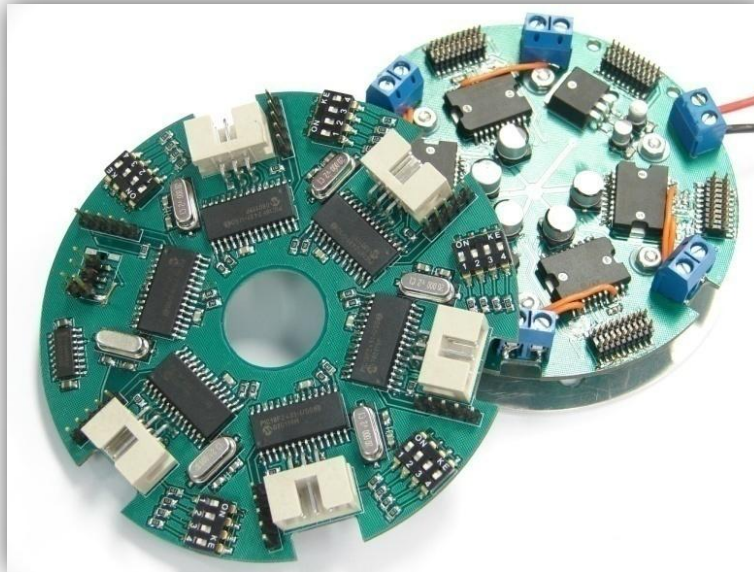


Figure 41: Digital Printed Circuit Board

An 8-bit PIC18F2550 from Microchip was used as the master for the system. This microcontroller includes 32 kB of flash memory, allowing for all the parameters of all the slaves to be backed up effortlessly. It also includes an Enhanced USART (EUSART) module to allow it to connect to a PC-based host using an RS-232 communication link while an on-board MSSP module allows it to interface to and control the communication with the slave microcontrollers. Also, with its 2048 bytes of RAM and 48 MHz external clock mode capability, the microcontroller will seamlessly perform all the necessary tasks with little delay.

For the slaves, PIC18F2431 (also from Microchip) microcontrollers were used. These 8-bit microcontrollers were purposely designed for motor control applications and include a Motion Control Module (MCM) for position feedback, a Power Control Pulse Width Modulator module (PCPWM) to drive an H-Bridge and a 10-bit High-Speed Analogue-to-Digital Converter module (ADC) to sample the current feedback. These microcontrollers have 16 kB of memory, 768 bytes of RAM and are capable of 40 MHz processing using an external clock. Also, an integrated SSP module allows for interfacing with the master microcontroller.

The electronic circuit configuration associated with the master is shown in Figure 42 and the circuit associated with all the slaves are as shown in Figure 43. Common components in the master and slave schematics are the 20 MHz crystals with their 15 pF capacitors, the 100 nF capacitor across the power pins (VDD and VSS) and the programming 1x5 header connector indicated in Figure 42 and Figure 43 by U1 and U2 respectively. In the master's schematic, 2.2 k Ω pull-up resistors (R4 and R5) are used on the I2C wires. The master is then connected to the I2C bus (SCL and SDA) through two 330 Ω resistors (R2 and R3).

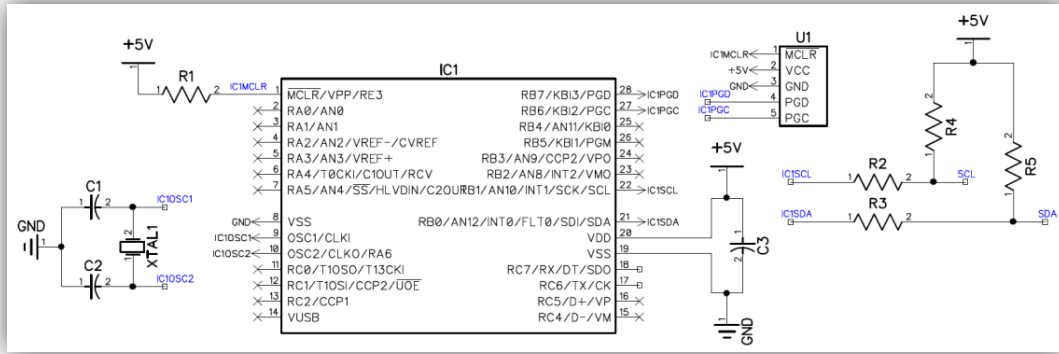


Figure 42: Master microcontroller schematic

In addition to the slave’s schematic, is the four-way DIL switch (DIL1) used to provide each slave with a unique identification number, and a 2x3 male header socket (QE1) for the motor encoder’s female plug. Each slave is also connected to the I2C bus through two 330 Ω resistors (R11 and R12).

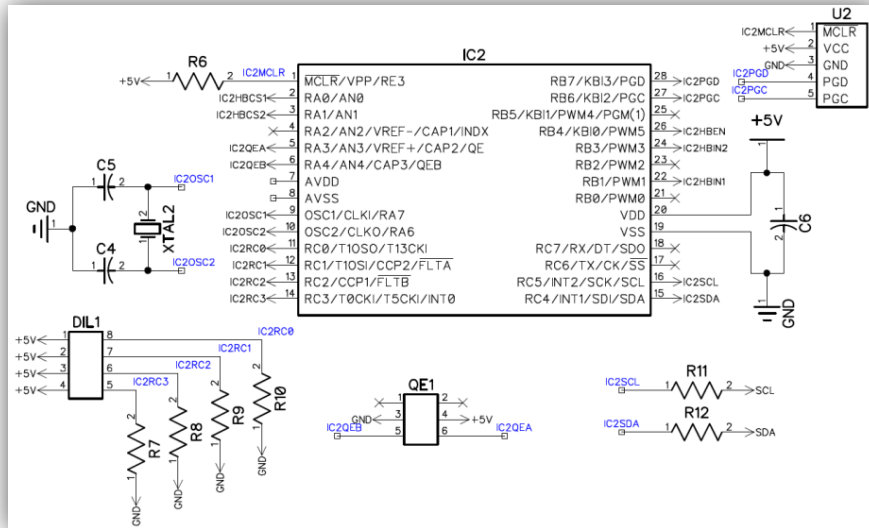


Figure 43: Slave microcontroller schematic

3.3 Power Drive PCB Board

The power drive board, shown in Figure 44, primarily consists of five H-Bridges to drive the motors. The board is supplied with 12 VDC and also includes a 5 V regulator circuit to supply the digital board with power. The digital board is mounted onto the power drive board by means of six 2x10 board-to-board surface mount header connectors from Samantec.

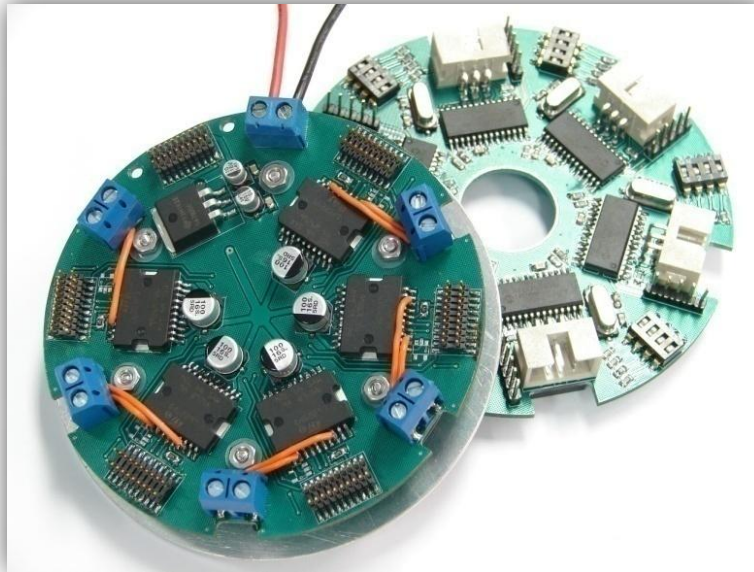


Figure 44: Power Printed Circuit Board

Five L6225 DMOS Dual Full H-Bridges from STMicroelectronics, specifically designed for motor control applications, were used to drive the motors bi-directionally. The chip allows a maximum operating supply voltage of 52 V with a 2.8 A peak current output (1.4 A DC). It has an operating frequency of 100 kHz, an overcurrent protection (OCP) capability and integrated thermal shutdown protection circuitry.

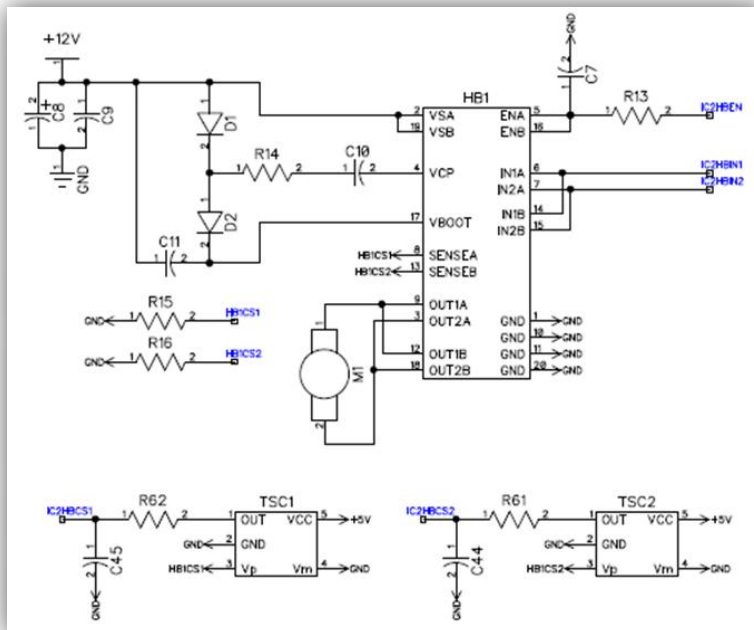


Figure 45: L6225 H-Bridge Parallel Configuration Schematic

In Figure 45 the load is connected such that Half Bridge 1 of Bridge A is paralleled with the Half Bridge 1 of the Bridge B, and the same for the Half Bridges 2, to increase the

output current capability and reduce the power dissipation in the device at a given current level. The High-Side and Low-Side switch ON Resistance of the H-Bridges on the same die (or chip) is well-matched, resulting in the current between the two integrated H-Bridges to be near equal.

Table 5: Recommended Values for the Components in Figure 45

Component	Value	Component	Value
C_8	100 μ F	D_1 & D_2	1N4148
C_9	100nF	R_{13}	100k Ω
C_{11}	220nF	R_{14}	100 Ω
C_{10}	10nF	R_{15} & R_{16}	1 Ω
C_7	5.6nF		

Table 5 lists the recommended values used, as per the datasheet from STMicroelectronics, for the schematic in Figure 45. The C_8 and C_9 capacitors provide low and high frequency filtering on the power supply. C_{11} , D_1 , D_2 , R_{14} and C_{14} are external components for the bootstrapped supply to realize a charge pump circuit for the N Channel Power MOS's upper transistors in the bridge requiring a gate drive voltage above the power supply voltage. IN1 and IN2 are TTL/CMOS and microcontroller compatible logic inputs which effectively allows control over the motor's direction of rotation. Pins EN_A and EN_B have identical input structures with the exception that the drains of the overcurrent and thermal protection MOSFETs are also connected to these pins causing the need for R_{13} and C_7 .

Figure 45 also shows the current sensing circuits utilizing the TSC101 amplifiers from STMicroelectronics (indicated by TSC1 and TSC2). The chip facilitates a wide common-mode operating range (2.8V to 30V) with a wide supply voltage range of 4 V to 24 V. It also has an internally fixed gain from which the 20 V/V, 50 V/V and the 100 V/V gains can be chosen from. The components C_{44} and R_{61} form a basic low-pass passive filter with a recommended cut-off frequency of 15 kHz (likewise for C_{45} and R_{62}). Although current sensing was made provision for through these current sensing circuits, the components were not physically soldered onto the board.

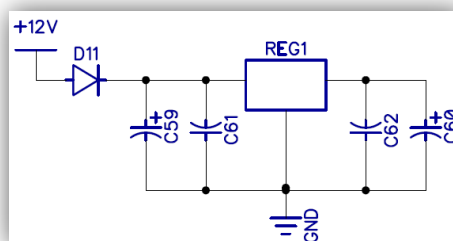


Figure 46: 5 V Regulator Circuit

The L7805CV voltage regulator from STMicroelectronics was chosen to serve as power supply to the digital circuitry. The regulator can deliver a maximum current of 1.5 A at 5

V, or otherwise 7.5 W. The corresponding 5 V power supply schematic is shown in Figure 46. It shows the 10 μF (C_{59} and C_{60}) and 100 nF (C_{61} and C_{62}) ripple rejection capacitors at the input and output of the regulator. It also includes a 'safety' diode (a 1N4007) which protects the system in the case that the power leads are connected the wrong way around.

4. Microcontroller Firmware Overview

Two different microcontroller programmes were written in Microchip's MPLAB using its MCC18 C compiler: the master controller (PIC18F2550) firmware and the slave controller (PIC18F2431) firmware. Although there are five slave controllers, the code was written such that the instructions executed depends on the unique identification number obtained from the DIL switches and therefore allowing for the same code to be loaded in all five slave microcontrollers. A different code was generated for the master due to it being a different microcontroller than the slaves.

4.1 Master Controller Firmware

Figure 47 illustrates the higher level of operation of the master controller firmware. At startup the microcontroller initializes the USART module for serial communication with the host controller at 115200 kbps. Then the MSSP is configured for master I2C communication. After the microcontroller is initialized correctly, the master sends all start up parameters to each slave microcontroller and then receives them back from the slaves and compares the data received to the data sent. If matched, the slaves are thought to be operating correctly. If incorrect, the master prints an error message to screen.

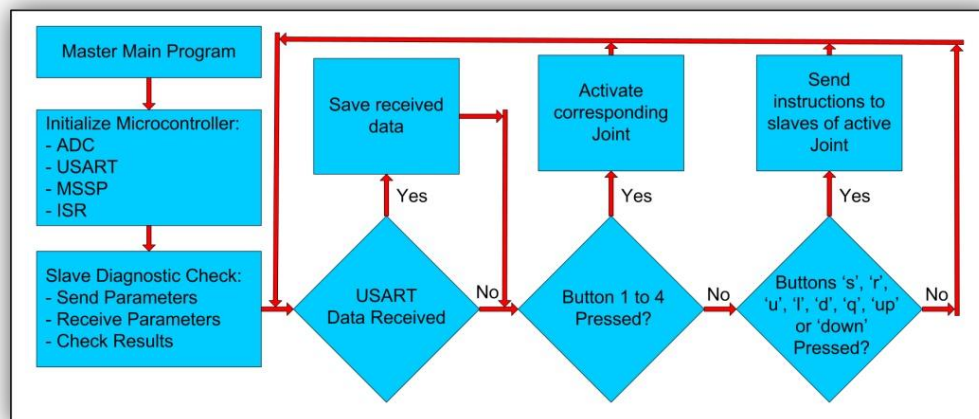


Figure 47: Master Controller Firmware Flowchart

After diagnostic checks are completed, the master enters an infinite while loop in which the USART data ready flag is polled. If data has been received it is saved in the 'userinput' variable, otherwise the old 'userinput' is carried forward and used. This variable is then checked to see if it matches any of the firmware instruction codes given

in Figure 47. If a match of buttons '1' to '4' occurs then the relevant joint is activated and the 'userinput' variable is set to zero to avoid the instruction to be performed again. If any other instruction codes match, the relevant instructions are then performed and the 'userinput' variable is again reset. The relevant instructions include the setting of parameters and sending these new parameter values to the active slaves.

4.2 Slave Controller Firmware

The slave controller firmware flowchart is shown in Figure 48. Similar to the master's firmware flowchart, this flowchart represents only the higher level of operation.

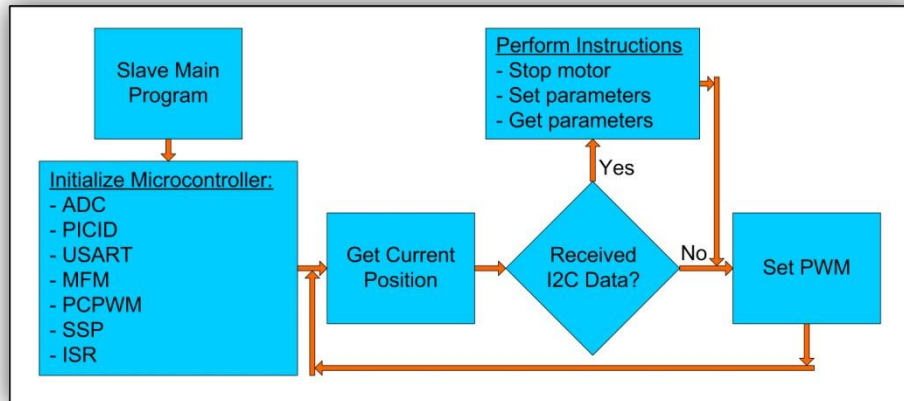


Figure 48: Slave Controller Firmware Flowchart

At startup, after all constants and global variables are defined, the microcontroller initializes all peripheral modules. It sets the microcontroller's ID, configures the MFM, initializes the PCPWM module and configures the SSP module for I2C communication. The microcontroller then enters an infinite while loop in which it gets the motor's current position from the MFM and looks to see if it received an instruction from the master controller. If no instructions were received, then the PWM is set in the PCPWM based on the current position and the reference position. However, if an instruction was received, the microcontroller checks the data's parity. If the data is valid, the instruction type is determined using the six most significant bits. Instruction types include: Stop motor, Set reference position, Set current position, Set upper or lower limits, Get reference position, Get current position and Get upper or lower limit. When a 'Set' instruction is given, the value to which the relevant parameter must be set to can be extracted from the remaining 9-bits of the original data received. With a 'Get' instruction, the relevant parameter's value is loaded into the SSP module's buffer awaiting it to be sent to the master. During a 'Get' and a 'Stop' instruction, the middle 9-bits of the original data received are ignored.

5. Control Electronics Costs

As the main reason for this thesis being to design and develop an MIRS system cost-effectively so that it can be more affordable to all medical institutes, the cost of the

control electronics are very important. Figure 49 shows the cost estimation related to the control electronics.

Control Electronics Cost Estimation				
No.	Description	Qty	Unit Price	Price
1	Digital PCB	1	R 1 423.56	R 1 423.56
2	Power Drive PCB	1	R 1 360.07	R 1 360.07
3	PIC18F2550	1	R 67.00	R 67.00
4	PIC18F2431	5	R 62.00	R 310.00
5	L6225 H-Bridges	5	R 86.00	R 430.00
6	DIL switches	5	R 6.50	R 32.50
7	2x3 Quadrature Encoder Male Header Sockets	5	R 15.00	R 75.00
8	20MHz Crystals	6	R 3.00	R 18.00
9	MAX3223E RS-232 Driver/Receiver	1	R 35.00	R 35.00
10	L7805CV 5V regulator	1	R 5.00	R 5.00
11	Other Connectors	NA	R 130.00	R 130.00
12	All Passives	NA	R 25.00	R 25.00
			Total:	R 3 911.13

Figure 49: Control Electronics Cost Estimate

The total cost of the electronics amount to an approximated R3911.13 with the manufactured PCB's making up nearly three quarters (R2783.63) of the total cost. It must be noted, however, that the prices provided above are only estimates and the total amount above does not include the labour costs (an estimated five hours) to solder and test the boards. The firmware can also only be loaded once the boards are fully soldered.

Chapter 5: System Evaluation

Another objective of this thesis is to determine the feasibility of the designed seven DOF primary slave manipulator. This chapter discusses the experiments done in order to verify the four DOF manipulator's capabilities with respect to the literature and the design requirements. The two experiments done were the repeatability test and the strength test experiment. Neither of these experiments was intended to be destructive, but instead see what the manipulator is capable of.

1. Repeatability Test Experiment

Repeatability is the ability of the end effector to move back to a previous position again and again. The system is, however, an open loop system and therefore the intention of this experiment was specifically aimed only at the mechanical repeatability of the primary slave manipulator end effector. This was achieved by moving the manipulator to certain positions repeatedly and measuring the manipulator links with a coordinate measuring machine (CMM).

1.1 Experimental Setup

The experimental setup shown in Figure 50 consisted of the manipulator placed securely onto two V-blocks positioned on the CMM's table. The manipulator was supplied with a 12 VDC power source and a serial connection to the PC based host controller. Basic manipulation instructions were sent from the PC, using HyperTerminal, to the manipulator controller PCB to drive the individual joints.



Figure 50: Repeatability test setup

The CMM was first calibrated by measuring a ceramic ball with a known diameter to determine the probe's diameter and position. After that the manipulator's elongated shaft centre line was found by measuring nine points along the shaft while positioned at its default or zero position. The centreline was then found again after rotating the elongated shaft approximately 60° about its centre axis to help determine whether the shaft was bent in any way. Once the shaft's straightness and cylindricity was verified, the coordinate system was set up with the z-axis along the elongated arm towards the actuator drive.



Figure 51: Repeatability test procedure

The main measurements were started by zeroing the elongated arm and moving the wrist's distal arm to an extreme flexion position. Both the elongated shaft's and the distal arm's centrelines were found by measuring nine points along each of their outer diameters. The wrist's distal arm was then moved 20 steps (in HyperTerminal) towards an extended position to find its centreline again. This was repeated for 35 steps from the original extreme flexion position before moving the wrist to its extreme extension position. The distal arm was then measured again at the 35 steps mark, but this time moving from a joint extension position rather than a flexion position, which allows for determining whether the joint positioning is path dependant or not. This was also done for the 20 steps mark (moving from the 35 steps mark) before moving back to the extreme flexion position.

The elongated arm is then rotated 60 steps anti-clockwise while the distal arm is in its extreme flexion position. The elongated arm is then measured again before measuring the wrist's distal arm in its extreme flexion, 20 steps, 35 steps and extreme extension positions. This was repeated in the 35 steps and 20 steps positions. This whole process is repeated for the 120 and 180 steps elongated arm positions before reversing the direction of rotation of the extension arm back to the 120, 60 and 0 steps positions. This one cycle was repeated 11 times before all measurements were completed and the data exported to a text file. Due to the amount of points measured, a macro was recorded for the CMM for one cycle and replayed for the other 10 cycles.

1.2 Results and Discussion

The test was performed over two days. Calibration of the CMM was done on the first day as well as a straightness and cylindricity test on the long manipulator arm. Samples one to four and half of sample five (only half of sample five was done due to a CMM malfunction) was also performed on day one whereas the second half of sample five and the remaining six samples were performed on day two. At the end of day one the manipulator joints were moved to their default or zero positions before switching the power source off. The joints were moved back to the positions of day one, taking the direction path into account, to continue with sample five's measurements on day two.

The data obtained from the CMM was exported into 11 text files, one for each sample. Each text file contained the point coordinates, cylinder diameter, its cylindricity and the centre line unit vector angles for each cylinder measured. The unit vector angles were then imported into an Excel spreadsheet to find the deflection angle of the distal arm as well as the roll or rotation angle of the long arm. Appendix F shows an example Excel sheet for a single sample data set.

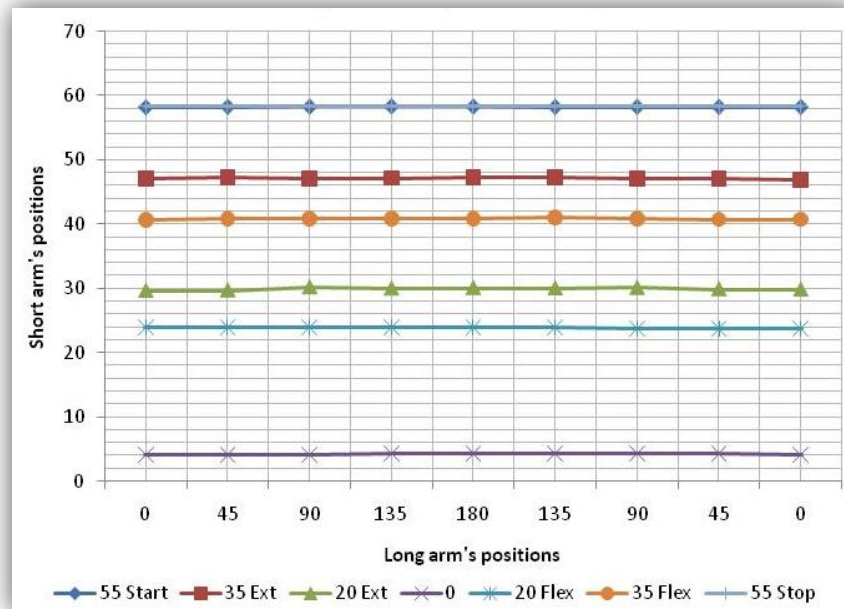


Figure 52: Sample 1 repeatability graph

The straightness and cylindricity test showed an error of 0.319 mm which was thought to be mainly due to the deflection of the long arm from the force exerted by the CMM probe on the shaft while measuring. For this reason it was thought that an uncertainty of approximately 0.4 mm or less could be expected in all the data. Figure 52 shows a line graph of the short arm's position versus the long arm's position for Sample 1. It clearly shows that the short arm's position is independent of that of the long arm and therefore the repeatability within a sample can be determined using the short arm's positions for all the long arm's positions. The short arm was found to be repeatable in Sample 1 with a maximum standard deviation of 0.193° for the '20 Ext' position shown in Figure 52.

Table 6 shows the mean and standard deviation of each short arm's position for the different sample sets. Due to the CMM's malfunction on day one and the manipulator having to be restarted on day two, the data is represented as shown in the table.

Table 6: Mean and standard deviation for short arm

Position	Sample 1 to 4		Samples 5		Sample 6 to 11		Across all Samples	
	Mean (degrees)	Std. dev.	Mean (degrees)	Std. dev.	Mean (degrees)	Std. dev.	Mean (degrees)	Std. dev.
55 Start	58.28	0.03	58.26	0.021	58.19	0.11	58.23	0.09
35 Ext	47.06	0.16	47.41	0.47	48.22	0.18	47.73	0.59
20 Ext	30.07	0.19	30.47	0.95	31.60	0.38	30.94	0.84
0	4.28	0.08	4.67	0.51	5.40	0.20	4.92	0.57
20 Flex	23.74	0.16	24.05	0.58	24.32	0.16	24.09	0.35
35 Flex	40.72	0.17	40.98	0.59	41.21	0.17	41.01	0.33
55 Stop	58.31	0.05	58.27	0.07	58.21	0.13	58.25	0.11

From the table it can be seen that for sample sets '1 to 4' and '6 to 11', the mean as well as the standard deviation changed. The main reason for this change is thought to be due to an accidental failure in properly resetting the manipulator back to its default or zero position before switching it off. This caused the manipulator, on startup, to adopt the starting position as its new zero position. The sudden jump in the mean is therefore due to this change in the zero position and can clearly be seen from the mean values in the first half of sample five's data compared to the second half. Furthermore, the macro recording to automatically measure the manipulator cylinders was based on Sample 1's positioning. This caused the probe shaft to touch the cylinder at times during the new positioning and resulted in a changed standard deviation.

Still, in sample sets '1 to 4' and '6 to 11' it is apparent that the manipulator is repeatable with a maximum standard deviation of 0.38°. This, however, is only the case if the position obtained by the short arm is found using the same path followed previously. This path-dependency factor is made clear in Figure 52 and Table 6 when comparing '35 Ext' and '20 Ext' to '35 Flex' and '20 Flex' respectively. It shows in both cases that even though the motor output shaft position is the same, the position of the short arm measured differed by up to 7°. This hysteresis error is believed to be caused by the friction exerted on the cable by its various contact points and therefore cause the cable to stretch. Figure 53 shows the hysteresis error of the short arm for its whole range of deflection for the different sample sets defined in Table 6.

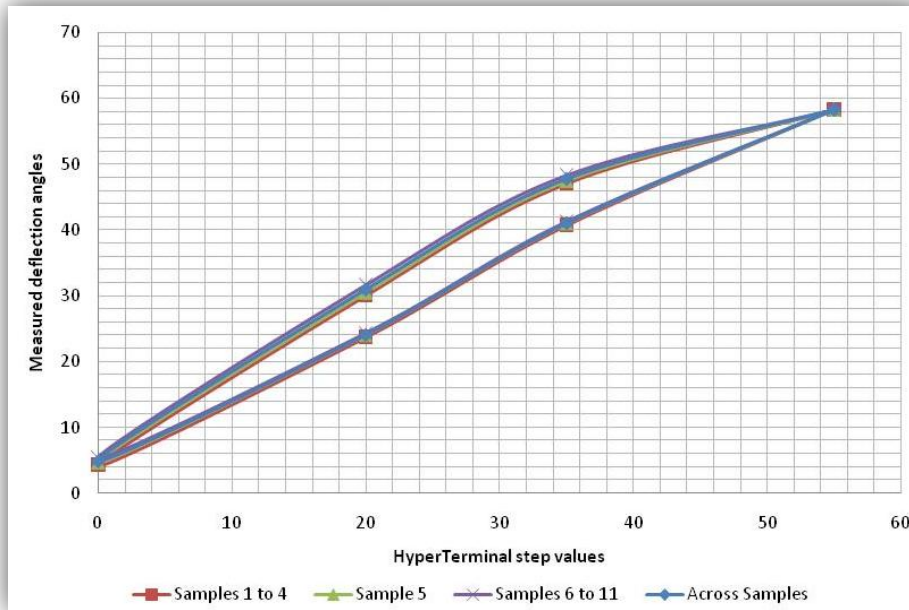


Figure 53: Short arm hysteresis error

Table 7 shows the mean and standard deviation values for the previously defined sample sets for the long arm. The table illustrates yet again that a change of about 0.3° in the mean occurred between sample sets ‘1 to 4’ and ‘6 to 11’ while the standard deviation values are similar for the different positions. The standard deviation within sample sets are near negligible and proves the repeatability of the long arm for a given path followed to a particular point.

A small hysteresis error is also noticed from the data shown in Table 7. This is believed to be due to backlash between the 28 tooth spur gear and the 84 tooth internal spur gear and can be eliminated by setting higher tolerances for the gear teeth or some other method to minimize backlash.

Table 7: Mean and standard deviation for long arm

Position	Sample 1 to 4		Samples 5		Sample 6 to 11		Across all Samples	
	Mean	Std. dev.	Mean	Std. dev.	Mean	Std. dev.	Mean	Std. dev.
0	0.97	0.18	1.05	NA	1.36	0.04	1.19	0.22
45	14.95	0.01	14.95	NA	15.27	0.01	15.13	0.17
90	29.91	0.01	29.93	NA	30.25	0.01	30.09	0.18
135	44.91	0.01	44.92	NA	45.25	0.003	45.098	0.177
180	59.88	0.01	59.89	NA	60.21	0.006	60.059	0.169
135	45.58	0.01	45.87	NA	45.88	0.01	45.77	0.16
90	30.52	0.01	30.85	NA	30.85	0.01	30.73	0.17
45	15.55	0.01	15.86	NA	15.86	0.01	15.75	0.16
0	0.57	0.01	0.88	NA	0.88	0.01	0.77	0.16

2. Manipulator Strength Test Experiment

A manipulator strength test was done to prove that the designed PSM is strong enough to perform the necessary tasks during a typical MIS procedure. One of the design requirements was that the manipulator should resist a 10 N opposing force at the manipulator tip. Also, from the literature (de Visser *et al.*, 2002), a gripping force of at least 5 N is needed during an MIS procedure for grasping a needle during suturing or pulling and stretching tissue.

During the experiment, the intention was not to find the maximum opposing or gripping force, but rather to prove that it is able to at least reach the minimum. The reason for this was because there was no real way to quantify how successfully the manipulator was able to oppose a certain force. It either could or it couldn't. Also, due to the expense of the manipulator, the author did not want to break the cables and possibly damage the components while trying to oppose forces which are much higher than what can be expected during an MIS procedure.

2.1 Experimental Setup

The experimental setup for the strength test is shown in Figure 54. It consisted of the manipulator placed securely on two V-blocks, initially with the revolute joint deflected and the distal part showing upwards, more or less parallel with the vertical plane. The revolute joint was then moved to its extended position to tie a 200 g weight (2 N) to the tip using a thin nylon cable. The revolute joint was then flexed and then extended. The weight was then increased to 500 g (5 N) and the revolute joint flexed and then extended again. This was repeated for an 800 g weight (8 N) and a 1 kg weight (10 N).



Figure 54: Manipulator Strength Test Experimental Setup

The weights were then loosened and the manipulator was rotated so that the deflected revolute joint's distal part was parallel with the horizontal plane. A 200 g weight was then tied again to the tip, but this time the manipulator's long arm was rotated about its own axis to lift the weight as it turned. This was repeated for the 500 g, 800 g and 1 kg weights as well. The manipulator was then again rotated (with the weights untied) such that the deflected revolute joint's distal part showed downward, parallel to the vertical plane. The weights were then tried with the manipulator moving from a deflected position to an extended position repeatedly. Again, the 200 g, 500 g, 800 g and 1 kg weights were used. A combination of the weights shown in Figure 55 made up the desired weights to be applied.



Figure 55: Strength test weights

During the experiment it was realized that a gripping force could not be measured, due to the gripper jaws not being able to close completely. This was because, the jaws used were intentionally designed that way to hold a needle. Even though this was known while designing the gripper, this experiment was not considered during the design.

2.2 Results and Discussion

During the experiment, there was no real way to quantify how successfully the manipulator was able to oppose a force applied at the tip of the manipulator. Therefore, it was marked that it either could or it couldn't oppose the tip force and any additional observations were noted. Appendix F shows the results in a tabular form.

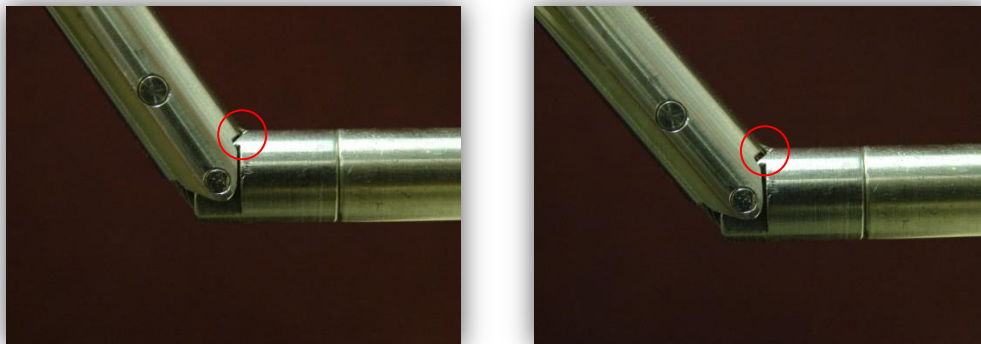


Figure 56: Strength test deflection moving from extension to flexion

One observation made during the experiment was that when the manipulator was in its extreme flexion position, the distal part did not move right up against the proximal part's chamfer anymore as shown in Figure 56. Figure 56 (left) shows the manipulator with a 200 g weight and Figure 56 (right) shows the manipulator with a 1 kg weight hanging vertically downwards. This was also noted when the deflected manipulator was facing downwards and the weights were being lifted with the manipulator moving from a deflected position to an extended position. Figure 57 shows the 'error' in position due to the applied weight at the tip.

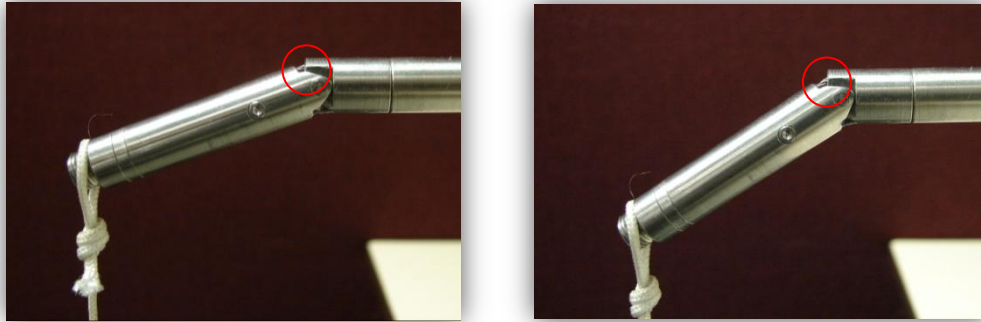


Figure 57: Strength test deflection moving from flexion to extension

The reason for this 'error' in position is due to the increased weight at the tip, causing an increased tension in the cables manipulating the revolute joint, therefore causing these cables to stretch. From the cable strength test (see Appendix A) it was shown that the cable's ultimate tensile strength is approximately 1000 N and can stretch approximately 2% before breaking.

It was also noted during the experiment that there was a slight deflection of the long arm and this was also due to the weights being placed at the tip of the manipulator.

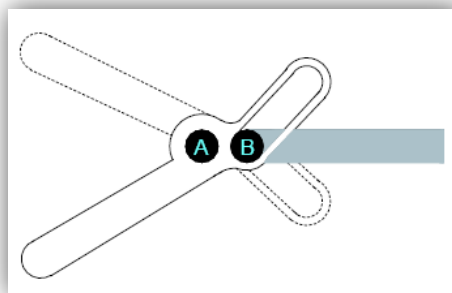


Figure 58: Drawing of the Gripper jaws and the drive rod (Peeters, 2002)

As mentioned in the experimental setup section, the gripping force was not found due to the nature of the gripper jaws. However, the gripping force can be calculated using the maximum tensile force in the revolute joint's manipulation cables from the weights applied at the tip and using this force to determine what the theoretical gripping force will be according to Peeters (2002). Figure 58 shows that the jaws rotate about point A and point B moves within the slots in the jaws, causing the gripper jaws to close. The

gripper force can be calculated through finding the resulting torque at point A due to the applied force at point B.

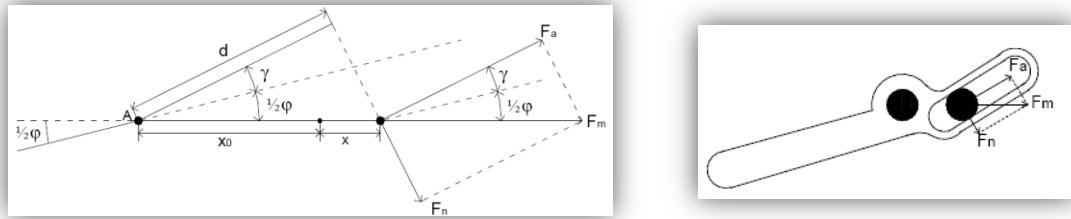


Figure 59: Force factorisation for the torque balance

From the gripper jaws used, the variables of the motion mechanism as from Peeters (2002) are as shown in Table 8.

Table 8: Variables of gripper motion mechanism

Variable	Value
x_{max}	5 mm
x_0	2.25 mm
φ_{max}	60 mm
γ	30 mm

Using these variables, the grasping torque around point A can be calculated through the following equation (Peeters, 2002):

$$T_g = \frac{1}{2} F_m (x_0 + x) \sin(\varphi + 2\gamma)$$

Using a tensile force of approximately 115 N in the gripper actuation cable and assuming $x_{max} = 5 \text{ mm}$, the grasping torque is calculated to be an estimated 0.3 N.m; this therefore giving a 15 N gripping force at the gripper jaw tip, taking the tip to be 20 mm from the pivoting pin (or point A).

3. System Evaluation Discussion

In the repeatability study it was found that the manipulator has a 0.38° standard deviation which translates into a 0.53 mm positional error when assuming an 80 mm distal tip part length. This is thought to be adequate due to the intention of the manipulator is that it be used in simple and more frequent surgeries, leaving those more complex procedures to more sophisticated MIRS systems, such as the da Vinci. Lobontiu and Loisanca (2007) showed that the da Vinci has a $220 \mu\text{m}$ mean error on three subjects with eight touches each and a $150 \mu\text{m}$ standard deviation on a beating target. The repeatability study also showed that the designed PSM has a 7° hysteresis error (or 9 mm positional error) and this is thought to be due to friction on the cable, therefore causing it to stretch. The gearhead's output shaft therefore moves to its desired position

while the manipulator's end effector does not. This positional error cannot be necessarily countered automatically by the control electronics due to there being no positional feedback from the end effector (open loop system) but can, instead, be countered by the surgeon through visual feedback and moving the end effector till it reaches the desired position.

During the strength test experiment it was found that the manipulator is able to resist a 10 N opposing tip force. However, the manipulator showed an increased positional error with increased applied opposing tip force. This was again due to the cables stretching, but in this case it was believed that a larger torque had to be produced at the revolute joint pivoting axis to lift the weights, therefore causing an increased tension in the cables rather than friction. This could again be countered through the visual feedback by the surgeon but with the increase in force at the tip, the tension in the cable may become large enough to damage or break the cable (although, current sensing should be implemented) permanently. Therefore, a cable tension force limit should firstly be programmed into the firmware, using current sensing, to safe keep the cables from breaking. Also, by implementing a small positional sensor into the revolute joint to allow the tip force to be calculated using the tensile force in the cable and the joint position would also prove beneficial.

A theoretical gripping force of 15 N was also calculated (a 115 N force in the actuation cable was assumed) using Peeters' (2002) gripper models and equations. This is much more than that suggested by de Visser *et al.* (2002) and that which Jaspers *et al.* (2004) accomplished with his passive mechanical manipulator (5 to 8 N). The da Vinci has a programmed gripping force of 1 N (Lehman *et al.*, 2007).

In conclusion, the experimental tests show that the manipulator could possibly perform the basic tasks in typical MIS procedures, considering only the repeatability and strength of the manipulator, however, before any such procedure can be done, many improvements should be done first. Friction on the cables must be reduced to reduce the hysteresis error in free movement. Positional feedback from the wrist joints and current feedback from the motors to determine cable tensile strength should also be implemented to further prevent the hysteresis errors in free movement and when an opposing tip force is applied. Through the current feedback ability, a cable tensile force limit can be implemented programmatically to prevent the cable and other parts being damaged. Furthermore, having the ability to measure the force in the cable, the gripping force can be limited and tactile feedback for the surgeon can be implemented at a later stage.

Chapter 6: Conclusion and Recommendations

Minimal invasive surgery benefits patients by giving surgeons the ability to work through only a few small incisions made in the patient's skin. Conventional instruments used in MIS are, however, constrained through having limited dexterity and are subjected to the fulcrum effect. Two-dimensional visualization also deprives the surgeon from hand-eye coordination and depth perception. Surgical robotics attempt to alleviate these drawbacks through increased manoeuvrability inside the operating cavity, eliminating the fulcrum effect and providing the surgeon with 3D visualization.

Existing MIRS systems are, however, hugely expensive and in some instances require the employment of additional staff to continually calibrate and clean the system. Therefore, even though MIRS systems reduce the time spent in the operating room compared to conventional MIS instrumentation, overhead costs involved in maintaining an MIRS system makes the 'per procedure' cost comparable to that of when using conventional MIS instrumentation. This alone causes many medical centres to discard the idea of obtaining such an expensive MIRS system and continue using conventional MIS instrumentation, accepting their related drawbacks.

This thesis therefore presents a new seven DOF manipulator for minimal invasive surgery applications. The scope included:

- focusing on the multi-DOF wrist of the manipulator → The four DOF PSM (with its multi-DOF wrist) is attached to a secondary slave manipulator (see Figure 12 (left) as an example), giving the PSM a further three DOF. It must be made clear that the SSM was not part of this thesis.
- designing the control electronics, which is used mainly to prove the manipulators functionality and do the repeatability and strength test experiments
- ignoring sterilizability in this stage of the design

The successfully designed manipulator is actuated through using five DC motors to wind up cables onto reels to ultimately manipulate the four DOF wrist. The further three DOF are made possible through the secondary slave manipulator. Figure 21 shows the PSM with its multi-DOF wrist. The control electronics used to drive the 12 VDC brushed motors include five slave PIC18f2431 microcontrollers with their Power Control PWM module and Motion Control Module to control the five L6225 H-Bridges which in turn drives the motors. A PIC18f2550 is used to receive instructions (via RS-232) from a PC-based host controller and send these instructions (using an I2C 2-wire bus) to the relevant slave(s). Appendix E, Section 4, shows some images of the control electronics' PCBs.

Two experimental tests were performed to determine the feasibility of the manipulator with respect to the preset manipulator specifications and the literature. The experiments were the repeatability test and the strength test. The repeatability study done on the manipulator showed that the manipulator is able to find the same position again and again (0.38° standard deviation or 0.53 mm positional error); but this depends on the path followed to find the same position again. This hysteresis error caused by the manipulator's path dependency was found to be nearly 7° which translates into a 9 mm positional error. It must be noted that this is an "unloaded" error.

The strength test experiment demonstrated that the manipulator is able to oppose a 10 N opposing tip force, although, in doing so a positional error occurred due to the applied weight at the tip. A theoretical gripping force of 15 N was also determined. In summary, the experimental tests show that the manipulator is at least repeatable and is able to resist and produce the necessary forces needed in a typical MIS procedure. However, before any such procedure can be done, a number of improvements must be made. For instance, friction on the cables must be reduced, positional feedback from the wrist should be considered and current sensing for the motors to determine the tensile force in the cables must be implemented. These improvements alone should reduce the hysteresis or positional error and in so doing prevent any damage to the components. Visual feedback will also help in that the surgeon can correct any positional error. Auto-calibration of the manipulator and even tactile feedback can also be implemented in the future.

The cost of the manipulator developed was determined to be R45000 for the making of the mechanical parts, R25000 for the five motors and R4000 for the control electronics, giving a total PSM cost of R74000. This is thought to still be relatively inexpensive for just the PSM but the cost can be reduced even more when in high production.

The strengths of the developed PSM are:

- Seven degrees of freedom (four DOF multi-DOF wrist, further three DOF are made possible through SSM), giving the surgeon more dexterity.
- Fulcrum effect can be eliminated through the firmware in the SSM when translating the movements of the master manipulator (controller with which the surgeon controls the slave manipulators).
- The manipulator consists of few parts made locally which are relatively easily assembled.
- The control electronics' firmware is easy to update to incorporate and make many improvements. Each slave microcontroller is responsible for its directly related tasks, therefore preventing other slave malfunctions to influence other slaves. The master keeps backups of each slave and can restart them when and if they malfunction to reload their data.
- The multi-DOF wrist is repeatable with a maximum standard deviation of 0.38° .
- The manipulator is capable of resisting high opposing tip forces and has a large theoretical gripping force compared to other manipulators.

- The prototype is thought to be relatively inexpensive and should be even more so when it is in high production using different, more economical manufacturing techniques e.g. moulding, using CNC machines and even using rapid prototyping machines to grow certain parts.

Limitations and weaknesses which were identified are:

- The cables are long and stretch up to 2% of the cable length, causing positional errors due to friction on the cables.
- The hysteresis error caused by the friction on the cables and the positional errors caused when applying opposing forces at the end effector tip, are major limitations, especially if no current sensing and positional feedback from the wrist is not implemented. Visual feedback to the surgeon may help this limitation to some extent, but will not eliminate it completely.
- The manipulator is not sterilisable at this stage and with the closed form factor and the woven cables used, cleaning of the manipulator may be very difficult.

Ongoing and Future work

In the future, a newly designed manipulator should be developed to reduce friction on the cable as well as incorporate the ability for the manipulator to be sterilized. Physically smaller motors with smaller gear reduction ratios which are capable of lower output torques should also be considered. This will then allow for current sensing to be implemented, allowing for auto-calibration and possibly even tactile feedback of the manipulator.

Furthermore, different tool tips for the manipulator should be designed to allow the surgeon to do all the different tasks necessary in a typical MIS procedure. Lastly, the rest of the MIRS system must be developed and tested extensively before starting the animal and human trials.

References

1. Ballantyne, G. H. (2002). Robotic surgery, telerobotic surgery, telepresence, and telemonitoring. *Surgical Endoscopy*, Vol. 12(1), pp.6-16.
2. Cavusoglu, M. C., Williams, W., Tendick, F., and Sastry, S. S. (2001). Robotics for Telesurgery: Second Generation Berkley/UCSF Laparoscopic Telesurgical Workstation and Looking towards the Future Applications. *In: In Proceedings of the 39th Allerton Conference on Communication, Control and Computing, 2001*. Monticello, IL.
3. Craig, R. R. (2000). *Mechanics of Materials*. USA: John Wiley & Sons Inc.
4. Davies, B. (2000). A review of robotics in surgery. *Proc Inst Mech Eng*, Vol. 214, pp.129-140.
5. de Visser, H., Heijnsdijk, E., and Herder, J. (2002). Forces and displacement in colon surgery. *Surgical Endoscopy*, Vol. 16, pp.16-20.
6. Diks, J., Jaspers, J., Wisselink, W., de Mol, B., and Grimbergen, C. (2007). The mechanical master-slave manipulator: an instrument improving the performance in standardized tasks for endoscopic surgery. *Surgical Endoscopy*, Vol. 21, pp.1025-1031.
7. Enderle, J. D., Blanchard, S. M., and Bronzino, J. D. (2005). *Introduction to Biomedical Engineering*. Burlington: Elsevier.
8. Funda, J., Gruben, K., Eldridge, B., Gomory, S., and Taylor, R. (1995). Control and evaluation of a 7-axis surgical robot for laparoscopy. *In: 1995 IEEE International Conference on Robotics and Automation, 1995*. Nagoya, Japan:, pp.1477-1484.
9. Gilbertson, R. G. and Busch, J. D. (1996). A survey of Micro-Actuator Technologies for the future spacecraft missions. *The Journal of the British Interplanetary Society*, Vol. 49, pp.129-138.
10. Greeff, G. P. (2007). *The Determination of the Forces Involved in Minimally Invasive Surgical Operations*. Stellenbosch: University of Stellenbosch.
11. Heemskerk, J., Zandbergen, R., Maessen, J. G., Greve, J. W. M., and Bouvy, N. D. (2006). Advantages of advanced laparoscopic systems. *Surgical Endoscopy*, Vol. 20, pp.730-733.
12. Hockstein, N. G., Gourin, C. G., Faust, R. A., and Terris, D. J. (2007). A history of robots: from science fiction to surgical robotics. *Journal of Robotic Surgery*, Vol. 1, pp.113-118.
13. Howe, R. D. and Matsuoka, Y. (1999). Robotics for Surgery. *In: Annual Review of Biomedical Engineering, 1999*. Annual Reviews, pp.211-240.

14. Intuitive Surgical Inc. (2007). *The da Vinci Surgical System*. [online]. [Accessed 8 February 2007]. Available from World Wide Web: <http://www.intuitivesurgical.com/products/davinci_surgicalsistem/index.aspx>
15. Jaspers, J. 2005. *Manipulator for an instrument for minimal invasive surgery and such an instrument*. 0119641 A1.
16. Jaspers, J., Shehata, M., Wijkhuizen, F., Herder, J., and Grimbergen, C. (2004). Mechanical manipulator for intuitive control of endoscopic instruments with seven degrees of freedom. *Minimal Invasive Theroscopy and Allied Technologies*, Vol. 13(3), pp.191-198.
17. Kingsnorth, A. N. and Majid, A. A. (2006). *Fundamentals of Surgical Practice*. Cambridge University Press.
18. Kobeissi, I. (2004). *Noise Reduction Techniques for Microcontroller-Based Systems*. Freescale Semiconductor Inc.
19. Kode, V., Cavusogle, M., and Azar, M. (2005). Design and Characterization of a Novel Hybrid Actuator Using Shape Memory Alloy and DC Motor for Minimal Invasive Surgery Applications. In: *IEEE International Conference on Mechatronics and Automation, 2005*. Niagara Falls, Canada.
20. Kode, V. and Cavusoglu, M. (2007). Design and Characterization of a Noval Hybrid Actuator Using Shape Memory Alloy and DC Micro-Motor for Minimal Invasive Surgery Applications. *IEEE/ASME Transactions on Mechatronics*, Vol. 12(4), pp.455-464.
21. Kwoh, Y. S., Hou, J., and Jonckheere, E. A. (1988). A robot with improved absolute positining accuracy for CT guided stereotactic brain surgery. *IEEE Transactions on Biomedical Engineering*, Vol. 35, pp.153-161.
22. Lanfranco, A. R., Castellanos, A. E., Desai, J. P., and Meyers, W. C. (2004). Robotic Surgery: A Current Perspective. *Annals of Surgery*, Vol. , pp.239:14-21.
23. Lawrence, C. L., Panting, G., and Raine, M. (2002). *An introduction to Dermatological Surgery*. Elsevier Health Science.
24. Lee, Y.-J., Kim, J., Ko, S.-Y., Lee, W.-J., and Kwon, D.-S. (2003). Design of a Compact Laparoscopic Assistant Robot : KaLAR. In: *ICCAS2003, 2003*. Gyeongju, Korea.
25. Lehman, A. C., Rentschler, M. E., Farritor, S. M., and Oleynokov, D. (2007). The current state of miniature in vivo laparoscopic robotics. *Journal of Robotic Surgery*, Vol. 1, pp.45-49.
26. Lobontiu, A. and Loisanse, D. (2007). Robotic Surgery and Tele-Surgery: Basic principles and description of a noval concept. *Jurnalul de Chirurgie*, Vol. 3(3), pp.208-214.

27. Martini, F. H. and Bartholomew, E. F. (2007). *Essentials of Anatomy & Physiology*. California, United States of America: Pearson Education.
28. Mediflex. (2006). *System Overview: Modular Laparoscopic Instrument System*. [online]. [Accessed 1 February 2007]. Available from World Wide Web: <<http://www.mediflex.com/system-overview.asp>>
29. Morley, T. A. and Wallace, D. T. 1994. *Roll-pitch-roll surgical tool*. 6902560.
30. NJCPCU. (2006). *Minimally Invasive Robotic Surgery*. [online]. [Accessed 1 February 2007]. Available from World Wide Web: <http://www.roboticurology.com/minimally_invasive_robotic_surgery.htm>
31. Ortmaier, T. (2003). *Concepts for an advanced (tele-) surgical robot system*. [online]. [Accessed 1 February 2007]. Available from World Wide Web: <<http://www.lirmm.fr/manifs/UJEE/docs/slides/Ortmaier.pdf>>
32. Pattenale, P. (2004). *Tasks for Veterinary Assistant*. Blackwell Publishing.
33. Peeters, J. M. (2002). *Medical robotics: A SMA actuated laparoscopic forceps with force feedback*. Eindhoven: University of Technology.
34. Peirs, J., Reynaerts, D., and van Brussel, H. (1999). A Miniature Hydraulic Parallel Manipulator for Integration in a Self-Propelling Endoscope. *In: The 13th European Conference on Solid-State Transducers, 1999*. Hague, Netherlands:, pp.753-756.
35. Peirs, J., Reynaerts, D., and van Brussel, H. (2000). A Miniature Manipulator for Integration in a Self-Propelling Endoscope. *In: The 14th European Conference of Solid-State Transducers, 2000*. Copenhagen, Denmark:, pp.309-312.
36. Reynolds, W. (2001). The First Laparoscopic Cholecystectomy. *Journal of the Society of Laparoendoscopic Surgeons*, Vol. 5, pp.89-94.
37. Ruurda, J. P.-H. (2003). *Robot-assisted endoscopic surgery*. Netherlands: University Utrecht.
38. Satava, R. (2006). *The early chronicles: a personal historical perspective*. [online]. [Accessed 2 February 2007]. Available from World Wide Web: <<http://www.websurg.com/ref/doi-ed01en0021.htm>>
39. Schur, M. O., Buess, G. F., Neisius, B., and al., e. (2000). Robotics and telemanipulation technologies for endoscopic surgery: a review of the ARTEMIS project. *In: Surgical Endoscopy, 2000.*, p.375–381.
40. Seibold, U., Kuebler, B., and Hirtzinger, T. (2005). Prototype of Instrument for Minimal Invasive Surgery with 6-Axis Force Sensing Capability. *In: IEEE International Conference on Robotics and Automation, 2005*. Barcelona, Spain: IEEE.
41. Shammas, E. A., Wolf, A., Brown, H., and Choset, H. (2003). New Joint Design for Three-dimensional Hyper Redundant Robots. *In: International Conference on Intelligent Robots and Systems., 2003.*, pp.3594 - 3599.

42. Shigley, J. E., Mischke, C. R., and Budynas, R. G. (2004). *Mechanical Engineering Design*. Singapore: McGraw Hill.
43. Shin, W.-H., Ko, S.-Y., and Kwon, D.-S. (2006). Design of a Dextrous and Compact Laparoscopic Assistant Robot. *In: SICE-ICASE International Joint Conference, 2006*. Bexco, Busan, Korea:, pp.233-237.
44. Sim, H. G., Yip, S. K. H., and Cheng, C. W. S. (2006). Equipment and technology in surgical robotics. *World Journal of Urology*, Vol. 24, pp.128-135.
45. Smith, S. T. and Seugling, R. M. (2006). Sensor and actuator considerations for precision, small machines. *Precision Engineering*, Vol. 30, pp.245-264.
46. Trueforce. (2004). *Industry Profile: Computer Motion Inc.* [online]. [Accessed 8 February 2007]. Available from World Wide Web: http://trueforce.com/Medical_Robotics/Medical_Robotics_Companies/aesop.htm
47. Yamashita, H., Kim, D., Hata, N., and Dohi, T. (2003). Multi-Slider Linkage Mechanism for Endoscopic Forceps Manipulator. *In: Conference on Intelligent Robots and Systems, 2003*. Las Vegas:, pp.2577-2582.
48. Yamashita, H., Matsumiya, K., Masamume, K., Liao, H., Chiba, T., and Dohi, T. (2006). Two-DOFs Bending Forceps Manipulator of 3.5 mm diameter for Intrauterine Fetus Surgery: Feasibility Evaluation. *International Journal of Computer Assisted Radiology and Surgery*, Vol. 1(1), pp.218-220.

Appendix A: Cable Tension Test

A tendon mechanism or cable actuating technique was proposed to actuate the wrist joints. In concept, it was thought that the cable would be fixed to the wrist joints and would then extend up a $\varnothing 10$ mm tube or pipe with a 1 mm wall thickness. The cable would then be wound around a reel which when turned would wind up the cable. It was thought that the tool tip should resist a 10 N opposing tip force. Therefore, if the tool tip is 100 mm long (from the end point to the rotation axis) and the moment arm is roughly 3.8 mm, a minimum tensile force of 263 N in the cable is required to produce the 1 Nm torque in the revolute joint.

The experiment serves to test the cable's tensile strength and the methods in which it is fixed on either end. The cable, otherwise known as trace wire, used was purchased at a local sports shop for R59.00 and is rated at 220 lbs/99.79 kg (Material: Stainless Steel) with an approximated bending radius of 2 mm. The cable is made up of many thin (approximately $\varnothing 0.1$ mm) wires which are woven together to make a strong, but flexible, $\varnothing 1.1$ mm cable. A 600 mm long cable was used during the experiment.

1. Experimental Setup

The tensile test rig was used during the experiment with a load cell attached to the top check. The apparatus shown in Figure 60 will be clamped in the bottom and top checks. Figure 60 (left) shows the $\varnothing 10$ mm reel around which the cable is to be wound up on and in Figure 60 (right) the $\varnothing 3$ mm pin is shown.

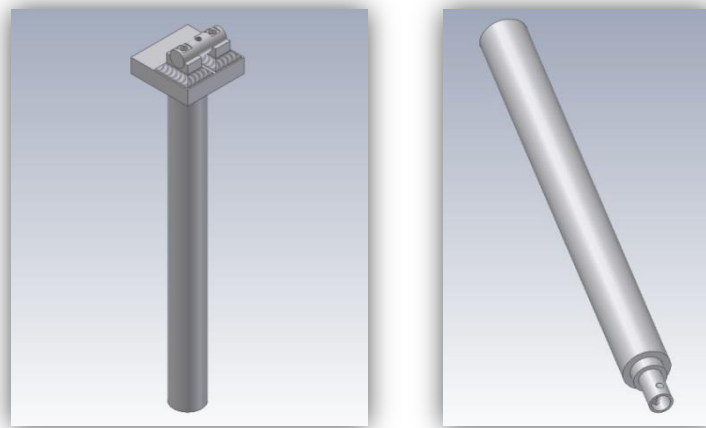


Figure 60: Cable Tension Test Apparatus

During the experiment, the cable wound around the reel, was wound up over itself to cause the cable to clamp itself when pulled tight. At the $\varnothing 3$ mm pin, the cable was wrapped around the pin and with the loose end then clamped onto the approaching cable with a $\varnothing 1.5$ mm tube. Figure 61 shows how the cable was fixed on each end; the picture on the left shows the reel and the one on the right, the pin.



Figure 61: Cable Tension Test Setup

2. Results and Discussion

During the experiment, the cable was pulled until breaking point. The HBM Spider bridge amplifier box was used to sample the tensile force and the displacement due to stretching in the cable.

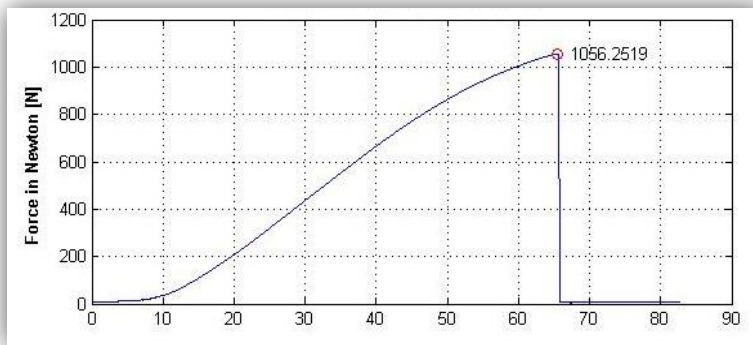


Figure 62: Force vs. Time plot for first trail

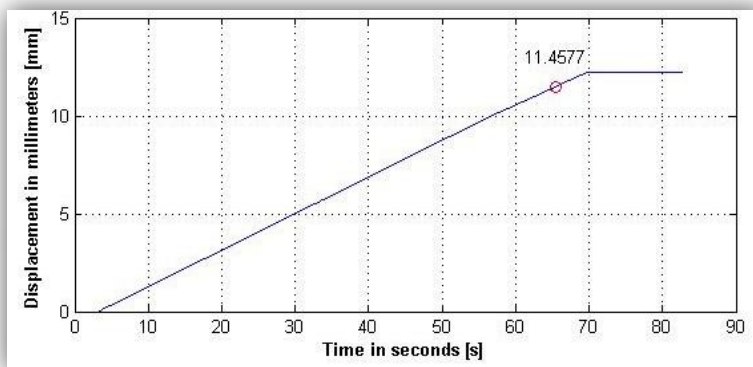


Figure 63: Displacement vs. Time plot for first trail

Figure 62 and Figure 63 show the Force vs. Time and the Displacement vs. Time plots respectively for the first trial. Red circles with the indicated values of each show the cable's breaking point. Figure 64 and Figure 65 show the results for the second trail.

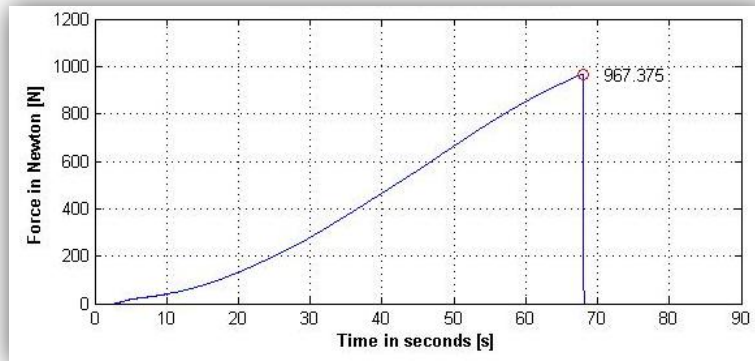


Figure 64: Force vs. Time plot for Second Trail

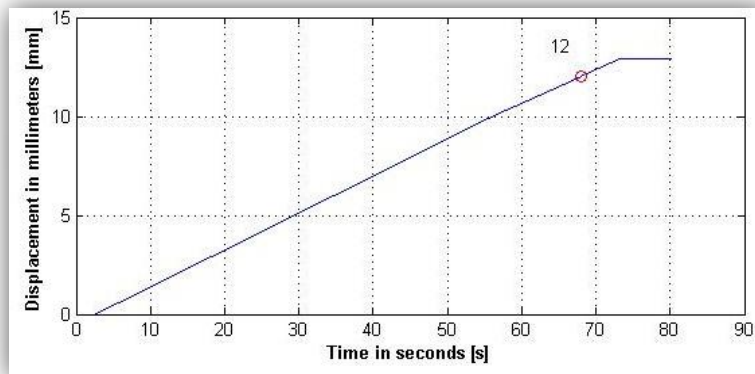


Figure 65: Displacement vs. Time for Second Trail

Although each of the above trails showed that the maximum tensile strength was approximately 1000 N (as was specified by the manufacturers), the cable did break in a third trail at 555 N. Figure 66 and Figure 67 show the third trial's associated plots. During this third trail the cable broke exactly there where it was clamped near the $\varnothing 3$ mm pin. It was therefore thought that the tube which clamped the cable may have damaged the cable when being clamped shut. Figure 66 also shows that only a few strands initially broke when reaching the 555 N peak while the rest of the strands broke only later.

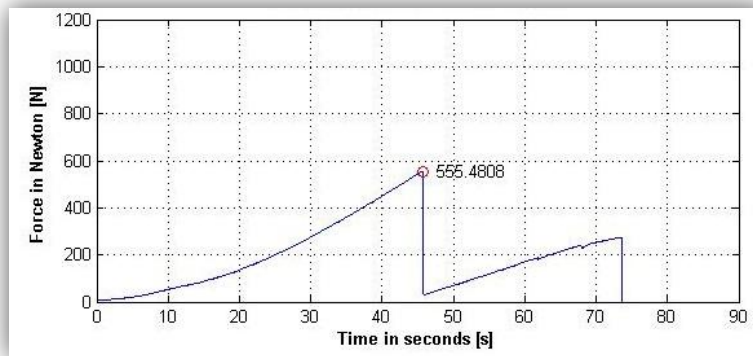


Figure 66: Force vs. Time plot for Third Trail

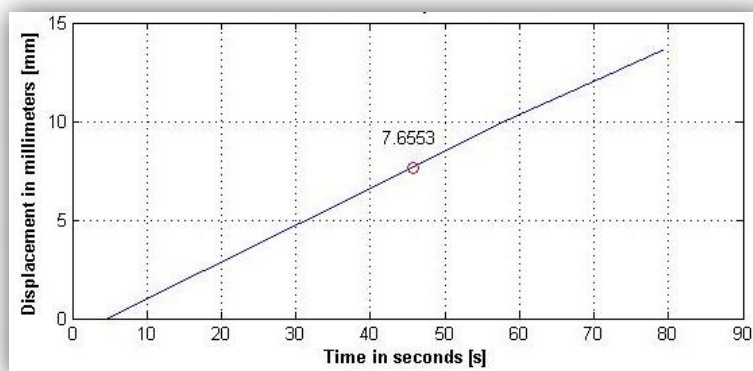


Figure 67: Displacement vs. Time for Third Trail

From the experiment it was concluded that the cable has an ultimate tensile strength of approximately 1000 N, but the method in which the cable was fixed at either end was crucial to the cable's ability to withstand high tension forces. It was also found that the cable stretches about 2% until breaking point. In this experiment, other methods of fixing the cable were not explored experimentally.

One such concept was to silver solder a ball onto the end point of the cable and pulling the cable through a hole with a size near to that of the cable's diameter. The ball would then be held back at the hole due to it being too big to go through the hole. Depending on the size of the hole, the soldered ball on the cable was able to withstand forces of up to 90 kg. This therefore gave a basic method to actuate the wrist joints and would also take up little space in the wrist. The bending radius of the cable also became less important.

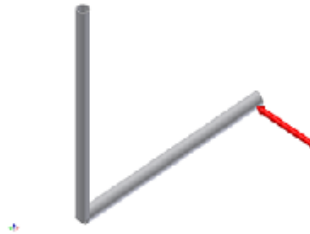
Appendix B: Basic Manipulator Calculations

1. Torsional and Bending Analysis of Manipulator

%Given parameters

$$\begin{aligned}
 d_o &:= 10\text{mm} & F_{\text{end}} &:= 10\text{N} \\
 x_1 &:= 170\text{mm} & sf &:= 1.6 \\
 x_2 &:= 150\text{mm} \\
 \tau_{\text{SS316}} &:= 515\text{MPa} & \sigma_{\text{SS316}} &:= 205\text{MPa}
 \end{aligned}$$

%Calculate the minimum inner diameter of a link as followed in (Craig, 2000) using torsional analysis. The Figure below illustrates where the force works in. The maximum torsional stress is assumed to be at the top of the link, proximal to the joint.



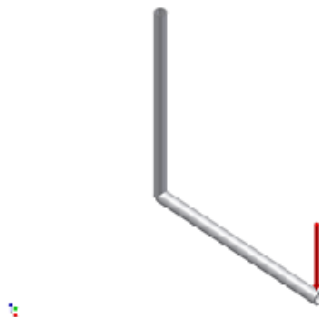
$$T_{\text{max}} := sf \cdot F_{\text{end}} \cdot x_2$$

$$T_{\text{max}} = 2.4 \text{ N}\cdot\text{m}$$

$$d_{\text{torsion}} := 2 \cdot \sqrt[4]{\left(\frac{d_o}{2}\right)^4 - \frac{T_{\text{max}} \cdot \left(\frac{d_o}{2}\right)}{\left(\frac{\pi}{2}\right) \cdot \tau_{\text{SS316}}}}$$

$$d_{\text{torsion}} = 9.94 \text{ mm}$$

%Calculate the minimum link inner diameter, following the procedure in (Craig, 2000), using the bending analysis. The Figure below shows where the force works in and it is assumed that the maximum bending will occur just next to the elbow joint, distal to that joint.



$$M_{\max} := sf \cdot F_{\text{end}} \cdot x_2$$

$$M_{\max} = 2.4 \text{ N}\cdot\text{m}$$

$$d_{\text{bending}} := 2 \cdot \sqrt[4]{\left(\frac{d_o}{2}\right)^4 - \frac{M_{\max} \cdot \left(\frac{d_o}{2}\right)}{\left(\frac{\pi}{2}\right) \cdot \sigma_{\text{SS316}}}}$$

$$d_{\text{bending}} = 9.847 \text{ mm}$$

%Calculate the minimum wall thickness

$$wt := \frac{d_o - (\max(d_{\text{torsion}}, d_{\text{bending}}))}{2}$$

$$wt = 0.03 \text{ mm}$$

2. Torsional Spring Calculations

$$d_{\text{wire}} := 0.9 \text{ mm}$$

$$N_{\text{turns}} := 6.5$$

$$D_{\text{shaft}} := 6 \text{ mm}$$

$$D_{\text{Coil_OD}} := 9 \text{ mm}$$

From Table 10-4 in Shigley *et al.* (2004) we find for SS302:

$$m_{\text{exp}} := 0.146$$

$$A_{\text{int}} := 1867 \text{ MPa} \cdot \text{mm}^{0.146}$$

$$S_{\text{ut}} := \frac{A_{\text{int}}}{d_{\text{wire}}^{0.146}}$$

$$S_{\text{ut}} = 1.896 \times 10^3 \text{ MPa}$$

$$S_y := 0.61 \cdot S_{\text{ut}}$$

$$S_y = 1.157 \text{ GPa}$$

$$D_{\text{mean}} := D_{\text{Coil_OD}} - d_{\text{wire}}$$

$$D_{\text{mean}} = 8.1 \text{ mm}$$

$$C_{\text{index}} := \frac{D_{\text{mean}}}{d_{\text{wire}}}$$

$$C_{\text{index}} = 9$$

$$K_1 := \frac{4 \cdot C_{\text{index}}^2 - C_{\text{index}} - 1}{4 \cdot C_{\text{index}} \cdot (C_{\text{index}} - 1)}$$

$$K_1 = 1.09$$

$$T_{\text{max_torque}} := \frac{\pi d_{\text{wire}}^3 \cdot S_y}{32 \cdot K_1}$$

$$T_{\text{max_torque}} = 0.076 \text{ N}\cdot\text{m}$$

Design and Development of a Minimal Invasive Surgical Robot Manipulator

Appendix B: Basic Manipulator Calculations

$$E_{SS302} := 193 \cdot \text{GPa}$$

$$\theta_c := \frac{10.8 \cdot T_{\text{max_torque}} \cdot D_{\text{mean}} \cdot N_{\text{turns}}}{d_{\text{wire}}^4 \cdot E_{SS302}}$$

$$\theta_c = 0.341 \text{ turns}$$

$$\theta_{c_deg} := \theta_c \cdot 360$$

$$\theta_{c_deg} = 122.728 \text{ degrees}$$

$$N_{\text{active}} := N_{\text{turns}} + \frac{10\text{mm}}{3 \cdot \pi \cdot D_{\text{mean}}}$$

$$N_{\text{active}} = 6.631 \text{ turns}$$

$$k_{\text{spring_rate}} := \frac{d_{\text{wire}}^4 \cdot E_{SS302}}{10.8 \cdot D_{\text{mean}} \cdot N_{\text{active}}}$$

$$k_{\text{spring_rate}} = 0.218 \frac{\text{N}\cdot\text{m}}{\text{rad}}$$

$$\theta := \frac{T_{\text{max_torque}}}{k_{\text{spring_rate}}}$$

$$\theta = 0.348 \text{ turns}$$

$$\theta_{\text{deg}} := \theta \cdot 360$$

$$\theta_{\text{deg}} = 125.201 \text{ degrees}$$

$$D_{\text{Coil_OD_new}} := \frac{N_{\text{turns}} \cdot D_{\text{mean}}}{N_{\text{turns}} + \frac{90}{360}}$$

$$D_{\text{Coil_OD_new}} = 7.8 \text{ mm}$$

$$D_{\text{Coil_ID_new}} := D_{\text{Coil_OD_new}} - 2 \cdot d_{\text{wire}}$$

$$D_{\text{Coil_ID_new}} = 6 \text{ mm}$$

$$D_{\text{shaft}} = 6 \text{ mm}$$

Appendix C: Manipulator Concept Development

The conceptual design phase was to only look at possible methods to actuate the revolute or rotational joint. This phase was done primarily through the use of the literature study and brainstorming. Each concept, when found, was taken further until proved to not work or thought to be impractical due to know standard parts being able to achieve the same. The revolute and rotational joint concepts are described briefly.

1. Revolute joint

Three subcategories were found from all the concepts generated, namely: cable, gearing and other. The concepts were divided into these categories and described briefly while also listing each's pros and cons.

1.1 Cable

1.1.1 Pulleys (One turn)

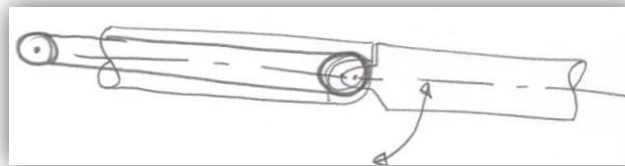


Figure 68: Pulley concept

Figure 68 shows the pulley concept generated. At the joint a pulley is fixed to the pin which holds the distal link to the proximal link. A cable or belt is wrapped around the pulley to actuate the distal link around the pin. To actuate joints distal to this joint, a 'double' pulley can be attached to the current joint and a normal pulley on the distal joint. The 'double' pulley will serve as an idler and when rotated by exterior manipulation, the second cable attached to the 'double' pulley turns and consequently turns the normal pulley on the distal joint to the current.

- Pros:
- Easy manipulation
 - Easy control
 - Easy to find link angles with sensors (perhaps with mini sensors)
- Cons:
- Cable will slip on pulley → not enough grip
 - Cable will not withstand the needed force to produce the required torque
 - Not enough space for too many pulleys on one pin → Also with the round profile, the space gets less on the sides
 - Pin would also have to be relatively big to withstand big forces
 - Small parts are expensive to manufacture

1.1.2 Pulleys (Multiple turns)

To increase the grip of the cable on the pulley, the cable can be wound around a reel type pulley to increase the contact surface area between the cable and pulley.

Pros: Greater torques are possible

Cons: Bigger pulleys or reels are needed and therefore more space at each joint
Cable will also probably not hold the required force
Pin would also have to be big to withstand big forces
Small parts are expensive to manufacture

1.1.3 Ball-'n-Chain

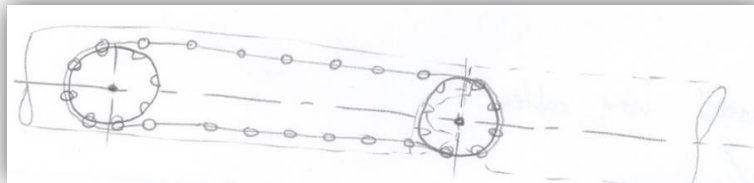


Figure 69: Ball-'n-Chain concept

Similarly to the pulley concept, Figure 69 shows a belt with equa-distant balls fixed to it which mesh with machined holes or gaps in the pulley to achieve better grip and therefore produce greater torques.

Pros: Higher torques are achievable

Cons: Manufacturing process for the 'chain' would need to be designed
Manufacturing of chain would be expensive due to the very small tolerance needed
Cable will not hold the large forces needed to produce the required torque

1.1.4 Pneumatic piston

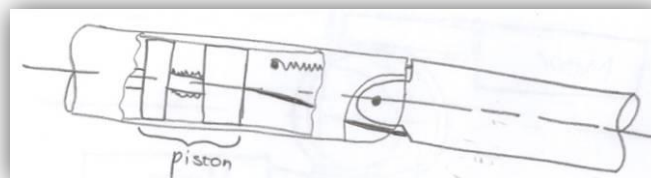


Figure 70: Pneumatic piston concept

Figure 70 shows the pneumatic piston. When expanded, the piston will pull the cable to manipulate the distal link about the pin which holds the distal link to the proximal link. The pin will produce an opposing moment about the pin to actuate the distal link in the opposite direction about the pin. The piston would therefore need to oppose the moment produced by the spring and by any external forces exerted on the link.

Pros: Simple concept

Cons: Large pressure is needed to produce the required linear force
Spring would also need to be very stiff and probably expensive
Pin would have to withstand large forces

Large wall thicknesses are needed due to large pressure

1.1.5 Magnets in series

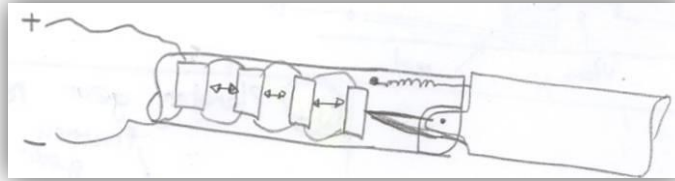


Figure 71: Magnets in series concept

Alternatively to the pneumatic piston, ferrous metal blocks can be placed in series (see Figure 71) and used to produce a linear force. When a current is induced into the blocks a magnetic attraction force will be created and cause the blocks to attract each other, consequently producing a linear force. The block on the left most side in Figure 71 will be fixed to the link to produce a force in the direction to the left.

Pros: Relatively simple mechanism

Cons: Large currents will be needed, making it very dangerous for invasive surgery
Small linear forces will be produced relative to what would be needed

1.1.6 Spur gear runner

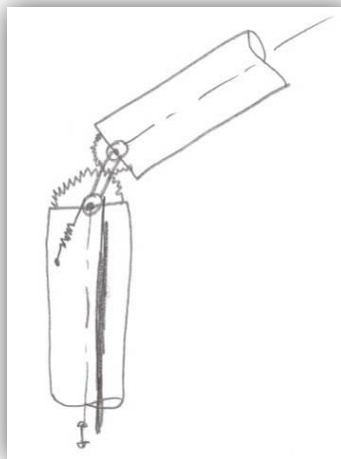


Figure 72: Spur gear runner concept

A cable is pulled which actuates an intermediate link, consequently causing the distal link to run on a gear, around the gear on the proximal link (shown in Figure 72). A spring is used to oppose this moment and actuate the link in the opposite direction to that of the cable.

Pros: Simple operating principle

Easy to determine distal link position or angle with respect to proximal link

Cons: Large force in cable would be necessary

Large spring to produce an equivalent moment about the pin is needed

Pin would need to withstand large forces exerted on it

1.1.7 Spring joint, cable actuated

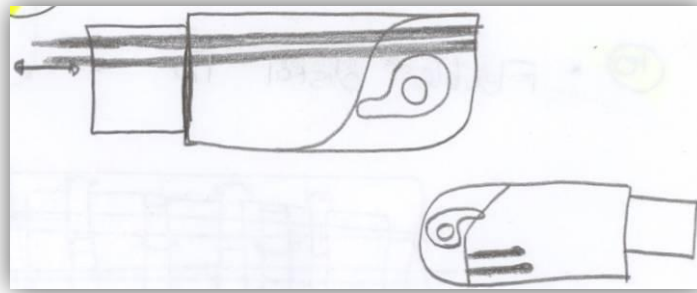


Figure 73: Spring joint, cable actuated concept

One or two cables can be attached to the distal link as shown in Figure 73 to produce a moment about the pin. A torsional spring placed in the joint (see Figure 73), around the pin, would allow the joint to oppose the moment produced when pulling the cable and therefore actuate the joint in the opposite direction to the movement produced by the cables.

- Pros: Built-in spring to allow the link to move back to its initial position using a torsion spring
- Cons: Limited space for more cables to actuate distal joint to this joint
All cables for distal joint would influence this joint
Torsional spring would need to be large to produce a large enough moment
Pin would need to withstand large linear and moment (due to the joint type/design) forces

1.1.8 Three-link joint

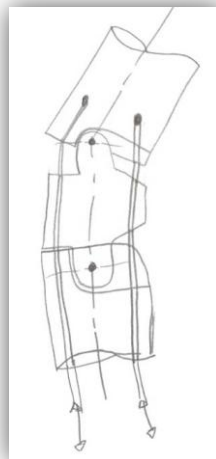


Figure 74: Three-link concept

The joint consists of three parts (see Figure 74): the proximal (bottom part in Figure 74), intermediate and distal part. The cable is guided through small holes as shown in the figure. The holes of the proximal and the distal do not line up with the intermediate part when they are placed in a straight line. For this reason, when the cable on the right is pulled, it produces a force normal to the contact area on the intermediate part,

consequently producing a force which then creates a greater moment around the pin between the proximal and intermediate parts. As the joint bends, the normal force becomes larger and creates a bigger moment (assuming that the pulling force on the cable stays the same). The moment at the pin between the intermediate and the distal part will however be equal to the force in the cable times the perpendicular distance of the cable from the pin.

Pros: Larger torques are possible

Cons: Large forces are needed in the cables

Pins would need to withstand the forces exerted on it

The moment on the second (upper) pin will be the same of just exerting a large force at a small perpendicular distance

1.2 Gearing

1.2.1 Worm gear

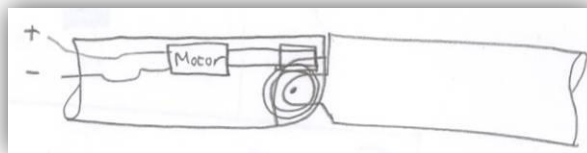


Figure 75: Worm gear concept

A small motor is attached to the side of the link as shown in Figure 75. A worm is attached to the output of the small motor that meshes with the worm gear. The worm gear is fixed to the pin which holds the distal and proximal links with respect to the joint (Peirs *et al.*, 2000).

Pros: Easy mechanism

Easy to determine position and angle of distal link relative to the proximal link'

Cons: The motor can only produce a small torque, even with a gearhead

Gear teeth may not hold the torque necessary

1.2.2 Double worm gear

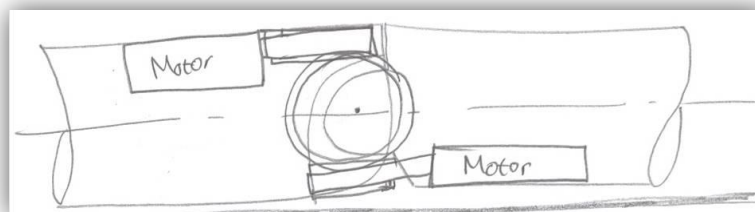


Figure 76: Double worm gear concept

To possibly increase the torque, two worm gears can be implemented. The motors can be placed as shown in Figure 76 and drive the same worm gear.

Pros: Larger torque would be produced compared to single worm gear

The torque required would be divided between the 2 motors

The forces would then also be divided between the 2 worms

- Cons: Torque produced would still be too small
Controlling the two motors could be complicated

1.2.3 Worm gear with big motor

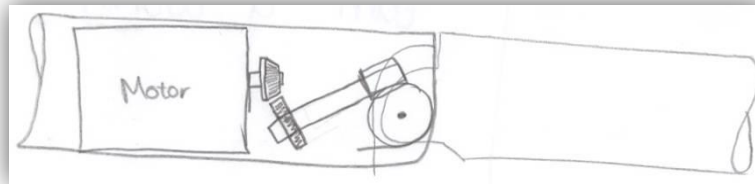


Figure 77: Big motor worm gear concept

A bigger motor which fills the space available in the link can also be used and implemented as shown in Figure 77. A bevel gear, fixed to the output shaft of the motor, would drive a spur gear which then turns the worm. The worm meshes with the worm gear to actuate the joint similarly to the worm gear mechanism with a smaller motor.

- Pros: Greater torque per motor is possible
- Cons: Gears will be very small (non-standard) and therefore expensive
The teeth may not be able to handle the forces exerted on them
The overall torque produced at the pin will still be too small

1.2.4 Bevel gear

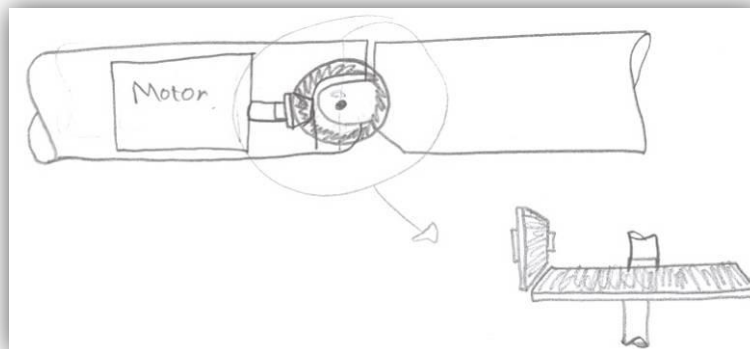


Figure 78: Bevel gear concept

Instead of a worm gear, a bevel gear can be used as shown in Figure 78. The motor would fill the space available in the link to produce the maximum torque possible in the given dimensions. A bevel pinion is used to drive the bevel gear which is fixed to the pin.

- Pros: Simple mechanism
Easy to determine the position or angle of distal link with respect to the proximal link
- Cons: Motor will not be able to produce torque required
Custom gears would need to be made → therefore expensive
Gear teeth may not be able to handle the forces exerted on it

1.3 Other

1.3.1 Pneumatic, three cylinder joint

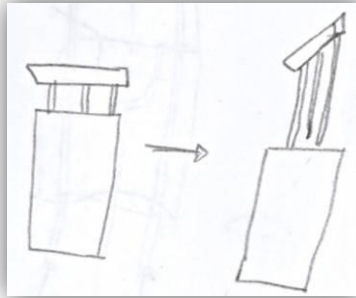


Figure 79: 3 Cylinder pneumatic joint concept

This tip is made up of a pipe in which holes are cut out to allow the pipe to bend in any direction. Figure 80 shows an example of the tip which was designed and tested by (Peirs *et al.*, 1999). The tip is manipulated by four small rods which are pushed or pulled to bend the tip in nearly any direction. Due to the tip size and the stresses in segments, only a certain amount of torque is possible.

Pros: The tip can bend in almost any direction

Cons: No, big forces can be exerted on the tip

The grasping force of the gripper should be limited

The actuation mechanism to manipulate the tip with the rods will be complicated

1.3.2 Flexible distal tip

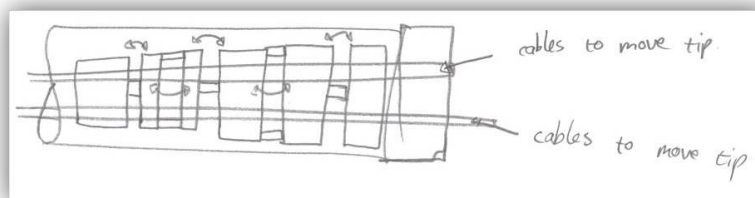


Figure 80: Flexible distal tip concept

1.3.3 Planetary gear reel for cable actuation

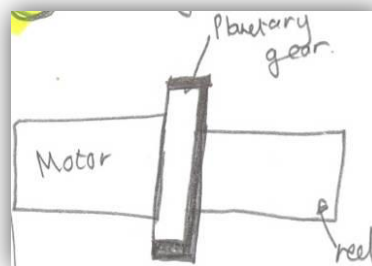


Figure 81: Planetary gear reel concept

A mechanism to pull a cable is shown in Figure 81. A motor is attached to drive a planetary gear system which turns the reel shown in the figure. The planetary gear system serves as a speed reduction and a means of increasing the torque to reel the cable in while keeping it at a certain tension.

- Pros: Basic way of winding up the cable
 High speed reduction and a means to increase torque (due to the planetary gearing system) to produce higher tensions in the cable
- Cons: Will not produce the required tension in the cable
 Two are needed, one for pulling the joint to one side and another to pull it to another side
 Due to the cable having to be perpendicular to the reel's centre line (centre line of the pipe), the overall mechanism will be too long to fit into the inner diameter of the link. It has to be placed outside the link.

1.3.4 Worm gear reel for cable actuation

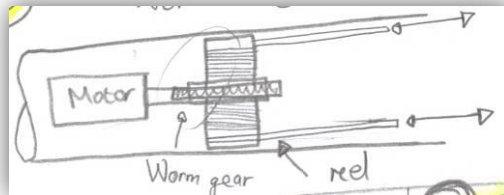


Figure 82: Worm gear reel concept

The worm gear reel mechanism shown in Figure 82 allows the cable to be reeled in on one side and another to be let go on the other side. This would allow the joint to be held firmly in a certain position and be actuated steadily.

- Pros: Can handle the actuation of a single joint in both directions
 Could be placed in link, but custom parts (gears) would be needed
 The reels on both sides do not have to be the same diameter and the cables therefore do not have to be reeled in or out the same amount
- Cons: Will not produce enough torque

2. Rotation joint

Three subcategories were found from all the concepts generated, namely: cable, gearing and other. The concepts were divided into these categories and described briefly while also listing each's pros and cons.

2.1 Cable

2.1.1 Cable rotation mechanism

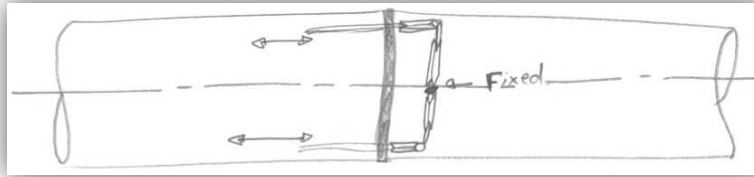


Figure 83: Cable rotation joint concept

Two cables are placed around a set of pulleys and are fixed at one point on the inside of the link as shown in Figure 83. When one of the cables are pulled and the other is released, the distal link is rotated.

Pros: Simple mechanism

Cons: Small pulleys are needed

Pins in pulleys will not hold the forces exerted on the pulley by the cable

Pulleys will be expensive to manufacture

2.2 Gearing

2.2.1 Direct drive actuation

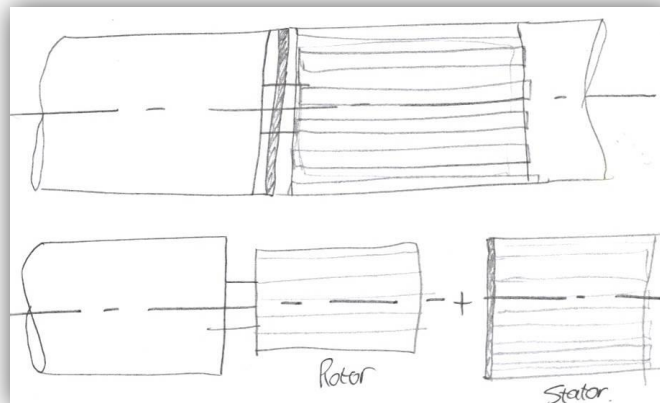


Figure 84: Direct drive rotational joint concept

Due to the link being approximately 130 mm from the elbow to the wrist, it was thought to embed a motor into the link (see Figure 84) to utilise the space available as best as possible. The link would act as the stator and be manufactured of a ferrous type material. On the inside, the link would have slots to place the copper windings. A shaft which connects to the distal link would act as the rotor on which permanent magnet strips will be fixed. By allowing current to flow through the stator windings in some slots, a magnetic field would be created to rotate the rotor and consequently the distal link.

Pros: Utilising of space available as best as possible

Cons: Difficult to actuate distal joint to this link due to all the space being used for the motor imbedded

Will be expensive due to a custom build
Torque that will be achieved will be far less than what is needed

2.2.2 Spur/Helical rotational joint

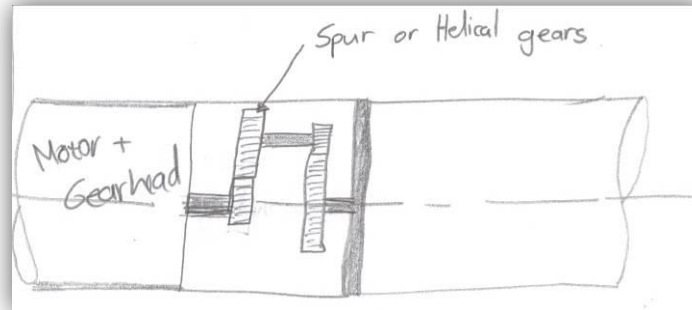


Figure 85: Spur/Helical rotational joint concept

A spur or helical gear driving mechanism is shown in Figure 85. A small gear is connected to the output shaft of the motor to drive an idler shaft which consequently acts as a means to increase the torque. The idler shaft then drives another spur or helical gear which is fixed to the distal link.

Pros: Simple working principle

Cons: Small, custom gears are needed

Gear teeth may not be able to withstand the forces to produce the required torque

The motor will not exert enough torque to drive the distal link with external forces

2.2.3 Multi-stage planetary gear rotation joint

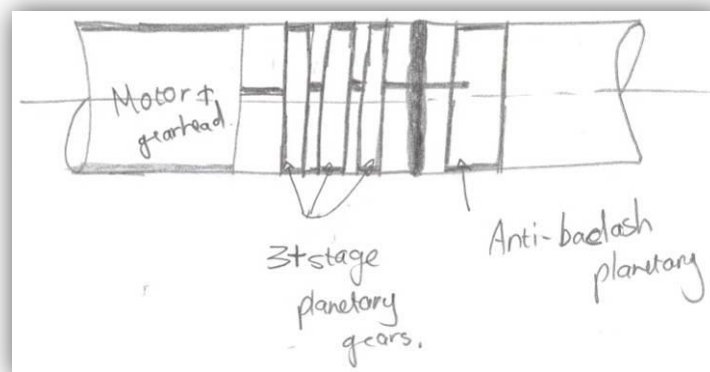


Figure 86: Multi-stage planetary gear rotational joint concept

Figure 86 shows a motor which is placed inside the link to drive a set of planetary gears. Each planetary gear system increases the torque and reduces the output speed. In the last stage, the planet gears' shafts or the outer ring gear is fixed to the distal link to manipulate it.

Pros: Simple means of actuating a rotational joint

- Cons: Difficult to actuate distal links due to all the space being utilised
Torque required may not be obtainable due to forces on gear teeth will be too large
The more stages there are the bigger the backlash and the less accurate

2.2.4 Harmonic gear joint

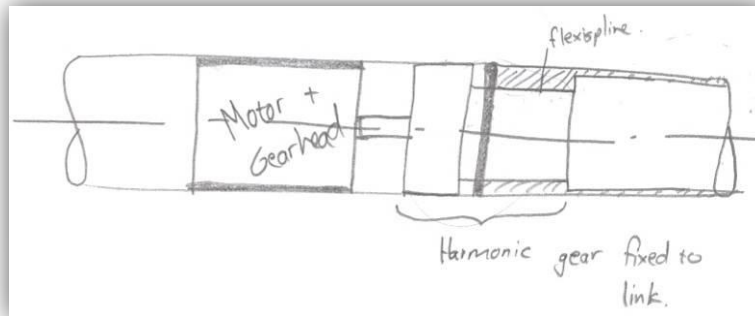


Figure 87: Harmonic gear rotational joint concept

Alternatively to the planetary gear system, a harmonic gearing mechanism could be used (illustrate in Figure 87). The motor would drive a 'wave creator' which causes the flexi spline and the outer spline to mesh, but due to the flexi spline having two less teeth than the outer spline, the flexispline rotates slowly with respect to the outer spline. The flexispline is fixed to the distal link and therefore the distal link rotates with the flexispline. This mechanism also acts as a means to increase the torque from the motor.

- Pros: Large speed reduction is possible
No backlash
- Cons: Required torque will still not be obtained due to motor not exerting a great enough torque
The torque required will also cause a too large a force on the teeth of the flexispline and the outer spline

2.2.5 Harmonic & Planetary joint

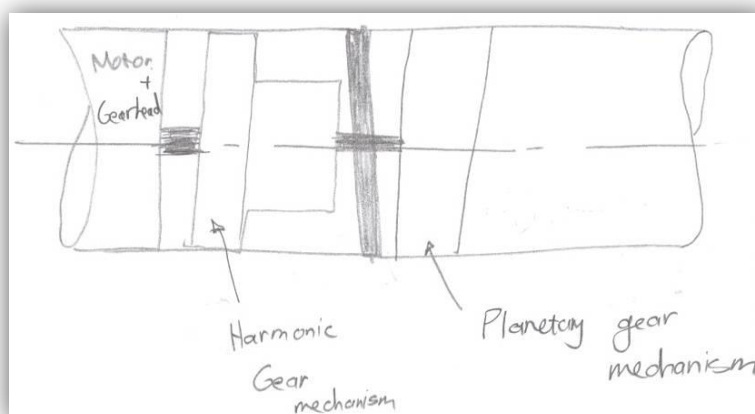


Figure 88: Harmonic & Planetary gear rotational joint concept

To further increase the torque, Figure 88 shows a planetary gearing system and a harmonic gearing system which is placed in series to increase the torque produced by the motor.

- Pros: Less backlash than a planetary gearing system on its own
 A larger torque could be obtained
- Cons: The torque cannot be achieved due to the forces on the gear tooth would be too large
 Custom part would be expensive

2.2.6 Helical worm gear mechanism with two motors

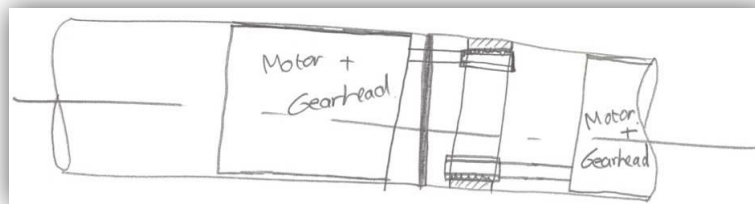


Figure 89: Helical worm gear rotational joint concept

A helical worm gear mechanism is shown in Figure 89. Two motors, one in the distal link and one in the proximal link drive to worms which mesh with a helical type gear and ultimately rotate the distal link with respect to the proximal link.

- Pros: Larger torques can possibly be achieved than those with the single motor concept
- Cons: Complex control system
 High forces on gear teeth
 Custom parts and therefore expensive
 Torque required will not be achieved

2.2.7 Bevel & Spur/Helical gear rotation joint

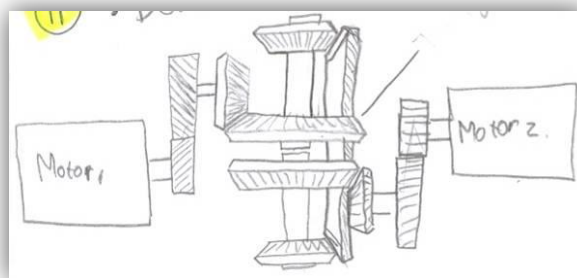


Figure 90: Bevel & Spur/Helical gear rotational joint concept

Two motors drive a complex configuration and are independent on each other. Each motor drives a shaft which allows then another shaft to be driven using a bevel gear system. The shaft with the bevel gear then meshes with an outer ring bevel gear which is attached to the link itself and therefore causing the link to rotate.

- Pros: Two motors with some good speed reduction and torques being increased

- One motor, on its own, can turn the joint while the other stands still (smaller overall torque will be produced in this case)
- Cons:
- Complex gearing system
 - Gears are very small and need to be custom made
 - The gear teeth may not be able to withstand the forces due to the torques

2.2.8 Angular swivel joint

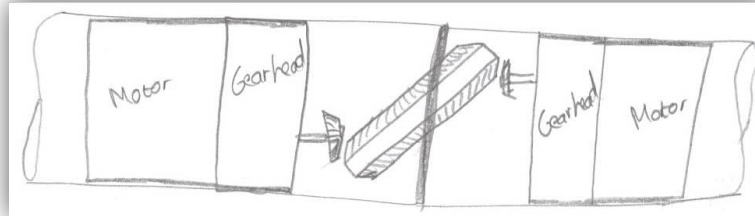


Figure 91: Angular swivel joint concept

The working principle of the joint shown in Figure 91 is explained in (Shammas *et al.*, 2003) and a short piece was extracted and given below:

Angular swivel joints were introduced by Takanashi [7]. The basic idea of this design is to use two angular shafts (Figure 5a), or two obliquely cut cups (Figure 5b), with supplementary angles (the shaft angles sum to 180 degrees). These two shafts are connected by a bearing, hence, rotating one shaft around the other sweeps a cone of revolution. Rotating the other shaft orients this cone of revolution. By coordinating both rotations, the joint can perform two pure motions: in-plane bending (the joint bends in one plane) and orienting (the joint orients the bending plane).

- Pros:
- Both a rotational and a hinge type motion is possible
 - Possibly high torques can be achieved
- Cons:
- Complex design
 - The design as given in (Shammas *et al.*, 2003) is much larger (typically 80 mm in diameter) than what is required, 10 mm.
 - The design is patented

2.3 Other

2.3.1 Drive shaft

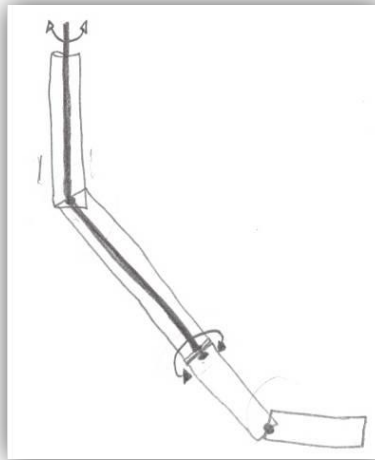


Figure 92: Drive shaft concept

Figure 92 shows a drive shaft that runs through the length of the arm up to the rotation joint. The drive shaft is rotated on the exterior by a motor allowing bigger torques to be achieved. At the revolute joints which it passes through, a universal joint will be used to allow bending at this joint.

Pros: High torques can be achieved

Cons: The universal joint will restrict the movement of the revolute joint

The shaft will take up a lot of space which can be used for other cables, etc

Due to the length of the drive shaft, torsional deflection could be a big problem since small diameter shafts would need to be used

When the revolute joint is bent, the universal joint would cause the shaft, distal to the joint, to rotate faster or slower depending of the position and orientation of the universal joint.

2.3.2 Inner tube guided joint

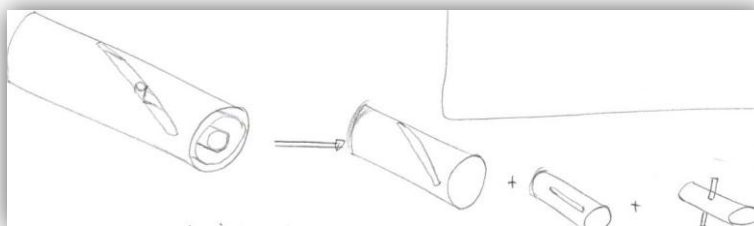


Figure 93: Inner tube guided rotational joint concept

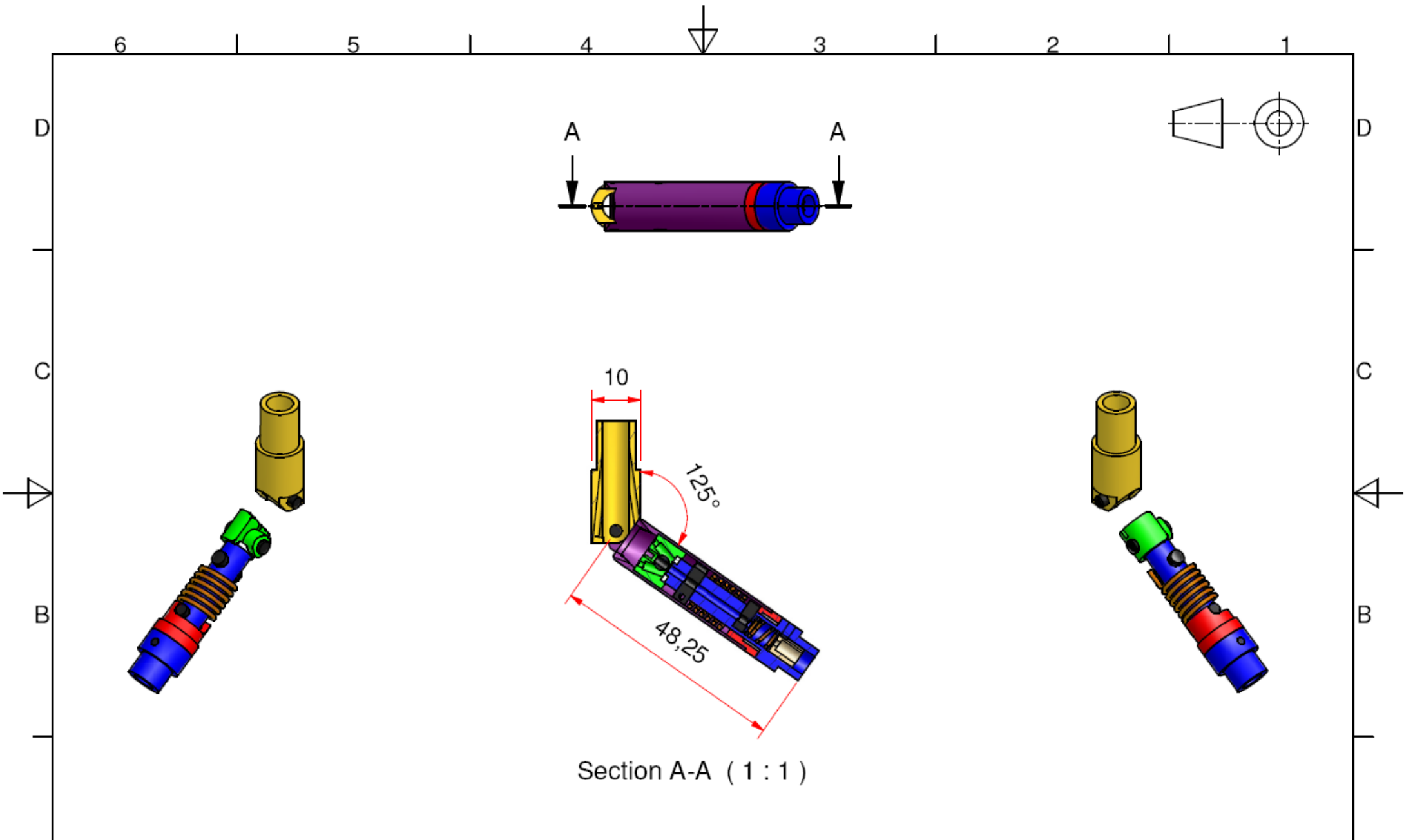
Figure 93 shows 3 tubes with the right most placed in the second right most and that into the the third right most to eventually form the assembly on the left. The two rods stretching from the pipe seen on the right is guided in the slotsof the two other pipes. It can also be seen that the third picture from the right has a scew slot where the second

one from the right has a straight slot. Due to these straight and scREW slots, when the inner pipe with its rods outstretched on either side is pushed forward the rod forces the middle pipe to rotate relative to the inner and outer pipes.

Pros: Linear actuation is implemented (greater linear forces are possible in the meso scale rather than in than with rotational motion)

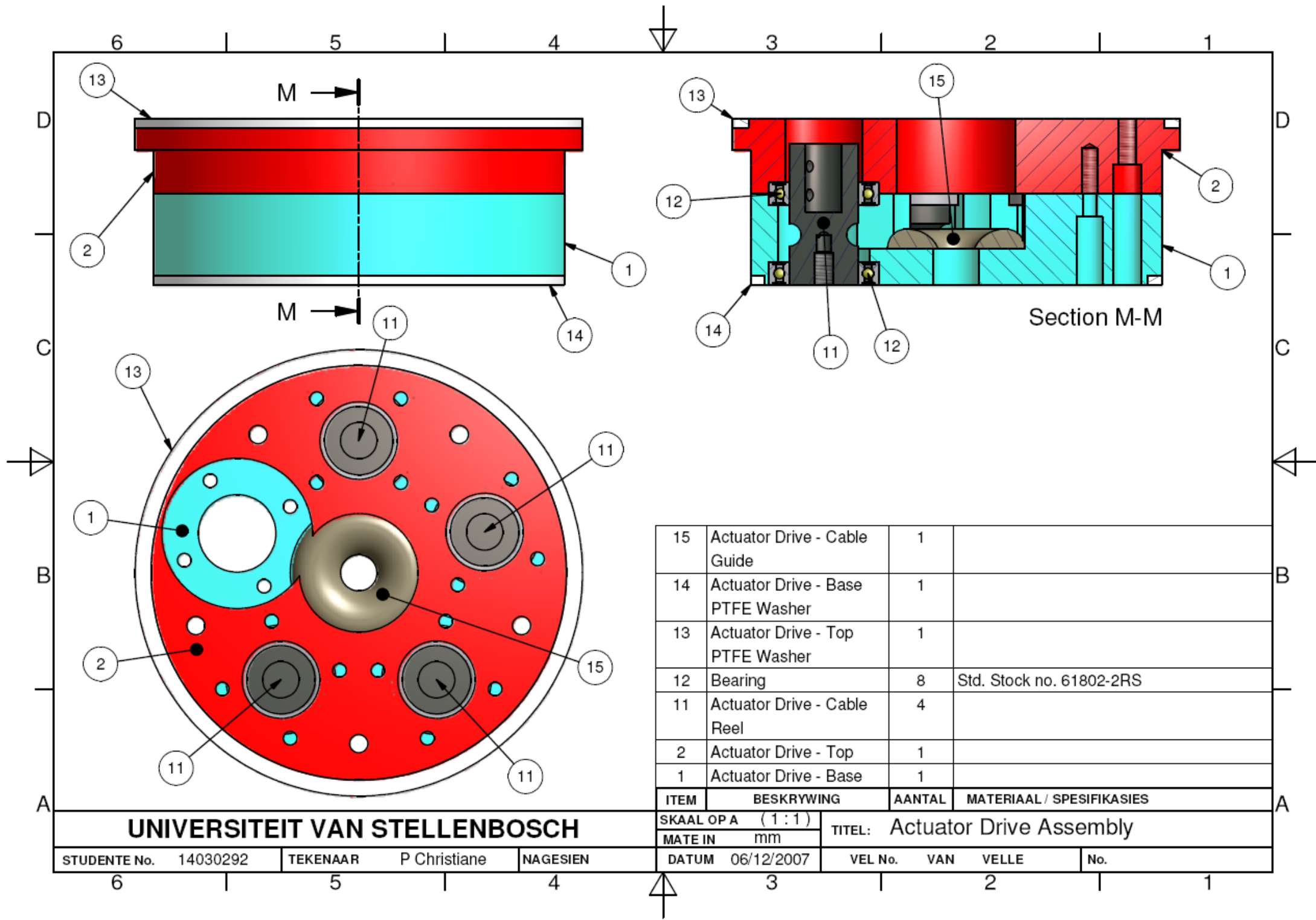
Cons: Large linear actuation force is needed due to friction and so on.
Accuracy could be a problem

Appendix D: Technical Drawings



Section A-A (1 : 1)

UNIVERSITEIT VAN STELLENBOSCH				ITEM	BESKRYWING	AANTAL	MATERIAAL / SPESIFIKASIES		
				SKAAL OP A (1 : 1)		TITEL: Manipulator Wrist Assembly			
				MATE IN mm					
STUDENTE No.	14030292	TEKENAAR	P CHRISTIANE	NAGESIEN	DATUM	VEL No.	VAN	VELLE	No.



15	Actuator Drive - Cable Guide	1	
14	Actuator Drive - Base PTFE Washer	1	
13	Actuator Drive - Top PTFE Washer	1	
12	Bearing	8	Std. Stock no. 61802-2RS
11	Actuator Drive - Cable Reel	4	
2	Actuator Drive - Top	1	
1	Actuator Drive - Base	1	

ITEM	BESKRYWING	AANTAL	MATERIAAL / SPESIFIKASIES
------	------------	--------	---------------------------

UNIVERSITEIT VAN STELLENBOSCH

SKAAL OP A (1:1)

MATE IN mm

TITEL: Actuator Drive Assembly

STUDENTE No. 14030292

TEKENAAR P Christiane

NAGESIEN

DATUM 06/12/2007

VEL No. VAN VELLE

No.

Appendix E: Electronic Design

1. Noise Reduction Techniques

There are three ways to prevent interference between devices (Kobeissi, 2004):

1. Suppress the noise at its source
2. Make the coupling path between the source and receptor inefficient
3. Make the receptor less susceptible to any noise

Kobeissi (2004) listed a number of noise reduction techniques at device and PCB levels. These techniques are not intended to be a complete EMI solution, but if implemented can greatly affect the performance of a system in a noisy environment. A few noise reduction techniques at board level from Kobeissi are listed below (Kobeissi, 2004).

1.1 Board-Level Techniques

Board structure, routing, and filtering board-level techniques are discussed here.

1.1.1 Board-structure techniques

- Use ground and power planes
- Maximize plane areas to provide low impedance for power supply decoupling
- Minimize surface conductors
- Use narrow traces (4 to 8 mils) to increase high-frequency damping and reduce capacitive coupling
- Separate circuits on PCB according to frequency and type
- Use multipoint grounding to keep ground impedance low at high frequencies
- Use single-point grounding only for low-frequency, low-level circuits
- Use 45-degree, rather than 90-degree, trace turns. Ninety-degree turns add capacitance and cause change in the characteristic impedance of the transmission line.
- Keep clock signal loop areas as small as possible.
- Keep high-speed lines and clock-signal conductors short and direct.
- Do not run sensitive traces parallel to traces that carry high current, fast-switching signals.
- Eliminate floating digital inputs to prevent unnecessary switching and noise generation:
 - Configure multipurpose device pins as outputs.
 - Set three-state pins to high impedance.
 - Use appropriate pullup or pulldown circuitry.
- Avoid running traces under crystals and other inherently noisy circuits.
- Keep clock traces, buses, and chip-enable lines separate from input/output (I/O) lines and connectors.

1.1.2 Filter techniques

- Filter the power line and all signals entering a board.
- Bypass all power feed and reference voltage pins for analog circuits.
- Bypass fast switching transistors.
- Decouple locally whenever possible.

- Decouple power/ground at device leads.

1.1.3 Other design techniques

- Mount crystals flush to board and ground them.
- Use shielding where appropriate.
- Use the lowest frequency and slowest rise time clock that will do the job.
- Route adjacent ground traces closer to signal traces than other signal traces for more effective interception of emerging fields.

2. Electronic schematics

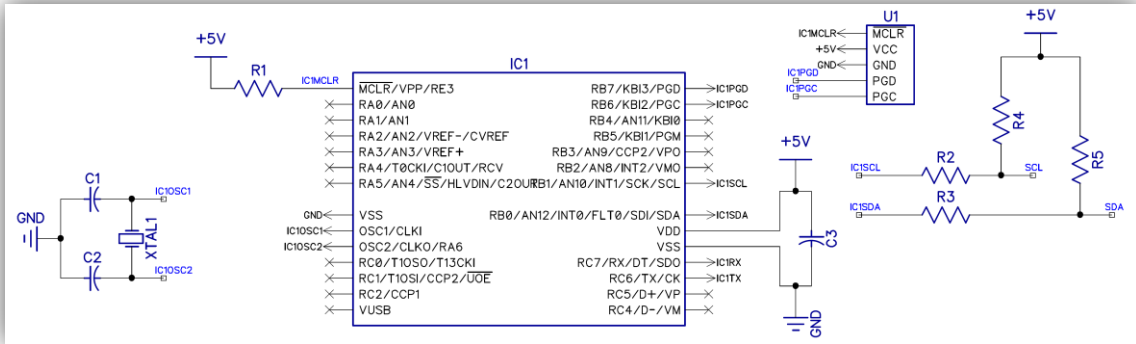


Figure 94: PIC18F2550 (Master) Schematic

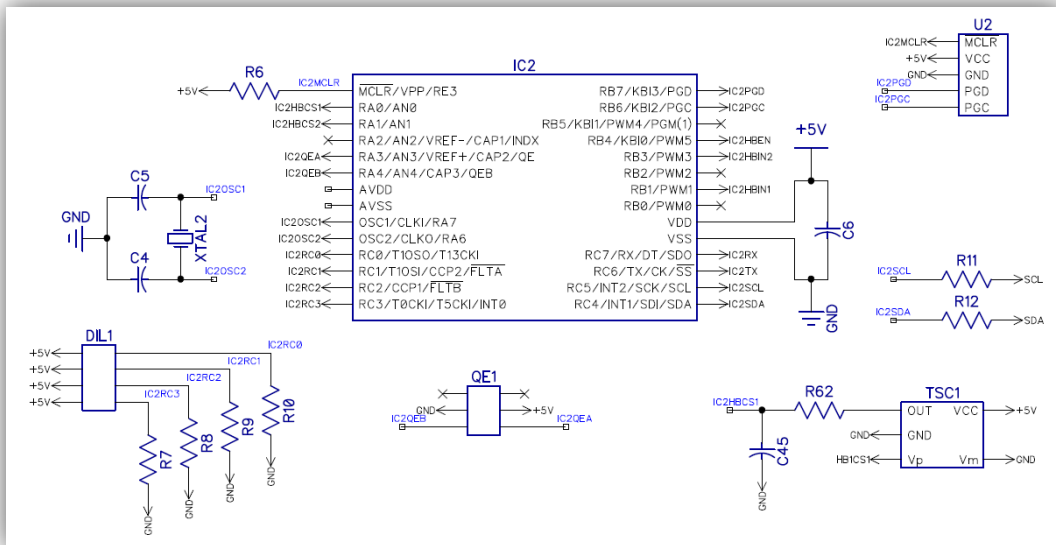


Figure 95: PIC18F2431 (Slave) Schematic

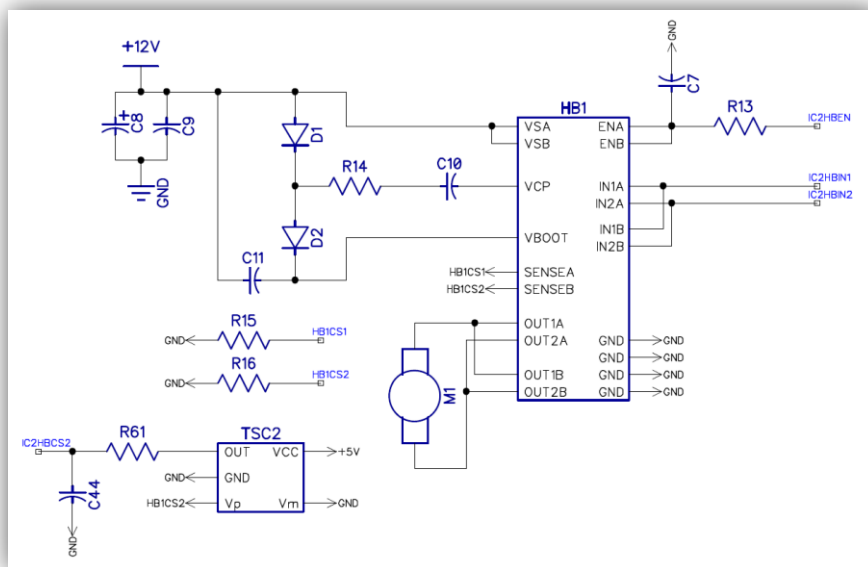


Figure 96: L6225 H-Bridge Schematic

3. PCB Layouts

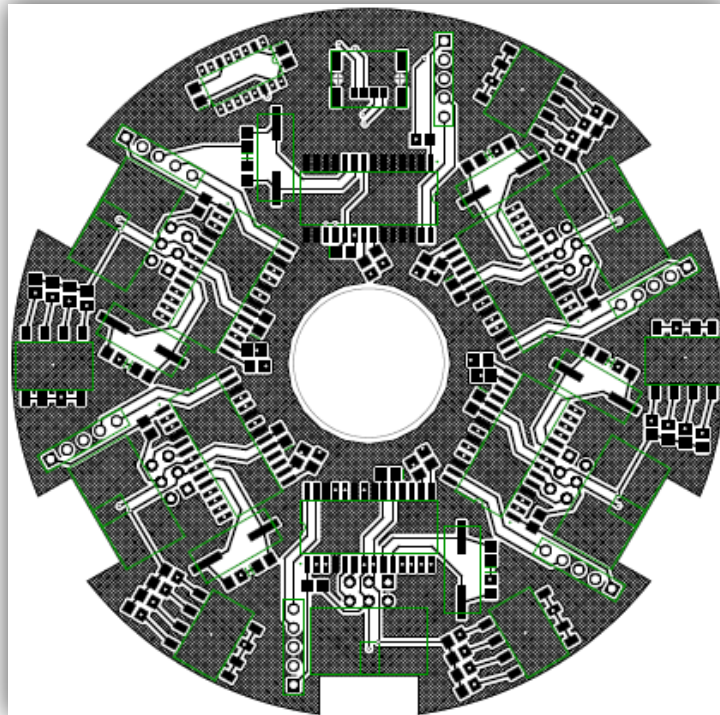


Figure 97: Digital PCB Top Layout (Not to scale)

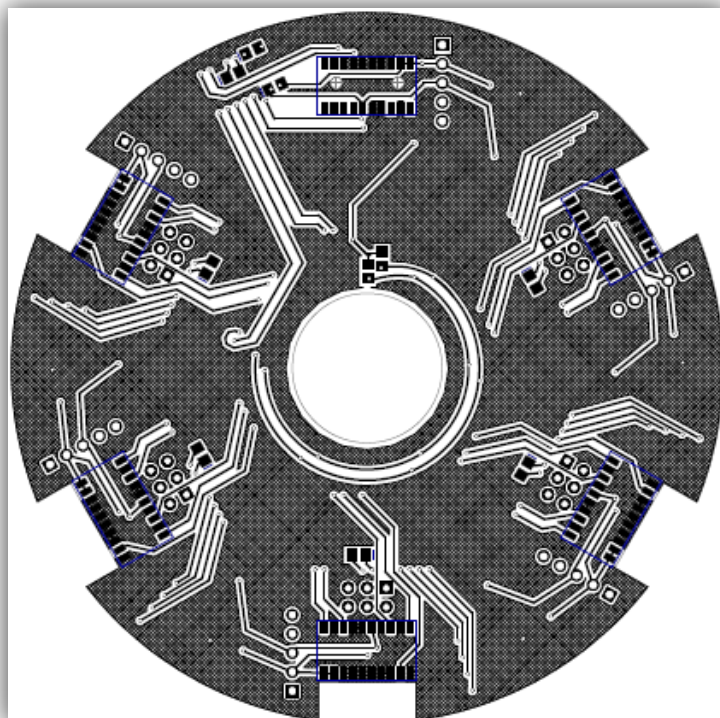


Figure 98: Digital PCB Bottom Layout (Not to scale)

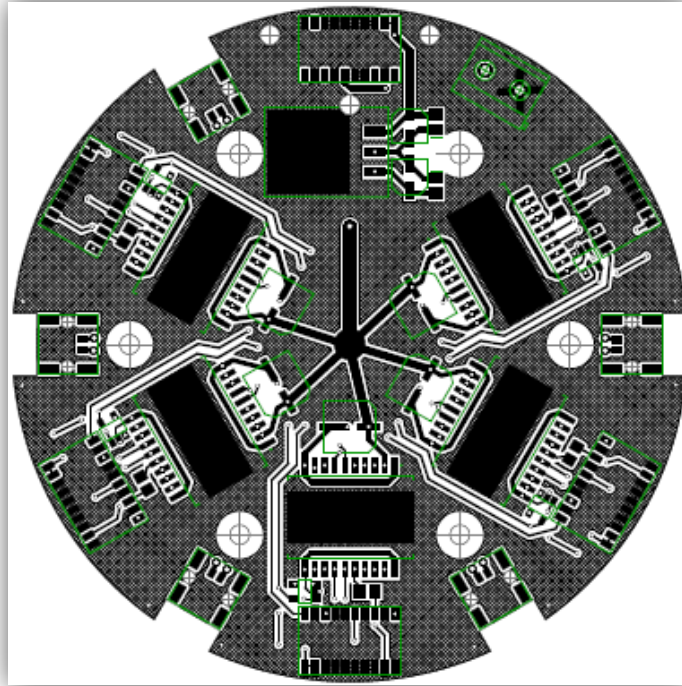


Figure 99: Power PCB Top Layout (Not to scale)

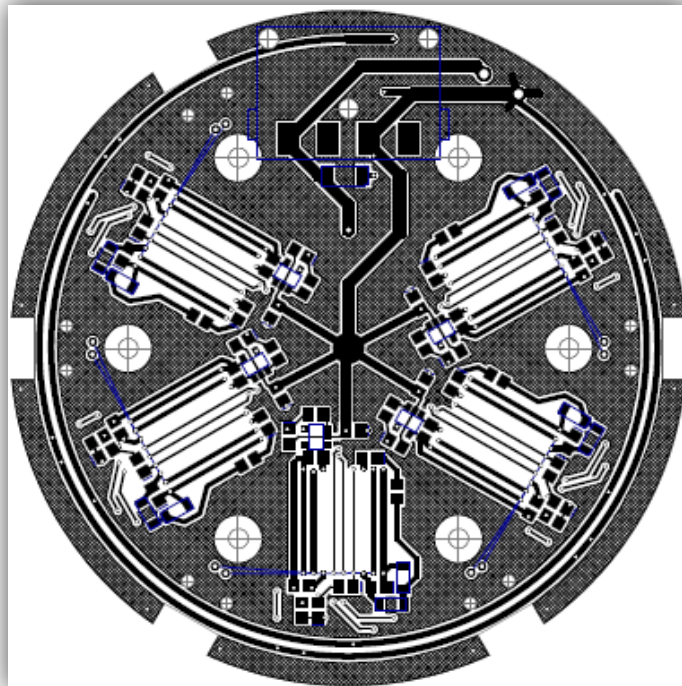


Figure 100: Power PCB Bottom Layout (Not to scale)

4. PCB Images

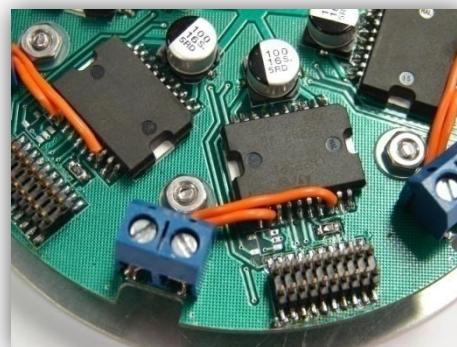
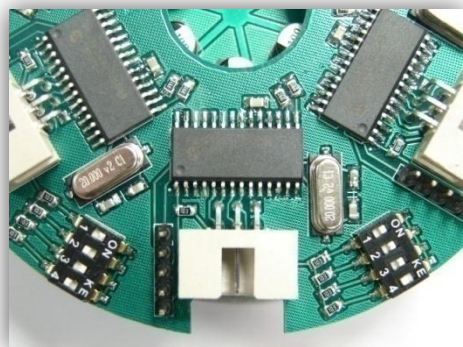
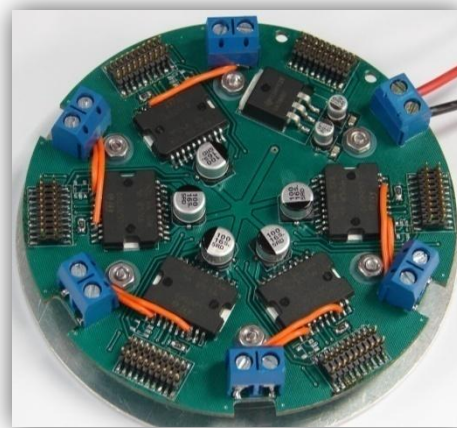
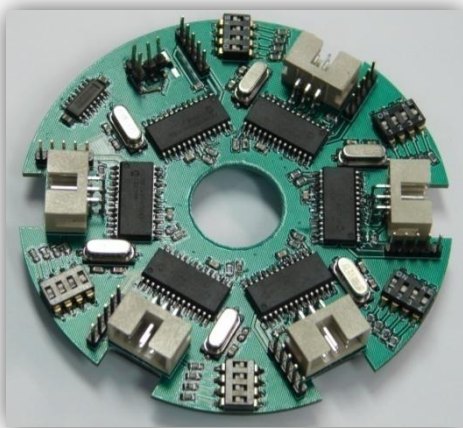
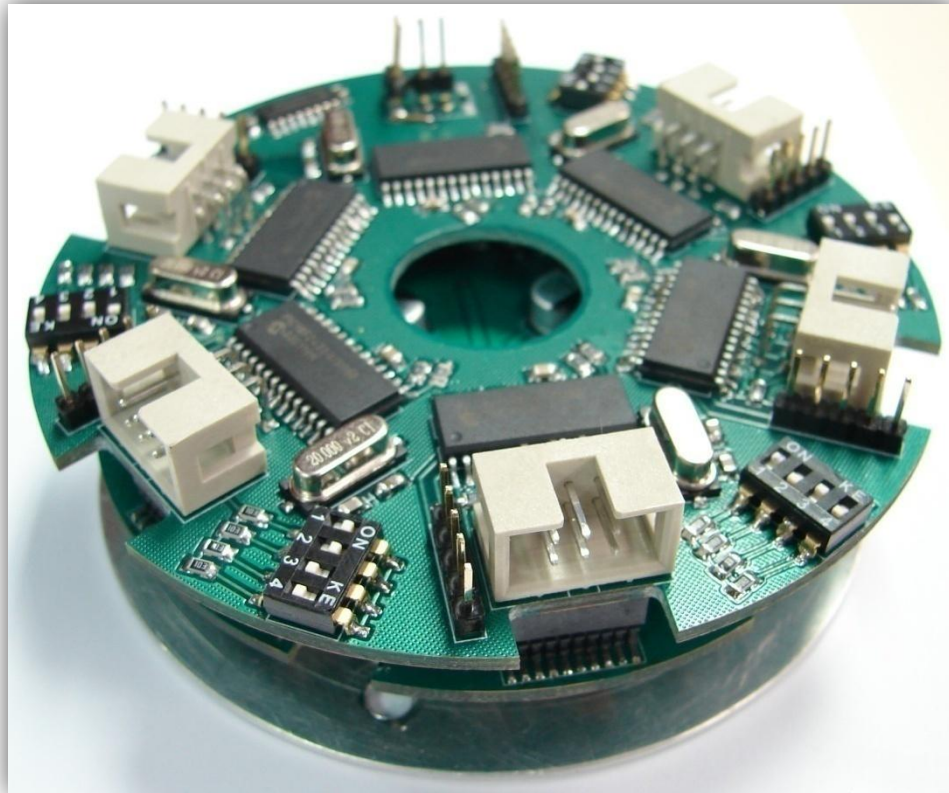


Figure 101: Close ups of Digital PCB (left) and Power PCB (right)

Appendix F: Experimental Data

1. Repeatability Test

Table 9: Repeatability Test Experimental Data

Sample 1										
No.	Joint Position		Vector Angle			Unit Vector Coordinates			Ext-Distal Angle	Ext Rotation Angle
	Extension	Distal	X-Angle	Y-Angle	Z-Angle	X-Coordinate	Y-Coordinate	Z-Coordinate		
1	0		89.926	90.004	0.074	0.001291543	-6.98132E-05	0.999999166	NA	0.702348127
2		55	90.597	31.794	58.213	-0.010419427	0.849947871	0.526762947	58.21793627	
3		35	89.915	137.049	132.951	-0.001483529	0.731936687	0.681372649	47.05319433	
4		20	90.704	60.312	29.698	-0.012286809	0.495276732	0.868648809	29.70391725	
5		0	89.874	85.807	4.195	0.002199113	0.073116352	0.997320865	4.197424281	
6		20	89.687	114.012	155.985	-0.005462853	0.406927967	0.913438943	24.02009958	
7		35	90.386	49.303	40.7	-0.00673692	0.652058707	0.758134336	40.70481958	
8		55	89.814	148.29	121.71	-0.003246307	0.850719384	0.525620138	58.29431181	
9	45		89.989	90.009	0.014	0.000191986	-0.00015708	0.99999997	NA	14.95394542
10		55	77.323	145.251	121.739	-0.219454582	0.821656886	0.526050658	58.28398654	
11		35	101.1	44.952	47.174	-0.192521967	0.707698917	0.67977419	47.19732448	
12		20	81.923	118.439	150.23	-0.1405038	0.476222857	0.868025549	29.79485093	
13		0	89.045	94.03	175.858	-0.016667123	0.070278787	0.997388105	4.163571708	
14		20	95.856	66.874	23.941	-0.10202863	0.392754478	0.913963808	23.96357477	
15		35	80.362	129.282	139.088	-0.167422647	0.633137732	0.755716324	40.93483481	
16		55	103.019	34.743	58.434	-0.225274155	0.82171657	0.523480389	58.45744926	
17	90		90.042	90.054	0.068	-0.000733038	-0.000942478	0.999999296	NA	29.89828673
18		55	115.083	42.499	58.264	-0.423930716	0.737289128	0.526006128	58.30437443	
19		35	68.642	129.349	133.013	-0.364194187	0.634042438	0.682164281	47.0273576	
20		20	104.907	64.348	30.237	-0.257250856	0.432904048	0.863949786	30.27829768	
21		0	91.981	86.329	4.173	-0.034568084	0.06402721	0.997348879	4.212144436	
22		20	78.241	110.591	156.016	-0.203795537	0.351694608	0.913659004	24.02463688	
23		35	109.079	55.425	40.912	-0.326871535	0.56748453	0.755716324	40.95243944	
24		55	64.914	137.47	121.768	-0.423978138	0.736923498	0.526481044	58.27239081	
25	135		90.084	90.107	0.136	-0.001466076	-0.001867501	0.9999997183	NA	44.91103312
26		55	126.916	52.95	58.295	-0.600643516	0.602511735	0.525545896	58.35009023	
27		35	58.87	121.239	132.923	-0.516981598	0.518609117	0.681014876	47.13209661	
28		20	110.655	69.222	30.018	-0.352740039	0.354747989	0.865868281	30.07305051	
29		0	87.047	93.029	175.768	-0.051516758	0.052841401	0.997273418	4.286815393	
30		20	106.6	73.261	23.933	-0.285688367	0.288012422	0.914020459	23.98800195	
31		35	62.495	117.637	139.114	-0.461826018	0.463868224	0.75601343	40.94107047	
32		55	126.898	52.98	58.243	-0.600392311	0.602093763	0.52631781	58.29809735	
33	180		90.107	90.169	0.2	-0.001867501	-0.002949602	0.9999993908	NA	59.88119049
34		55	137.359	64.739	58.259	-0.735612536	0.426742375	0.526080344	58.32502201	
35		35	50.624	111.603	132.819	-0.634406776	0.368173235	0.679684581	47.24701925	
36		20	115.701	75.414	30.098	-0.433674811	0.251832895	0.865168926	30.16401991	
37		0	93.71	87.867	4.281	-0.064706476	0.037219274	0.997209943	4.347265595	
38		20	69.435	101.795	156.021	-0.351269777	0.204410629	0.913694473	24.04495513	
39		35	124.496	70.784	40.922	-0.566348701	0.329130354	0.755602011	40.98800254	
40		55	42.647	115.26	121.749	-0.735541595	0.426726591	0.526199082	58.31702147	
41	135		90.089	90.11	0.141	-0.001533342	-0.001919861	0.999996972	NA	45.56574794
42		55	127.372	53.479	58.218	-0.606987543	0.595117376	0.526688768	58.27365322	
43		35	58.484	120.89	132.888	-0.522736646	0.513391484	0.680567431	47.16761762	
44		20	110.967	69.46	30.076	-0.357830186	0.350861216	0.865361417	30.13167378	
45		0	92.989	87.008	4.232	-0.052144232	0.052196521	0.997273418	4.287402028	
46		20	73.227	106.549	156.079	-0.288580639	0.284835234	0.914105402	23.97652329	
47		35	118.079	62.698	41.088	-0.470688533	0.458680573	0.753701056	41.14381288	
48		55	52.629	126.57	121.731	-0.606973673	0.595804439	0.525931907	58.32462459	
49	90		90.049	90.054	0.073	-0.000855211	-0.000942478	0.999999188	NA	30.52838273
50		55	115.589	42.911	58.242	-0.431912601	0.732412196	0.52633265	58.28305546	
51		35	68.239	129.085	132.996	-0.370735749	0.630472617	0.6819473	47.04498833	
52		20	104.944	64.462	30.155	-0.257874841	0.431109619	0.864669606	30.19647683	
53		0	92.044	86.304	4.225	-0.035666963	0.06446264	0.997282426	4.264784905	
54		20	78.239	110.43	156.158	-0.203829711	0.349062759	0.914663608	23.88284461	
55		35	109.318	55.639	40.859	-0.33081088	0.564405236	0.756321798	40.89990909	
56		55	64.417	137.104	121.747	-0.431818151	0.73259042	0.526169399	58.2940432	
57	45		89.999	90.009	0.009	1.74533E-05	-0.00015708	0.999999988	NA	15.55821779
58		55	103.183	35.002	58.243	-0.228061993	0.819132022	0.52631781	58.26672805	
59		35	78.632	134.739	133.033	-0.197109823	0.703878366	0.682419476	46.99084651	
60		20	97.836	61.299	29.948	-0.136338051	0.480238806	0.866478833	29.97213189	
61		0	91.04	85.886	4.243	-0.018150427	0.071741163	0.997259232	4.265616251	
62		20	83.931	112.966	156.155	-0.105726067	0.390184821	0.914642442	23.86831111	
63		35	100.054	50.993	40.782	-0.17457626	0.629415333	0.757200296	40.80568216	
64		55	76.811	145.004	121.747	-0.228163952	0.819192085	0.526169399	58.27673464	
65	0		89.928	89.978	0.075	0.001256637	0.000383972	0.999999143	NA	0.569113543
66		55	90.484	31.744	58.261	-0.008447293	0.850407325	0.526050658	58.26576424	
67		35	89.177	136.827	133.161	-0.014363566	0.729291132	0.684050754	46.84450094	
68		20	89.98	60.091	29.909	0.000349066	0.498623905	0.866818436	29.91303102	
69		0	89.883	85.875	4.126	0.002042034	0.071932653	0.997408236	4.128560475	
70		20	90.053	113.806	156.194	0.000925024	0.403641108	0.914917404	23.80993842	
71		35	90.234	49.204	40.797	-0.004084059	0.653367754	0.757025268	40.80151763	
72		55	89.531	148.267	121.728	-0.008185503	0.850508318	0.525887373	58.27674136	

2. Strength Test Data

Table 10: Strength Test Experimental Data

Strength Test Experimental Results			
Joint	Weight	Success/Failure	Notes
Revolute (up)	200g	Yes	
	500g	Yes	Noticable change in stop position (against the flange)
	800g	Yes	
Long Arm rotation	1kg	Yes	Noticable increase in change in stop position (against the flange)
	200g	Yes	
	500g	Yes	
	800g	Yes	
	1kg	Yes	
Revolute (down)	200g	Yes	Noticable Deflection due to weight
	500g	Yes	Increased Deflection due to weight
	800g	Yes	Increased Deflection due to weight
	1kg	Yes	Large deflection due to weight!